DEFENSE DOCUMENTATION CENTER

FOR

SCIENTIFIC AND TECHNICAL INFORMATION

CAMERON STATION ALEXANDRIA, VIRGINIA

INSTITUTE

FOR

AEROSPACE STUDIES

UNIVERSITY OF TORONTO

TURBULENCE-INDUCED PANEL VIBRATION

by

M. Y. elBaroudi

FEBRUARY, 1964

UTIAS REPORT NO. 98
AFOSR 64-0883

TURBULENCE-INDUCED PANEL VIBRATION

by

M. Y. elBaroudi

TURBULENCE-INDUCED PANEL VIBRATION

M. Y. el Baroudi

Errata

Page 2
Section 2.2 - paragraph 2 - line 3 - "The clamping surfaces ..." instead of "The clamping area ....".

Page 5
Eq. (3.2.1) - numerator - "$p(x'+\Delta x, y'+\Delta y, t'+\tau)....$" instead of "$p(x'+\Delta x, y'+\Delta y, t'+\tau)....$".

Page 10
Section 4.3 - paragraph 2 - line 3 - "All odd panel modes (m, n odd) with ..." instead of "All panel modes with ....".

Section 4.3 - paragraph 2 - line 3 - ".... with modal lines ..." instead of "... with model lines...".

Page 11
Section 4.4 - paragraph 1 - line 15 - "... running wave, $\sin k(x' - U_c t')$, is a ...." instead of ".... running wave, $\sin k(\Delta x - U_c \tau)$ is a .....".

Section 4.4 - paragraph 1 - line 18 - "... standing wave, $\sin(kx') \cdot \cos(\omega t')$, is a ..." instead of "... standing wave, $\sin(k\Delta x) \cos(\omega \tau)$, is a ...".

Page 12
last paragraph - line 4 - "... electromagnet fed to ....." instead of "... electromagnet feed to ....".

Page 18
last paragraph - line 11 - "Second, that ..." instead of "Third, that a ....".

Appendix A
Eq. (A.4) "$4A \bar{p}^2$ ...." instead of "$A \bar{p}^2$ ....".

Eq. (A.8) - expression for x - term 2 of 2 terms - "$C(-EB - DA/D----)$" instead of "$C(EB - DA/D---)$".

Eq. (A.8) - expression for Y - term 1 of 2 terms - "$[-A(AB/E + AD/G)---]$" instead of "$[-A(AB/E + AD/G.]$"

Eq. (A.9) - expression for BB - "$[1/\theta(-a_{mn}+1/\theta) - \alpha_m(\alpha_m + \omega_{mn})]$" instead of "$[1/\theta(-a_{mn}+1/\theta) - \alpha_m(\alpha_m - \omega_{mn})]$".

Eq. (A.9) - expression for EA - "$4(a_{mn}/\theta)/(a_{mn}^2 + \omega_{mn}^2)$" instead of "$4(a_{mn}/\theta)(a_{mn}^2 + \omega_{mn}^2)$".

Eq. (A.9) - expression for EB - "$4(\omega_{mn}/\theta)/(a_{mn}^2 + \omega_{mn}^2)$" instead of "$4(\omega_{mn}/\theta)(a_{mn}^2 + \omega_{mn}^2)$".

Eq. (A.14) - p. 25 - first line - "$E_2 = OQ^2 + OO^2$; $E_3 = OI^2 + OF^2$; $F_1 = OL^2 + OJ^2$".

Eq. (A.15) - expression for OM - "$1/2(a_{mn} - a_{pn}) - 1/\theta$" instead of "$1/2(a_{mn} - a_{pn}) + 1/\theta$".

Appendix E
title - "... Simply-Supported Plate..." instead of ".... Simply-Supported Panel ..."

Figure 12B   figure $(U_c)_{f_o}$ /U vs f_o - frequency scale, major divisions
              100, 1000, 10000 instead of .01, .1, 1 .

Figure   caption, upper right hand corner of figures -
21b, c   1 in. Duct instead of 8 in. Duct.

Figure 34   vertical scale - $\left| R_p (\Delta x, o, \tau) \right|_{max} = 1$
              - vertical scale from $0 \rightarrow 1.0$ instead of from $0 \rightarrow 1.2$ as
              shown.

ACKNOWLEDGEMENT

SUMMARY

Motivated by the problem of boundary-layer induced panel noise, a detailed study has been made of the transverse vibration of 11 x 11 inch steel panels flush-mounted in the wall of a turbulent flow duct. Panel thicknesses were .002 and .008 inch. Duct cross sections were 1 x 12 and 8 x 12 inches, and flow speeds were about 60 to 200 feet per second.

The characteristics of the exciting pressure field at the wall and of the resultant vibration of the sample panels were investigated using statistical techniques. Relief charts of the experimental two-point space-time correlation of panel vibration versus longitudinal separation and time-delay showed pronounced oblique ridges and valleys discernable in a more random pattern. These are interpreted as running waves (with a speed equal to that of the pressure field convection) with an irregular pattern superposed.

Such running waves were predicted by Ribner's idealized infinite-panel model of the flexural response. On the other hand, a superposition of stationary unsteady oscillations in the various modes of a finite panel forms the basis of the more realistic but more complex theories. To test the compatibility, Dyer's idealized theoretical model of the panel response was developed and programmed for a digital computer. The calculated relief plot of correlation showed qualitative agreement with the experimental results.

TABLE OF CONTENTS

NOTATION

A; A, A'	eddy size parameter; spectral amplitudes
a_{mn}	plate modal damping
B	plate bending stiffness - $Eh^3/12 (1 - \sigma^2)$
D	duct depth
d	capacitance probe static displacement
d_m	microphone pinhole diameter
d_w	capacitance probe sensing element diameter
E	Young's modulus
$e_1(t), e_2(t)$	two arbitrary electrical signals at time t
f	frequency
f_c	coincidence frequency
f_{cL}	clamped panel modal frequency
f_{co}	frequency of lowest order mode considered in computations
$f_{max}, f_{min};$ f_o	filter upper and lower cut-off frequencies, filter band center frequency
f_{ss}	simply supported panel modal frequency.
g	impulse response
h	panel thickness
$I_{mn}, I_{mpn},$ I_{mnpq}	functions related to Dyer's displacement covariance
k; k_x, k_y	wave number; wave number components
L_x, L_y	plate lengths
ℓ_x, ℓ_y	turbulence integral scales
M; M, N, P	plate mass; highest order plate loop lines considered in computations $M = (m)_{max}$, $N = (n)_{max}$, $P = (p)_{max}$

m, n; p, q	plate loop lines
p	fluctuating static pressure
R; R_p, R_w	correlation function; wall pressure and panel displacement correlation function
$_{f_o}R_p$, $_{f_o}R_w$	1/3 octave band pressure and displacement correlation function
$_{f_o}\bar{R}_p$, $_{f_o}\bar{R}_w$	1/3 octave band pressure and displacement correlation function maximum amplitude
$\mathcal{R}$; $\mathcal{R}_p$, $\mathcal{R}_w$	covariance function; pressure and displacement covariance functions
S; S_w	spectral density function; panel displacement spectral density function
U; U_p	duct center-line mean flow speed; plate flexural wave speed
U_c; $\bar{U}_c$	pressure field convection speed; average pressure field convection speed
$(U_c)_{f_o}$, $(\bar{U}_c)_{f_o}$	1/3 octave band pressure field convection speed; 1/3 octave band average pressure field convection speed
u	local duct flow speed
w	panel or plate displacement
w_{mn}	plate modal displacement
x', y'; x, y	observation points in plane of panel or plate surface
$_3$(or z)	coordinate along duct depth
α_m	pressure wave convection frequency (m π U_c/L_x); at coincidence α_m = ω_{mn}.
β_o	plate or panel acoustic damping
γ	$\cos^{-1}$ (U_p/U_c)
Γ_{mn}	eigenvalue
$\zeta*$	turbulent duct flow displacement thickness

Δf	equivalent rectangular filter bandwidth
$\Delta x, \Delta y$	spatial separations: $\Delta x = x - x'$, $\Delta y = y - y'$
η	plate or panel structural damping
θ	eddy lifetime
$\lambda; \lambda_x$	wave length; wave length component
ξ	damping ratio
σ	Poisson's ratio
τ	time delay: $\tau = t - t'$
ϕ_{mn}	plate or panel eigenfunction
ω_{mn}	plate or panel modal frequency
cps	cycles per second
fps	feet per second
in., "	inch
ips	inches per second
ms	millisecond
rms	root mean square
thou.	one thousandth of an inch

The coordinate system used in this investigation is defined in Section 3.2 and in figures 2, and 9.

The terms vibration and displacement are used interchangeably in this investigation.

1. INTRODUCTION

The noise level in the interior of flight vehicles due to the turbulent flow bathing their exterior can be of large magnitude. The dominant noise existing in present day high subsonic speed transport aircraft under most cruise conditions is the noise due to boundary-layer excitation (Ref. 1).

The fluctuating static pressure in a turbulent boundary layer of a flow over a flexible skin causes motion of the skin transverse to its surface. The skin behaves like the diaphragm of a loudspeaker and radiates sound into the interior of the fuselage as well as into the flow field.

A body of theoretical treatments of this mechanism of panel excitation is to be found in the literature (Refs. 2, 3, 12, 13, 14, 15, 16, and 17). Two levels of approximation were used. Ribner (Ref. 2) whose work is representative of the simpler approach, idealized the panels as infinite. He treated the response in terms of running flexural waves which were excited by a convected turbulent pressure pattern moving over the panel surface on one side. Dyer (Ref. 3) whose work typifies the second approach, considered the motion of a finite plate excited by a convected decaying pressure pattern in terms of its normal modes.

The present investigation was initiated to study experimentally as well as theoretically, the vibration of panels excited by turbulent flow on one side and in particular to determine whether this motion was best described physically in terms of running waves (Ref. 2) or standing waves (e.g., Ref. 3).

The physical environment used for the experiments was identical to the one used by Ludwig (Ref. 4) in his investigation of the sound radiation from panels excited by turbulent flow. The statistical quantities measured were the two-point space-time correlation of the turbulent wall-pressure field and the two-point space-time correlation of the resultant panel vibration as well as its magnitude.

2. EXPERIMENTAL EQUIPMENT

2.1 Air Duct

A schematic of the UTIAS low-noise air duct (Ref. 5 and 4) is given in Fig. 1. The facility was basically an open circuit wind-tunnel with interchangeable rectangular duct sections twelve inches wide and one or eight inches deep. Test panels were fitted in a cut-out portion of the top of the duct, flush with the inner surface. Fully developed turbulent duct flow was achieved at the panel station center which was 35.5 D and 35 D downstream of the duct entrance for the eight inch and one inch duct respectively.

1

The interior of the duct sections were lined with acoustic tile to absorb acoustical disturbances generated by the blower. The duct sections in the vicinity of the panel station were enclosed in a 1/2 inch plywood shell forming a 1-1/2 inch gap between shell and duct section which was filled with sand to eliminate duct vibration.

A port-hole in the bottom of the duct, directly below the panel station, was removable for checking the mounting of the panel frame in the duct wall.

Blower rpm was monitored by means of a Hewlett-Packard electronic counter and tachometer system.

A pitot-static probe system of conventional design mounted on a screw traversing mechanism was used in conjunction with a Meriam water manometer to measure flow velocities and pressures.

Flow temperatures were measured by means of a total temperature dial thermometer whose probe end was inserted into the settling chamber.

Atmospheric temperatures and pressures were measured by a laboratory thermometer-barometer unit. (Cenco, Cambridge, Mass.)

2.2 Panels

The panel material was commercial shim steel in 12 inch by 120 inch rolls (precision Steel Warehouse Inc., Downers Grove, Illinois). Two thicknesses were used, .002 and .008 inch.

A panel to be tested was mounted in a steel frame (Ref. 4). All four panel edges were clamped, leaving an exposed area of 11 inches by 11 inches (Fig. 2). The clamping area of the two panel edges perpendicular to the flow direction were bent through an angle of 30 degrees and fixed between machined steel surfaces. This bending was necessitated by the requirement that panel and frame present a smooth flat surface to the duct flow. The remaining two edges were clamped flat between machined steel surfaces imbedded for the most part in the duct wall. The protrusions formed a minute portion of the duct   cross-sectional area.

The outside dimensions of the panel frame were carefully matched with the dimensions of the cut-out portion of the top of the duct in order to seal off the duct interior from the atmosphere of the test room.

2.3 Fluctuating Wall Static Pressure Transducer

The measurement of the fluctuating wall pressure was made with an Altec Lansing (type 21 BR-18-15) pinhole microphone (Fig. 3). The pinhole (d_m = .040 inches) in the microphone surface was offset so

that the minimum distance between two microphone pinholes in a correlation measurement would be small. The free field-parallel incidence microphone calibration provided by the manufacturer indicated resonances at 5,000 cps and 11,000 cps. A full shunt-type amplitude equalization filter (Ref. 4) was used to flatten the microphone response to 12,000 cps.

The electrical signal from a microphone was fed in sequence through a General radio (type 1551-P1) battery powered cathode follower, a General radio (SLM type 1551-A) battery powered amplifier, and the equalization filter. Two high pass filters were available for use with the General Radio Amplifier. Both filters were series m-derived with center T sections and had cut-off frequencies of 100 cps (Ref. 4) and 120 cps (George Kelk, Ltd., Toronto). All electrical connections were made with short cables (Fig. 5a).

2.4 Panel Vibration Transducer

The measurement of the panel transverse displacement was made with a Shattuck (Ref. 6) capacitance-type probe (Fig. 4). The sensing element (d_W = .125 inches) of the stationary probe acts as one plate of a two plate capacitor and the grounded vibrating panel acts as the other plate. Measurements of the mechanical response of capacitance probes of this same general type made by Shattuck (Ref. 6) and Koidan (Ref. 7) indicate flatness up to a frequency of 10,000 cps.

The same electronics as described previously in Section 2.3, with the exception of the equalization filter, were used to process the capacitance probe signal.

2.5 Electronic Correlator

A data processing system, the electronic correlator, was used to obtain the two point space-time correlation function of the wall pressure fluctuations and of the panel vibration separately (Fig. 5B).

Two signals to be correlated, $e_1(t)$ and $e_2(t)$, were recorded at constant tape speed (15 ips) with a conventional head assembly on an Ampex (type 351-2P) tape recorder whose two channels had identical characteristics.

When the two recorded signals were played back, a finite time delay, $\mathcal{T}$ (0 → 30 milliseconds), was inserted between them. The time delay was achieved by mechanically staggering the playback heads (Ref. 8) on a special assembly (Fig. 6). Provision was made to break contact between playback head and tape during the rev nd mode of operation in order to decrease head wear.

The two signals, $e_1(t + T)$ and $e_2(t)$, were then passed through idential low frequency amplifiers which extended the lower limit of the tape recorder frequency response from 50 cps down to 18 cps. A low frequency amplifier (George Kelk, Ltd., Toronto) was made up of cascaded R-C low pass filters with a transistor amplifier stage between each network.

The outputs from the low frequency amplifiers were passed through two identical Muirhead Pametrada (type D-489 E) wave analyzers only when limited portions of the frequency spectra were of interest. Otherwise the signals were passed through a switching box with manual selection of e_1 and e_1, or e_1 and e_2, or e_2 and e_2, as inputs to two identical high gain voltage amplifiers which brought up the levels of the signals to that required at the input of a Philbrick MU/DV analogue multiplier.

The multiplier output, $e_1 \cdot e_2$, or e_1^2, or e_2^2, was averaged by an active R-C integrator (Electronic Associates, Ltd., Toronto) whose averaging time, T, was 10 seconds and whose meter readout was $T\overline{e_1 e_2}$, or $T\overline{e_1^2}$, or $T\overline{e_2^2}$.

The correlation function was then

$$R = \frac{\overline{e_1(t+T) \cdot e_2(t)}}{\sqrt{\overline{e_1^2(t+T) \cdot e_2^2(t)}}} \qquad (2.5.1)$$

The system, whose frequency response extended from 18 cps to 10,000 cps (Fig. 7), accurately auto-correlated sine waves (Fig. 8). The constancy of tape speed was checked by monitoring stroboscopically and otherwise the capstan drive rpm under start-stop and steadystate conditions. High output Scotch magnetic tape (type 120A) was used throughout and the system overall signal-to-noise ratio was never less than 45 db.

A talk-in circuit was available for data identification in the record mode of operation.

3. MEASUREMENT PROCEDURES

3.1 Spectra

A three minute sample of a displacement signal was first recorded permanently on tape. The recorder output on playback was passed repeatedly through a Muirhead wave analyzer at different filter settings. The analyzer filters used were "1/3 octave", "narrow band", and "in tune high selectivity" with an equivalent rectangular passband, $\Delta f/f_0$, of 25.7%, 5.25%, and 1.25%. The analyzer output was averaged by a Flow Corporation random signal voltmeter (type TBM-2). Readout

4

of this instrument was taken after a minute of sampling. Overall displacement signals were also processed through the voltmeter.

For each displacement signal sample, the transducer location over and above the panel was noted as well as instrument gains.

3.2 Space-Time Correlations

A cartesian coordinate system was chosen to describe the observation points in the plane of the duct top wall. The positive x-axis was defined in the flow direction and the origin of the coordinates was at the intersection of the upstream panel edge and an edge parallel to the flow direction.

Two pinhole microphones were used in the measurement of the correlation of the wall pressure fluctuations. These microphones were placed in a steel and mahogany solid frame (Fig. 9) whose outside dimensions were equal to those of the panel frame. The microphone frame was then mounted in the cut-out portion of the duct at the panel station flush with the inner surface of the duct.

The frame had a series of equally spaced openings for microphone insertions. These openings formed a cruciform pattern in the frame, one line parallel to the flow direction and the other perpendicular to it with the cruciform center located at the panel station center. Small increments in the distance between pinholes were achieved by rotation of the microphones within frame openings. Larger increments were achieved by transferring one of the two microphones to ar'·ther frame opening. Holes not being used were plugged with steel dowels of the same dimensions as the microphones.

A sample of a microphone pressure signal at x', y', p(x',y',t'), was time correlated with a sample of the microphone pressure signal at x' + Δ x, y' + Δ y, p(x' + Δ x, y' + Δ y, t) to give

$$R_p = \frac{\overline{p(x'+\Delta x, y'+\Delta y, t'+\tau) \cdot p(x', y', t')}}{\sqrt{\overline{p^2(x'+\Delta x, y'+\Delta y, t'+\tau)} \cdot \overline{p^2(x', y', t')}}} \qquad (3.2.1)$$

The correlation was determined for various fixed microphone locations.

Two Shattuck displacement probes were used in the measurement of the correlation of the panel displacement. The probes were usually mounted at a height d < .1 inch above the test panel surface. Each probe was placed in a holder which was traversed by two circular rods. These two rods terminated in fixed supports located at the upstream and downstream edges of the panel frame when correlating in the flow direction, and at the opposite edges parallel to the flow direction when correlating

5

in the y-direction. Probe positioning was obtained by sliding its holder along the support rods. All components were held rigidly to each other and to the panel frame by multiple Allen screw connections.

A more elaborate traversing mechanism which allowed correlations to be carried out in any direction was also used.

The correlation of displacement signals from two panel observation points, was evaluated in a fashion similar to that for the pressure signals.

4. EXPERIMENTAL RESULTS

4.1 Duct Flow Velocity Profiles

Velocity profiles were measured along the duct depth, upstream and downstream of the panel station, in order to ascertain the fully developed nature of the turbulent flow (Fig. 10).

The velocity profiles in the 8 inch duct were similar when either the flexible panel or the rigid microphone frame was in position in the duct wall.

The velocity profiles in the 1 inch duct were similar when the rigid microphone frame was in position; however, with a thin panel and at the highest flow speed, the profiles were asymmetric about the duct centerline. This asymmetry in the one inch depth was concluded to be due to the panel deflecting inwards into the duct under the action of a static pressure differential across its thickness while the air duct was being operated.

Yaw of the pitot-static probe and its mount during the operation of the air duct was the cause of a slight but observable asymmetry in all velocity profiles.

The displacement thickness, δ^* , computed from the symmetric profiles according to the relation

$$\delta^* = \int_o^{D/2} \left(1 - u/U\right) dy \qquad (4.1.1)$$

was .434 inch for the 8 inch duct, and .054 inch for the 1 inch duct.

4.2 Space-Time Correlations of Wall Pressure Fluctuations

The wall pressure spectra (Ref. 4) measured in the 8 inch and the 1 inch ducts displayed a number of discrete peaks in the frequency range below 100 cps. The associated peak frequencies were observed to be

independent of the duct mean flow speed and the vibration response of a
microphone (mounted in its frame in the tunnel wall with its pinhole covered),
was determined to be over 40 db below the wall pressure fluctuations signal
level at all frequencies. The corresponding two-point space correlation
function measured in the flow direction had a constant value of . 6 for all
flow speeds and for all flow separations up to a test panel length (11 inches)
except at the smallest separation (.8 inch) where it increased.

On the basis of these observations it was concluded that the
low frequency pressure spectrum peaks were not associated with the wall
turbulence but rather with acoustic disturbances, presumably "organ pipe"
standing waves in view of the lengthy region of correlation. Accordingly
no frequencies below 100 cps were considered in the correlation measure-
ments by the use of identical high-pass filters.

The finite size of the pin-hole, . 040 inch diameter, in an
Altec Lansing microphone, put a limit on the latter's high frequency resolu-
tion. The pin-hole averaged the pressure over its area and at the high fre-
quencies (short wave lengths) the pressure was not uniformly distributed
over the sensing area, and above a certain limiting frequency the measured
output signal was progressively attenuated. This limiting frequency for the
present correlation measurements was estimated (Ref. 9) to be 6000 cps at
the high flow speeds and 1500 cps at the low flow speeds for about a 30%
attenuation of the measured pressure signals. It is to be noted that the ratio
of the pin-hole diameter to displacement thickness, d_m / δ^* , which should
be as small as possible for accurate high frequency resolution, was . 092
for the 8 inch duct and . 74 for the 1 inch duct. For comparison . 332 is the
lowest value of this ratio cited in the literature for turbulent boundary
layer measurements (Ref. 10).

The longitudinal two-point space-time correlation function,
$R_p (\Delta x, o, T)$, was measured at two flow speeds, 44. 5 fps and 170 fps, in the
8 inch duct and at two flow speeds, 84. 8 fps and 189 fps, in the 1 inch duct
at the panel station along the wall centerline in the flow direction (Fig. 11).

For each spacing, Δx , and duct flow speed, there was
an optimum time delay, T_{opt} , at which the correlation was a maximum.
The ratio, $\Delta x / T_{opt}$, was the effective average speed, U_c , at which the
pressure-producing eddies were convected downstream in the air duct
(Fig. 12A).

The decay of the locus of the correlation maxima was
approximated by the function exp $(-T/\Theta$), and Θ was interpreted as a
measure of the mean lifetime of a pressure-producing eddy (Fig. 13).

Because of the finite size of the microphones, the closest
possible separation between them was $\Delta x / \delta^*$ = 1. 84 in the 8 inch duct and
$\Delta x / \delta^*$ = 14. 82 in the 1 inch duct. Observation of the symmetry of the lines

7

of constant longitudinal correlation (Fig. 14) near the origin of the $\Delta x -\overline{U}_c \Upsilon$ plane, suggested the possibility of increasing the space correlation information given by $R_p(\Delta x, o, o)$ for very small separations by making use of the auto-correlation function, $R_p (o, o, U_c \Upsilon)$ (Fig. 15). A measure of the average longitudinal spatial extent of a pressure-eddy was given by

$$\ell_x = \int_o^\infty R_p(\Delta x, o, o) \, d(\Delta x) \tag{4.2.1}$$

The filtered longitudinal two-point space-time correlation function, $\left[f_o R_p(\Delta x, o, \Upsilon)\right]_{\Delta f}$, was measured in 1/3 octave bands whose equivalent rectangular frequency band was Δf, and whose center frequency was f_o at one flow speed, 170 fps, in the 8 inch duct and at two flow speeds, 84.8 fps and 189 fps, in the 1 inch duct at the panel station along the wall center-line in the flow direction.

A filtered correlation curve had the form of a damped "oscillation" with symmetry about a peak amplitude at an optimum time delay given by $\Delta x = U_c \Upsilon$ (Fig. 16A).

Now the theoretical correlation function for white noise passed through filters of vanishingly <u>narrow</u> band width (one cycle/second) is calculated to be of the form (Appendix D).

$$f_o R_p (\Delta x, o, \Upsilon) = f_o \overline{R}_p (\Delta x) \cos \left[2\pi f_o \Upsilon + \alpha(\Delta x, \Upsilon) \right] \tag{4.2.2}$$

For comparison, the auto-correlation function for white noise passed through flat filters of <u>finite</u> band width can be shown to be of the form (Appendix C)

$$R(\Upsilon) = \left[\sin(\pi\Upsilon\Delta f)/(\pi\Upsilon\Delta f) \right] \cos \left[\pi\Upsilon(f_{max} + f_{min}) \right] \tag{4.2.3}$$

where f_{max} and f_{min} are the upper and lower band cut-off frequencies,
$\Delta f = f_{max} - f_{min}$, $f_o = \dfrac{f_{max} + f_{min}}{2}$.

A correlation of these two results with the experimental observations suggests that the effect of finite band width was the amplitude modulation of the expected cosine correlation by sampling function such that the true amplitude of the correlation was given only at $\Upsilon_{opt} = \Delta x / U_c$ (Fig. 16A).

In other words:

$$[f_o R_p]_{\Delta f} / f_o R_p = \sin\left[\pi \Delta f (\tau - \Delta x/U_c)\right] / \left[\pi \Delta f (\tau - \Delta x/U_c)\right] \qquad (4.2.4)$$

Third octave band convection speeds were obtained at τ_{opt} as well as eddy lifetimes in much the same way outlined previously for the wide band correlations (Fig. 12B; 13). It is noted here that the 1/3 octave correlation amplitudes and convection speed ratios scaled reasonably with ($f_o \Delta x / U$) (Fig. 16B; Ref. 9).

At the highest frequency 1/3 octave bands the filtered correlation maxima fell very near to the zero. This was attributed to low signal-to-instrument noise ratio due to the pressure transducer's loss of high frequency response. The instrument noise in the two channels of the data processing system was uncorrelated and did not contribute to the covariance of the pressure signals but it did contribute to the rms signals in each channel leading to a reduction in the normalized covariance or correlation.

The lateral two-point space-time correlation function, $R_p(o,\Delta y,\tau)$, was measured at one flow speed, 170 fps, in the 8 inch duct and at two flow speeds, 84.8 fps and 189 fps, in the 1 inch duct at the panel station centerline transverse to the flow direction, (Fig. 17 and 18).

For each spacing, Δy , and duct flow speed the correlation was a maximum at zero time delay. The correlation function in the 8 inch duct at 170 fps had its first zero crossing for all Δy spacings at the same time delay.

A measure of the average lateral spatial extent of a pressure eddy was given by

$$\ell_y = \int_o^\infty R_p (o,\Delta y,o)\, d(\Delta y) \qquad (4.2.5)$$

The filtered lateral two-point space-time correlation function, $f_o R_p (o,\Delta y,o)$, was measured at one flow speed, 189 fps, in the 1 inch duct at the panel station center transverse to the flow direction (Fig. 19). The correlation maxima, $f_o \overline{R}_p$, all of which occurred at $\tau_{opt} = o$, fell to very low values at 1000 cps as compared to 5000 cps for the longitudinal correlation maxima.

The degree of homogeneity was determined (Fig. 20) by measuring $R_p (\Delta x,o,\tau)$ at two different observation points x, y and x', y and $R_p(o, \Delta y, \tau)$) at x, y and x, y'.

The following conclusions were reached on the basis of the correlation studies described. First, that a stochastic space pressure pattern was being convected downstream past the panel station. Second,

9

that the larger eddies of this pattern were travelling faster downstream than the smaller eddies. Third, that the longitudinal spatial extent of a mean pressure-eddy ($\ell_x \simeq .09$ inch) was of the order of one-quarter of the displacement thickness, and the lateral spatial extent of a mean pressure-eddy ($\ell_y \simeq .7$ inch) was of the order of twice the displacement thickness. Fourth, that the smaller eddies lost their identity by decay much faster than the larger eddies. Fifth, that the decay of the eddies was much more rapid in the flow direction than in the direction transverse to the flow. Sixth, that the pressure pattern was homogeneous in the flow direction and transverse to the flow direction in the vicinity of the duct center-line. Seventh, that the turbulence process was stationary in the statistical sense.

4.3 Spectra of Panel Vibration

The frequency spectrum of the transverse panel surface motion in response to turbulent wall pressure fluctuation was measured at the panel center for a .008 inch panel at a flow speed of 170 fps in the 8 inch duct and for a .002 inch panel at flow speeds of 84.8 fps and 189 fps in the 1 inch duct (Fig. 21). The bulk of the response was in the band, 100 cps to 1000 cps, and the largest values of the spectral density in this band were located in the sub-band, 100 cps to 500 cps.

A more detailed spectrum of the .008 inch panel motion was determined with the use of narrow band, and in-tune high selectivity filters (Fig. 22). All panel modes with model lines parallel to the panel edges or which the difference between m and n was an even number had loop lines passing through the panel center and contributed to local motion. An attempt was made to associate the frequencies of the major spectral peaks with the theoretically allowable modal frequencies (Appendix E) for a thin, undamped, clamped edge panel (Ref. 11). The approximate frequency relation used was obtained by an energy method based on Rayleigh's principle with the use of characteristic beam functions. Successful identification of a large numer of the observed peaks was achieved.

On the negative side, for some theoretically possible modes at the observation point, no displacement spectral spectral peaks were detected and vice versa (Fig. 22, Appendix E). This discrepancy was thought to be associated mainly with the effects of panel support. The areas at the panel affected by clamping-bending though small were different in magnitude at each lateral edge. Thus the geometrically square panel was efectively rectangular and off-centered and a transducer located at the geometric panel center would pick up some additional contributions and drop some others - this effect was most apparent at higher frequencies (higher order modes) where a large number of modes were crowded in between two allowable ones.

Half order modes were not anticipated in view of the fact that the panels were not exactly square and the modal frequency at which the capacitance type probe would attenuate the panel displacement by 10% because of its finite size, was estimated to be over 12,000 cps.

The measured rms displacement for a .008 inch panel at a flow speed of 170 fps in the 8 inch duct with the exclusion of frequencies below 100 cps is given in the following table:

$\sqrt{\overline{w^2}}$ 10^3 x inch	x' inch	y' inch
.14	5.5	5.5
.09	2.375	5.5
.01	.375	5.5
.09	2.0	3.0

4.4 Space-Time Correlation of Panel Vibration

The longitudinal two-point space-time correlation of the panel transverse displacement (vibration) with the exclusion of frequencies below 100 cps was measured for a .008 inch panel at 170 fps flow speed in the 8 inch duct and for a .002 inch panel at flow speeds of 189 fps and 84.8 fps in the 1 inch duct (Fig. 23, 24 and 25). The correlation curves (Fig. 29) had the form of damped "oscillations" with more rapid decay in space than in time. The correlation was highest for small separations (Δ x) and small delays (T) falling to a fairly constant range of magnitude -.30 < $R_w(\Delta x, o, T)$ < .20 at large separations and time delays. The major features - for example, the first valley of the correlation pattern was swept forward at an angle with the time delay axis, and in particular where the time delay was multiplied by the appropriate average convection speed of a pressure eddy, this angle was significantly close to 45 degrees (Fig. 23). It is to be noted here, first that the correlation function for a running wave, $\sin [k(\Delta x - U_c T)]$, is a running wave, $\cos [k(\Delta x - U_c T)]$, with the corresponding correlation pattern swept forward at an angle of 45 degrees with the $U_c T$ axis in the $\Delta x - U_c T$ plane and that, second, the correlation function of a standing wave, $\sin (k \Delta x) \cdot \cos (\omega T)$, is a standing wave, $\cos (\omega T)$, with its corresponding correlation pattern unswept and parallel to the Δ x axis in the $\Delta x - U_c \widetilde{T}$ plane.

The lateral two-point space-time correlation of the panel transverse displacement with the exclusion of frequencies below 100 cps was measured for a .008 inch panel at 170 fps flow speed and for a .002 inch panel at flow speeds of 189 fps and 84.8 in the 1 inch duct (Fig. 26,

27 and 28). The correlation curves had the form of damped "oscillations" with maxima at zero time-delay for every space separation, (Δ y), and such that the magnitude of these maxima fell with increasing separation. The correlation patterns were unswept over the spatial separation range examined, lying parallel to the Δ y-axis in the $\Delta y - \bar{U}_c \tau$ plane. This trend was not so well established for the 8 inch duct tests.

The filtered longitudinal and lateral two-point space-time correlation of the panel surface transverse motion in 1/3 octaves was measured for the minimum separation, .85 inch, for a .002 inch panel at a flow speed of 189 fps in the 1 inch duct (Fig. 30 and 31). The correlation curves had the form of unswept damped "oscillations," having their maxima at zero time delay.

The repeatability of the correlation measurements on the same panel for two different displacement signal samples (Fig. 32A) was good as was the repeatability of the correlation measurements on two different .008 inch panels (Fig. 32B). The repeatability tests on three different .002 inch panels showed a fair amount of data (Fig. 32C), although the nature of the correlation was the same. This data scatter was associated with small but visible non-uniformities (wrinkles) in the panel surface which were in part introduced at the manufacturing stage and in part introduced during the procedure of mounting the panel in its frame.

A qualitative investigation of the bending and clamping of the panel edge surfaces was first carried out by observing the motion of sand particles sprinkled around the edges of the panel. The motion of the sand particles was small up to a distance of 1 inch from the edges whose surfaces had been bent prior to clamping and up to a distance of no more than .375 inch from the other two edges. A quantitative investigation using a correlation technique was then carried out; this method consisted of measuring the space correlation function, $R_w(\Delta x, o, o)$, for a fixed Δ x at different longitudinal locations along the panel center-line. The space correlation (Fig. 33A) showed that for all test panels but one an inadequate correlation existed between any point located up to a distance of two inches from the edge and the rest of the panel. This effect shows up clearly in the two-point space-time correlation near the edge (Fig. 33B). The good correlation achieved for one of the panels tested was concluded to be associated with a chance perfect bend at that edge during the mounting procedure. All correlation measurements were carried out within an effective panel area of 7 square inches.

A check of the fundamental modal frequency for a typical test panel was made by exciting the panel with an electromagnet (Ref. 4), feeding the filtered panel displacement response to the y-input of an oscilloscope which had the voltage signal to the electromagnet feed to its x-input, and observing the Lissajous figure for the fundamental which was at 25 cps. The theoretical estimate for the fundamental (Ref. 11) was 23 cps.

Because of the uncertainty about the characteristics of the wall pressure field below 100 cps, all correlation measurements excluded these same frequencies.

At the highest flow speeds in the 1 inch duct, the static pressure differential across the thin .002 inch panel depressed the panel surface inwards into the duct (Fig. 10; page 6). This effect did not change the basic nature of the turbulence because the displacement correlation for a thin panel exhibited the same trends of a .008 inch panel in the 8 inch duct.

5. THEORETICAL RESULTS

5.1 Mathematical Formulation

5.1.1 Statement of the Problem

A number of workers ̇ave dealt, in varying degrees of idealization, with the problem of the excitation of plate vibratory motion by turbulent flow pressure fluctuation and in some of the cases with the concomitant problem of plate sound radiation (Ref. 2, 3, 12, 13, 14, 15, 16 and 17). The work of Dyer (Ref. 2) seemed best suited to numerical computations for physical circumstances approximating the present experimental arrangement. The following is a resume of the relevant parts of his theory and is presented here for completeness.

The problem considered was the determination of the response of a finite plate excited by a pressure field whose covariance was given by

$$\overline{p(x,y,t)\,p(x',y',t')} = \overline{p^2}\; A\; \delta(\Delta x - U_c \tau)\; \delta(\Delta y)\; exp\left(-|\tau|/\theta\right) \qquad (5.1.1)$$

The particular form of the panel response sought was the displacement covariance given by

$$\overline{w(x,y,t)\,w(x',y',t')} = \int_{-\infty}^{t} dt_o \int_{-\infty}^{t'} dt_o' \int_S dS_o \int_S dS_o'\; g(x,y,t\,|\,x_o,y_o,t_o)$$
$$\times g(x',y',t'\,|\,x_o',y_o',t_o')\; \overline{p(x_o,y_o,t_o)\,p(x_o',y_o',t_o')} \qquad (5.1.2)$$

The plate impulse response, $g(x,y,t\,|\,x_o,y_o,t_o)$, was evaluated in terms of the eigenfunctions or orthonormal modes of oscillation of the plate which were of the form

$$W_{mn}(x,y,t) \propto \phi_{mn}(x,y)\; exp\left[-(\beta_{mn} + i\,\omega_{mn})\,t\right] \qquad (5.1.3)$$

and which satisfied the plate equation

13

$$B(1-i\eta)\nabla^4 W_{mn} + M\frac{\partial^2 W_{mn}}{\partial t^2} + \beta_o\frac{\partial W_{mn}}{\partial t} = 0 \qquad (5.1.4)$$

giving the eigenfunction equation

$$\nabla^4\phi_{mn} - \Gamma_{mn}^4\phi_{mn} = 0 \qquad (5.1.5)$$

The impulse response function for low damping was found to be

$$g(x,y,t|x_o,y_o,t_o) \approx \sum_m\sum_n \frac{\phi_{mn}(x,y)\,\phi_{mn}(x_o,y_o)}{\omega_{mn}} \exp\left[-a_{mn}(t-t_o)\right] \\ \times \sin\left[\omega_{mn}(t-t_o)\right] \qquad (5.1.6)$$

and the expressions derived for the modal damping and frequency were

$$a_{mn} = \frac{\beta_o}{2M} + \frac{\eta\,\omega_{mn}}{2} \qquad ; \qquad \omega_{mn}^2 = \frac{B}{M}\Gamma_{mn}^4 \qquad (5.1.7)$$

The mode shape which satisfied the eigenfunction equation subject to the plate boundary conditions for simple support at the edges was

$$\phi_{mn}(x,y) \propto \sin\left[\left(\frac{m\pi}{L_x}\right)x\right]\sin\left[\left(\frac{n\pi}{L_y}\right)y\right] \qquad (5.1.8)$$

with the eigenvalues given by

$$\Gamma_{mn}^2 = \left(\frac{m\pi}{L_x}\right)^2 + \left(\frac{n\pi}{L_y}\right)^2 \qquad (5.1.9)$$

The particular form of the displacement covariance was

$$\overline{w(x,y,t)\,w(x',y',t')} = \sum_m\sum_n\sum_p\sum_q \frac{A\,\beta^2\,\phi_{mn}(x,y)\,\phi_{pq}(x',y')}{\omega_{mn}\,\omega_{pq}\,M^2} \\ \times \int_{-\infty}^{t}dt_o\int_{-\infty}^{t'}dt_o'\int_S dS_o\int_S dS_o'\;\phi_{mn}(x_o,y_o)\,\phi_{pq}(x_o',y_o') \qquad (5.1.10) \\ \times \exp\left[-a_{mn}(t-t_o) - a_{pq}(t'-t_o') - (|t_o - t_o'|/\theta)\right]\sin\left[\omega_{mn}(t-t_o)\right] \\ \times \sin\left[\omega_{pq}(t'-t_o')\right]\,\delta\left[(x_o-x_o') - U_c(t_o-t_o')\right]\,\delta(y_o-y_o')$$

Dyer evaluated the limiting case of the displacement covariance for zero time delay and spatial separation, subject to the condition $U_c\theta \ll L_x$.

The displacement covariance function as well as the corresponding power spectral density function were evaluated analytically as part of the present investigation and the results are given in Appendices A and B.

14

5.1.2 Discussion of the Assumptions

The idealized pressure field covariance given by Eq. 5.1.1 was used for mathematical convenience. This field (Fig. 34) was thought of as the limiting case of an exponential covariance

$$\lim_{\ell_x, \ell_y \to 0} \exp\left[-(|\Delta x - U_c \tau|/\ell_x)\right] \exp\left[-(|\Delta y|/\ell_y)\right] \exp\left[-(|\tau|/\theta)\right]$$

$$= 4\,\ell_x \ell_y\, \delta(\Delta x - U_c \tau)\, \delta(\Delta y)\, \exp\left[-(|\tau|/\theta)\right] \qquad (5.1.11)$$

The wave number spectral density function for the exponential covariance indicated that a plate excited by a force field with such a covariance would be subjected to a point source loading instead of a distributed loading as $\ell_x, \ell_y \to 0$. The frequency spectrum of the delta function covariance was flat as well and the time delay exponential envelope adequately represented the experimentally observed pressure eddy decay.

The back reaction of the panel on the tur .lent flow was assumed to be negligible. This seemed plausible because the rms displacement was very small ($\delta^*/\sqrt{w^2} \approx 2000$ and $\ell_x/\sqrt{w^2} \approx 500$). Moreover estimates of the back reaction made by Dr. H. S. Ribner (unpublished) in connection with reference 2 indicated such a conclusion.

For the highest order mode of significance, the plate was effectively subdivided into platelets of dimension $L_x/m \approx 1$, giving a ratio of $[h/(L_x/m)] \sim .008$. This excluded any appreciable contribution to the plate motion from shear deflection and rotary inertia (Ref. 19).

The use of simply-supp rted-plate eigenfunctions instead of those for a clamped plate, lead to a consistent underestimate of the modal frequencies—45% at the fundamental, 23% at 100 cps, 15.5% at 200 cps, and 7% at 1000 cps.

The requirement for low damping was met in practice. The experimentally measured damping ratio, ξ, (Ref. 4) went as $1/f^2$ from the fundamental to about 110 cps and as $1/f^{2/3}$ from then on. It was noted significantly that the modal damping, $a_{mn} = \xi\, \omega_{mn}$, (Fig. 35), increased above 110 cps and at 1000 cps had the same value as at 50 cps. Over the range of frequencies considered (100 cps and above), the structural damping, which was low, was thought to dominate over the acoustic damping.

When a driving pressure wave matched or nearly matched a possible plate flexural wave in speed and in wave length (note - the plate is a dispersive medium), a condition similar to resonance, called "coincidence", was met (Fig. 36). Dyer found that this condition was given by

$$\alpha_m = (m\pi/L_x)U_c = k_x U_c = \omega_{mn} \qquad (5.1.12)$$

and that the mean square plate displacement, $\sum_m \sum_n \left[\overline{w(x',y',t')^2} \right]_{m,n}$, was a maximum at coincidence. This result was derived earlier by Ribner (Ref. 2) in the consideration of the motion of infinite plates. For a given convection speed, a definite range of modal frequencies existed for which the coincidence condition could be met, (Fig. 37).

5.2 Result of Digital Computations

A number of functions derived from the theoretical covariance described in Section 5.1 were evaluated on an IBM 7090 Digital Computer.

The displacement power spectral density, $S_W(f)$, was evaluated for an .008" x 11" x 11" steel plate at the panel center (Fig. 38).

All spectra had sharp peaks at the modal frequencies (Appendix E) except for those modes that had a nodal line passing through the observation point. Some modes, the 2-4 and the 4-2, never contributed to the displacement along the center-line.

The panel damping was low enough that the elimination of some modes below a certain critical frequency, f_{co} , did not significantly change the remainder of the spectrum. For example, the elimination of modes below 100 cps in the calculation of the spectrum at the panel center (Fig. 38 and 39) changed the displacement at the modal frequency 113.4 cps, by -.18% and the displacement at the modal frequency, 466.2 cps by .0005%. The theoretical coincidence frequencies given by equation (5.1.12) matched or fell close to the allowable modal frequencies, and the coincidence frequency range (Fig. 37) matched the displacement spectrum bandwidth. Statistical modal intercoupling was found to be low and at the panel center it was non-existent. The coupling term which was proportional to

$$ \sin \left[(m\pi/L_x)x \right] \sin \left[(p\pi/L_x)x \right] \sin^2 \left[(n\pi/L_y)y \right] \left[m/(p^2-m^2) \right] \qquad (5.2.1)$$

had a non-zero value only when (p-m) was odd. At the panel center, this requirement made $\sin \left[(m\pi/L_x)x \right] \sin \left[(p\pi/L_x)x \right]$ equal to zero. The theoretical spectrum of the panel displacement response was very small above 1000 cycles per second. Modes resonant above 1000 cycles were found to make negligible change in the calculated spectrum below 1000 cycles: accordingly, these modes were eliminated from the calculations along with those (see above) below 100 cycles.

$\sqrt{\overline{w^2(x',y',t')}}$ The theoretical (or predicted) rms displacement, , was evaluated and is given below

x' inch	y' inch	M	N	P	f_{co} cps	$\sqrt{\overline{w^2}}$ $10^3 \times$ inch	x' inch	y' inch	M	N	P	f_{co} cp	$\sqrt{\overline{w^2}}$ $10^3 \times$ inch
5.5	5.5	11	11	11	0	1.832	2	5.5	11	11	11	0	*1.422
5.5	5.5	11	11	11	100	..620	2	5.5	11	11	11	170	.4257
5.5	5.5	11	11	11	120	.480	2	5.5	15	15	15	170	.4264
5.5	5.5	11	11	11	170	.387	2	5.5	15	15	15	170	*.4190

* with statistical modal intercoupling

The rms displacement was greatest at the panel center when the first few allowable modes were included. However, when the contribution of modes below 170 cps was excluded, the displacement was greater at 2 inches from the upstream edge than at the panel center. A geometric analysis of the mode shapes showed that a far greater number modes were contributing to the displacement at 2 inches above 170 cps than at the panel center because fewer nodal lines were going through the off-center location.

The correlation function defined by the relation

$$R_w (\Delta x, \Delta y, \tau) = \frac{\overline{w(x,y,t) \, w(x',y',t')}}{\sqrt{\overline{w(x,y,t)^2} \; \overline{w(x',y',t')^2}}}$$ (5.2.2)

was evaluated along the panel center-line in the flow direction with the fixed point (x') at 2 inches from the upstream edge and at the panel center for various modal cut-off frequencies (Fig. 41). The correlation curves had the form of damped "oscillations" for small separations (Δx) and time delays (τ). As the separation was increased, the oscillations were less damped. At the largest separation the correlation was lower but with the "oscillations" being more damped at smaller rather than at large time delays. The whole correlation pattern was swept forward at an angle with the time-delay axis and in particular when the time-delay was multiplied by the average convection speed of a pressure eddy, this angle was significantly 45 degrees (Fig. 40). An increase of the total number of allowable plate modes used in the computation as well as the allowance for statistical modal inter-coupling, produced no changes in the correlation. The period of a correlation curve was heavily dependent on the frequency of the largest amplitude spectral. Lowering the modal cut-off frequency, f_{co}, had the effect of expanding the whole correlation pattern in time delay (Fig. 41).

6. CONCLUSIONS

The nature of the fluctuating wall pressure in a fully developed turbulent flow duct (which is of interest in its own right) was investigated and its most important features - eddy convection, decay and length scales -- were studied and incorporated in an idealized analytical representation.

The main features of the observed panel motion in response to the turbulence were accounted for by a development of Dyer's theoretical model. The similarity between the measured and calculated spectra suggested, first, the importance of the "coincidence" effect in the increased panel response when a "coincidence" frequency matched or nearly matched a panel modal frequency as well as in the definition of the panel response bandwidth: (only a finite number of modes were necessary to describe the panel motion); second, the important effects of low panel damping on the peakiness of the spectra as well as in the abatement of the high frequency response within the bandwidth defined by the "coincidence" effect (for example, for an .008 inch panel, the modal damping at 800 cps was about twice its value at 100 cps). The calculated panel displacements though consistently higher in value were of the same order of magnitude as the measured displacements. This trend was thought to be associated with the fact that a point source loading of the panel by the turbulence was assumed instead of the distributed one that it is (this imlies a failure of the theoretical response to fall off fast enough with diminishing ripple wave length). The strong resemblance between the measured and calculated patterns of longitudinal space-time correlation - the pronounced ridges and valleys swept forward at 45 degrees - was interpreted as indicating that the response of the panels had a strong running wave content, as predicted by Ribner.

The present investigation was thought to bring to light three main results regarding the panel motion. First, that when the life span of an eddy was small compared to the physical size of the panel ($U_c \theta \ll L_x$), the latter responded primarily in running waves which decayed as quickly as the pressure waves; a part of the response consisted of fluctuating, irregular waves which resulted from the reflection processes of the running waves near the panel edges. This has the significance that the decay process of the running waves is essential to the mechanism of panel sound radiation in subsonic flow [in subsonic flow, the sound generated by a constant amplitude panel running wave carries no energy (Ref. 2)]. Third, that a concrete affirmation was obtained of the power of a classical analytical formulation of the panel motion which made use of a superposition of normal modes and a correlation format (due to Dyer) in describing the primary running wave nature of the motion as well as its secondary irregular wave content and in distinguishing between these two types of motion.

18

REFERENCES

1. Bishop, D. E.   Cruise Flight Noise Levels in a Turbojet Transport Airplane. Noise Control, Vol. 7, No. 2, March-April, 1962.

2. Ribner, H. S.   Boundary Layer Induced Noise in the Interior of Aircraft. UTIA Report No. 37, April 1956.

3. Dyer, I.   Sound Radiation into a Closed Space from Boundary Layer Turbulence. BBN Report No. 602, Dec. 1958.

4. Ludwig, G. R.   An Experimental Investigation of the Sound Generated by Thin Panels Excited by Turbulent Flow (Boundary Layer Noise). UTIA Report No. 87, Nov. 1962.

5. Maestrello, L.   UTIA Air Duct Facility for Investigation of Vibration Noise Induced by Turbulent Flow Past a Panel (Boundary Layer Noise). UTIA Tech. Note No. 20, April 1956.

6. Shattuck, R. D.   Capacitance-Type Displacement Probe. Jour. Acous. Soc. Amer., Vol. 31, No. 10, Oct. 1959.

7. Koidan, W. et al   Absolute Calibration of a Capacitance-Type Vibration Pickup. Tech. News Bull., Nat. Bur. of Standards, Vol. 42, No. 1, January 1958

8. Lawrence, J. C. et al   Special Electronic Data for the Analysis of Statistical Data. Proceedings of the IRE, Vol. 47, No. 5, May 1959.

9. Corcos, G. M.   Pressure Fluctuations in Shear Flows. Univ. of California, Inst. of Eng. Research, Series No. 183, Issue No. 12, July 1962.

10. Willmarth, W. W. Wooldridge, C. E.   Measurements of the Fluctuating Pressure at the Wall Beneath a Thick Turbulent Boundary Layer. The Univ. of Michigan, College of Eng., Tech. Report, April 1962.

11. Warburton, G. B.   Vibration of Rectangular Plates. Proc. Inst. Mech. Eng., Vol. 188, No. 12, 1954.

12. Corcos, G. M.
    Liepman, H. W.

On the Transmission Through a Fuselage Wall of a Boundary Layer Noise. Rep. No. S. M. - 19570, Douglas Aircraft Company, Santa Monica Div., Dec. 1955.

13. Kraichnan, R. H.

Noise Transmission from Boundary Layer Pressure Fluctuations. Jour. Acous. Soc. Amer., Vol. 29, No. 1, Jan. 1957.

14. Powell, A.

On the Fatigue Failure of Structures Due to Vibrations Excited by Random Pressure Fields. Aeronautical Research Council No. 17925, 1955.

15. Lyon, R.H.

Response of Strings to Random Noise Fields. Jour. Acous. Soc. Amer., Vol. 28, p. 391-398, 1956.

16. Tack, D. H.
    Lambert, R. F.

Response of Bars and Plates to Boundary Layer Turbulence. Journal of the Aerospace Sciences, March, 1962.

17. Eringen, A. C.

Response of Beams and Plates to Random Loads. Jour. Appl. Mechanics, Vol. 24, p. 46-52, 1957.

18. Davenport, W. B.
    Root, W. L.

Random Signals and Noise. McGraw-Hill Book Co., Inc., New York.

19. Timoshenko, S.

Vibration Problems in Engineering. D. Van Nostrand Co., Inc., New York.

20. Harrison, M.

Pressure Fluctuations on the Wall Adjunct to a Turbulent Boundary Layer. David Taylor Model Basin, Rep. 1260, Dec. 1958.

APPENDIX A

Results of the Evaluation of the Integrals of the Displacement Covariance

A typical term of the displacement covariance summation (page 14, equation 5.1.10) was

$$\left[\overline{w(x,y,t)\,w(x',y',t')}\right]_{mn\,pq} = \frac{A\,\bar{p}^2\,\phi_{mn}(x,y)\,\phi_{pq}(x',y')}{\omega_{mn}\,\omega_{pq}\,M^2} \int_{-\infty}^{t} dt_o \int_{-\infty}^{t'} dt_o' \int_{0}^{L_x} dx_o \int_{0}^{L_y} dy_o \int_{0}^{L_x} dx_o' \int_{0}^{L_y} dy_o'$$

$$\times \phi_{mn}(x_o,y_o)\,\phi_{pq}(x_o',y_o')\,\exp\left[-a_{mn}(t-t_o) - a_{pq}(t'-t_o') - |t_o - t_o'|/\theta\right] \sin\left[\omega_{mn}(t-t_o)\right] \sin\left[\omega_{pq}(t'-t_o')\right]$$

$$\times \delta\left[(x_o - x_o') - U_c(t_o - t_o')\right]\,\delta(y_o - y_o') \tag{A.1}$$

The evaluation of the space integrals gave

$$\left[\overline{w(x,y,t)\,w(x',y',t')}\right]_{mn\,pq} = \left[\overline{w(x,y,t)\,w(x',y',t')}\right]_{mn} + \left[\overline{w(x,y,t)\,w(x',y',t')}\right]_{mpn} \tag{A.2}$$

where

$$\left[\overline{w(x,y,t)\,w(x',y',t')}\right]_{mn} = \frac{A\,\bar{p}^2\,\phi_{mn}(x,y)\,\phi_{mn}(x',y')}{\omega_{mn}^2\,M^2}\,I_{mn}(t-t') \tag{A.3}$$

$$\left[\overline{w(x,y,t)\,w(x',y',t')}\right]_{mpn} = \begin{cases} \dfrac{A\,\bar{p}^2\,\phi_{mn}(x,y)\,\phi_{pn}(x',y)}{\pi\,\omega_{mn}\,\omega_{pn}\,M^2}\,\dfrac{m}{p^2 - m^2}\,I_{mpn}(t-t') & m-p\ \text{odd} \\ 0 & m-p\ \text{even} \end{cases} \tag{A.4}$$

and

$$I_{mn}(t-t') = \int_{-\infty}^{t} dt_o \int_{-\infty}^{t'} dt_o'\,\exp\left\{-a_{mn}\left[(t-t_o) + (t'-t_o')\right] - |t_o - t_o'|/\theta\right\}\cos\left[\alpha_m(t_o-t_o')\right]$$

$$\times \sin\left[\omega_{mn}(t-t_o)\right] \sin\left[\omega_{mn}(t'-t_o')\right] \tag{A.5}$$

$$I_{mpn}(t-t') = \int_{-\infty}^{t} dt_o \int_{-\infty}^{t'} dt_o'\,\exp\left[-a_{mn}(t-t_o) - a_{pn}(t'-t_o') - |t_o - t_o'|/\theta\right]$$

$$\times \sin\left[\alpha_p(t_o-t_o')\right] \sin\left[\omega_{mn}(t-t_o)\right] \sin\left[\omega_{pn}(t'-t_o')\right] \tag{A.6}$$

The evaluation of the time integrals (with proper accounting of the absolute magnitude signs) gave

$$8\,I_{mn}(T) = \exp\left(-a_{mn}T\right)\left[W\cos(\omega_{mn}T) + X\sin(\omega_{mn}T)\right]$$

$$+ \exp\left(-T/\theta\right)\left[Y\cos(\alpha_m T) + Z\sin(\alpha_m T)\right] \tag{A.7}$$

21

where

$$W = (1/A)(1/B) \left[EC(A+B) + A(AB/E - AD/G) + B(AA/D - AC/F) \right]$$
$$- C(EA + BA/D + BB/E - BC/F - BD/G)$$

$$X = (1/A)(1/B) \left[A(CB/E + CD/G) - B(CA/D + CC/F) \right] - C(EB - DA/D$$
$$+ DB/E - DC/F + DD/G)$$

$$Y = (1/A)(1/B) \left[-A(AB/E + AD/G - B(AA/D + AC/F) \right] - C(-BA/D - BB/E$$
$$- BC/F - BD/G)$$

$$Z = (1/A)(1/B) \left[A(CB/E + CD/G) + B(CA/D + CC/F) \right] - C(DA/D + DB/E$$
$$+ DC/F + DD/G) \tag{A.8}$$

and

$$A = \left[1/\theta^2 + (\alpha_m - \omega_{mn})^2 \right] \quad ; \quad B = \left[1/\theta^2 + (\alpha_m + \omega_{mn})^2 \right] \quad ; \quad C = 1/(1/\theta^2 + \alpha_m^2)$$

$$D = \left[(-a_{mn} + 1/\theta)^2 + (\alpha_m - \omega_{mn})^2 \right] \quad ; \quad E = \left[(-a_{mn} + 1/\theta)^2 + (\alpha_m + \omega_{mn})^2 \right]$$

$$F = \left[(a_{mn} + 1/\theta)^2 + (\alpha_m - \omega_{mn})^2 \right] \quad ; \quad G = \left[(a_{mn} + 1/\theta)^2 + (\alpha_m + \omega_{mn})^2 \right]$$

$$AA = \left[1/\theta(-a_{mn} + 1/\theta) - (\alpha_m - \omega_{mn})^2 \right] \quad ; \quad AB = \left[1/\theta(-a_{mn} + 1/\theta) - (\alpha_m + \omega_{mn})^2 \right]$$

$$AC = \left[1/\theta(a_{mn} + 1/\theta) - (c_{,m} - \omega_{mn})^2 \right] \quad ; \quad AD = \left[1/\theta(a_{mn} + 1/\theta) - (\alpha_m + \omega_{mn})^2 \right]$$

$$BA = \left[1/\theta(-a_{mn} + 1/\theta) - \alpha_m(\alpha_m - \omega_{mn}) \right] \quad ; \quad BB = \left[1/\theta(-a_{mn} + 1/\theta) - \alpha_m(\alpha_m - \omega_{mn}) \right]$$

$$BC = \left[1/\theta(a_{mn} + 1/\theta) - \alpha_m(\alpha_m - \omega_{mn}) \right] \quad ; \quad BD = \left[1/\theta(a_{mn} + 1/\theta) - \alpha_m(\alpha_m + \omega_{mn}) \right]$$

$$CA = \left[(-a_{mn} + 1/\theta) + 1/\theta \right] (\alpha_m - \omega_{mn}) \quad ; \quad CB = \left[(-a_{mn} + 1/\theta) + 1/\theta \right] (\alpha_m + \omega_{mn})$$

$$CC = \left[(a_{mn} + 1/\theta) + 1/\theta \right] (\alpha_m - \omega_{mn}) \quad ; \quad CD = \left[(a_{mn} + 1/\theta) + 1/\theta \right] (\alpha_m + \omega_{mn})$$

$$DA = \left[\alpha_m \left(-a_{mn} + 1/\theta\right) + 1/\theta \left(\alpha_m - \omega_{mn}\right)\right] \quad ; \quad DB = \left[\alpha_m \left(-a_{mn} + 1/\theta\right) + 1/\theta \left(\alpha_m + \omega_{mn}\right)\right]$$

$$DC = \left[\alpha_m \left(a_{mn} + 1/\theta\right) + 1/\theta \left(\alpha_m - \omega_{mn}\right)\right] \quad ; \quad DD = \left[\alpha_m \left(a_{mn} + 1/\theta\right) + 1/\theta \left(\alpha_m + \omega_{mn}\right)\right]$$

$$EA = 4 \left(a_{mn}/\theta\right)\left(a_{mn}^2 + \omega_{mn}^2\right) \quad ; \quad EB = 4 \left(\omega_{mn}/\theta\right)\left(a_{mn}^2 + \omega_{mn}^2\right)$$

$$EC = 2/a_{mn}\theta \tag{A.9}$$

and

$$8\, I_{mpn} = \exp(-a_{mn}\Upsilon) \left[I \cos(\omega_{mn}\Upsilon) + J \sin(\omega_{mn}\Upsilon)\right]$$
$$+ \exp(-\Upsilon/\theta) \left[K \cos(\alpha_p \Upsilon) + L \sin(\alpha_p \Upsilon)\right] \tag{A.10}$$

where

$$I = (OA)(BET_1) + (OB)(BET_2) + (OD)(BET_3) + (OF)(BET_4) + (OG)(BET_5 + BET_6)$$
$$+ (OH)(BET_7 + BET_8) + (OI)(BET_9 + BET_{10})$$

$$J = (OG)(BET_1 + BET_2) + (OH)(BET_{11}) + (OL)(BET_{12}) - (OA)(BET_5)$$
$$- (OB)(BET_6) - (OD)(BET_7 + BET_9) + (OE)(BET_8 + BET_{10})$$

$$K = (OD)(ZET_1) + (OF)(ZET_2) + (ON)(ZET_3) + (OO)(ZET_4) + (OQ)(ZET_5 + ZET_6)$$
$$+ (OI)(ZET_7 + ZET_8)$$

$$L = -(OI)(ZET_1 + ZET_2) + (OQ)(ZET_3 + ZET_4) + (OD)(ZET_7) + (OF)(ZET_8)$$
$$- (ON)(ZET_5) - (OO)(ZET_6) \tag{A.11}$$

and

$$BET_1 = (OL/D_2)(1/E_1 - 1/D_1) + (OM/D_2)(1/D_1' - 1/E_1')$$

$$BET_2 = (OL|D_2)(1|G_1 - 1|F_1) + (OM/F_2)(1|F_1' - 1|G_1')$$

$$BET_3 = (OL|D_3)(1/D_1 - 1|G_1) + (OM/D_3')(1|G_1' - 1|D_1')$$

$$BET_4 = (OL|E_2)(1|E_1 - 1|F_1) + (OM|E_3')(1|F_1' - 1|E_1')$$

$$BET_5 = (OC/D_2)(1|D_1' - 1|D_1) + (OE/D_2)(1|E_1' - 1|E_1)$$

$$BET_6 = (OJ/F_2)(1|F_1 - 1|F_1') + (OK|F_2)(1|G_1 - 1|G_1')$$

$$BET_7 = (1|D_3)(OC/D_1 - OK/G_1) \quad ; \quad BET_8 = (1|E_3)(OE/E_1 - OJ/F_1)$$

$$BET_9 = (1|D_3')(OK|G_1' - OC/D_1') \quad ; \quad BET_{10} = (1|E_3')(OJ/F_1' - OE/E_1')$$

$$BET_{11} = (OL|D_3)(1|D_1 - 1|G_1) + (OL|E_2)(1|F_1 - 1|E_1)$$

$$BET_{12} = (OM|D_3')(1|G_1' - 1|D_1') + (OM|E_3')(1|E_1' - 1|F_1') \qquad (A.12)$$

$$ZET_1 = (OM|D_3')(1|D_1' - 1|G_1') \quad ; \quad ZET_2 = (OM|E_3')(1|E_1' - 1|F_1')$$

$$ZET_3 = (OM|D_2')(1|D_1' - 1|F_1) \quad ; \quad ZET_4 = (OM|E_2')(1|E_1' - 1|G_1')$$

$$ZET_5 = (1|D_2')(OJ/F_1' - OC/D_1') \quad ; \quad ZET_6 = (1|E_1')(OK/G_1' - OE/E_1')$$

$$ZET_7 = (1|D_3')(OC/D_1' - OK/G_1') \quad ; \quad ZET_8 = (1|E_3')(OE/E_1' - OJ/F_1') \quad (A.13)$$

$$D_1 = OL^2 + OC^2 \quad ; \quad D_2 = OG^2 + OA^2 \quad ; \quad D_3 = OH^2 + OD^2$$

$$D_1' = OM^2 + OC^2 \quad ; \quad D_2' = OQ^2 + ON^2 \quad ; \quad D_3' = OI^2 + OD^2$$

$$E_1 = OL^2 + OE^2 \quad ; \quad E_2 = OH^2 + OF^2 \quad ; \quad E_1' = OM^2 + OE^2$$

$$E_2' = OQ^2 + OO^2 \quad ; \quad E_3' = OI^2 + OF^2 \quad ; \quad D_3 = OH^2 + OD^2$$

$$F_2 = OG^2 + OB^2 \quad ; \quad F_1' = OM^2 + OJ^2 \quad ; \quad G_1 = OL^2 + OK^2$$

$$G_1' = OM^2 + OK^2 \tag{A.14}$$

$$OA = (1/2)(\omega_{mn} - \omega_{pn}) \quad ; \quad OB = (1/2)(\omega_{mn} + \omega_{pn}) \quad ; \quad OC = \alpha_p + OB$$

$$OD = OC + OA \quad ; \quad OE = \alpha_p - OB \quad ; \quad OF = OE - OA$$

$$OG = (1/2)(a_{mn} + a_{pn}) \quad ; \quad OH = (a_{mn} + 1/\theta) \quad ; \quad OI = (a_{mn} - 1/\theta)$$

$$OJ = \alpha_p - OA \quad ; \quad OK = \alpha_p + OA \quad ; \quad OL = (1/2)(a_{mn} - a_{pn}) + 1/\theta$$

$$OM = (1/2)(a_{mn} - a_{pn}) + 1/\theta \quad ; \quad ON = OC - OA \quad ; \quad OO = OE + OA$$

$$OQ = a_{pn} + 1/\theta \tag{A.15}$$

APPENDIX B

Results of the Evaluation of the Fourier Transform of the Displacement Covariance

The power spectral density was defined as follows (Ref. 18)

$$S_w(f) = 4 \int_0^\infty \mathcal{R}_w \cdot (o,o,\tau) \cos(2\pi f \tau) d\tau \qquad (B.1)$$

The introduction of Eq. (5.1.10) into equation (B.1) gave (see Appendix A for expression for modal covariance)

$$S_w(f) = 4 \sum_m \sum_n \sum_p \sum_q \int_0^\infty \overline{\left[w(x',y',t) \, w(x',y',t) \right]}_{mnpq} \cos(2\pi f \tau) \, d\tau \qquad (B.2)$$

$$= \sum_m \sum_n \frac{4 \, A \, \bar{P}^2 \, \phi_{mn}^2 (x',y')}{\omega_{mn}^2 \, M^2} \, X_{mn}(f)$$

$$+ \sum_m \sum_p \sum_n \frac{16 A \bar{P}^2 \, \phi_{mn}(x',y') \, \phi_{pn}(x',y')}{\omega_{mn} \, \omega_{pn} \, M^2} \, X_{mpn}(f) \qquad (B.3)$$

where

$$X_{mn}(f) = (W)(COE)(1/COA + 1/COB) + (X)[-(COG/COA) + (COH/COB)]$$

$$+ (Y)(COF)(1/COC + 1/COD) + (Z)[-(COI/COC) + (COJ/COD)] \qquad (B.4)$$

$$COA = 2\left[a_{mn}^2 + (2\pi f - \omega_{mn})^2 \right] \quad ; \quad COB = 2\left[a_{mn}^2 + (2\pi f + \omega_{mn})^2 \right]$$

$$COC = 2\left[1/\theta^2 + (2\pi f - \alpha_m)^2 \right] \quad ; \quad COD = 2 \, {}_L 1/\theta^2 + (2\pi f + \alpha_m)^2 \right]$$

$$COE = a_{mn} \quad ; \quad COF = 1/\theta \qquad\qquad (B.5)$$

$$COG = (2\pi f - \omega_{mn}) \quad ; \quad COH = (2\pi f + \omega_{mn})$$

$$COI = (2\pi f - \alpha_m) \quad ; \quad COJ = (2\pi f + \alpha_m)$$

X_{mpn} (f) was identical in form to X_{mn} (f) but with I, J, K, L, instead of W, X, Y, Z, (see Appendix A) and α_p instead of α_m.

APPENDIX C

The Auto-Correlation of Band Limited White Noise

Consider a stationary stochastic process defined by its spectral density function, S(f). The auto-covariance function is then given (Ref. 18) by

$$\mathcal{R}(\tau) = \int_0^\infty S(f) \cos(2\pi f \tau) \, d\tau \tag{C.1}$$

If in particular

$$S(f) = \begin{cases} A & f_{min} < f < f_{max} \\ 0 & \text{otherwise} \end{cases}$$

Then the auto-correlation function

$$R(\tau) = \frac{\mathcal{R}(\tau)}{\mathcal{R}(0)} = \frac{\sin(\pi \tau \Delta f)}{(\pi \tau \Delta f)} \cos(2\pi f_0 \tau) \tag{C.2}$$

where $\Delta f = f_{max} - f_{min}$; $f_0 = (f_{max} + f_{min})/2$

The auto-correlation function has been evaluated for various combinations of f_{max} and f_{min} and the results are plotted in Figs. C-1, C-2. A widening of the bandwidth by extending f_{max} to higher frequencies can be seen to increase the number of zero crossings. On the other hand a decrease in f_{min}, produces a decrease in the magnitude of the most negative value of the correlation.

APPENDIX D

The Filtered Correlation Function for the Wall-Pressure Fluctuations

Harrison (Ref. 20) has shown that the cross covariance of the wall-pressure fluctuations could be written as

$$\mathcal{R}_p(\Delta x, \Delta y, \tau) = \mathcal{R}_{12}(\tau) = \int_0^\infty U_{12}(f)\cos(2\pi f\tau)\,df - \int_0^\infty V_{12}(f)\sin(2\pi f\tau)\,df \quad \text{(D.1)}$$

where the subscripts 1 and 2 denote two observation points, x, y and x', y', and U_{12} and V_{12} are real functions of Δx, Δy, f, even and odd respectively such that a cross-spectral density function, $P_{12}(f)$, could be written as

$$P_p(\Delta x, \Delta y; f) = P_{12}(f) = U_{12}(f) + i V_{12}(f) \quad \text{(D.2)}$$

If, now, the pressure signals were passed through filters of unit width band-pass at a frequency f_0, the correlation function would become (Ref. 20, 9)

$$_{f_0}\mathcal{R}_{12}(\tau) = U_{12}(f_0)\cos(2\pi f_0\tau) - V_{12}(f_0)\sin(2\pi f_0\tau) \quad \text{(D.3)}$$

or in another form

$$_{f_0}\mathcal{R}_{12}(\tau) = \sqrt{U_{12}^2(f_0) + V_{12}^2(f_0)}\ \cos\left[(2\pi f_0\tau) + \alpha\right] \quad \text{(D.4)}$$

where

$$\alpha = \tan^{-1}(V_{12}/U_{12}) \quad \text{(D.5)}$$

normalizing this filtered covariance

$$_{f_0}R_{12}(\tau) = \frac{_{f_0}\mathcal{R}_{12}(\tau)}{\sqrt{_{f_0}\mathcal{R}_1(0)\,_{f_0}\mathcal{R}_2(0)}} = \frac{\sqrt{U_{12}^2(f_0) + V_{12}^2(f_0)}}{\sqrt{P_1(f_0)\cdot P_2(f_0)}}\cos\left[(2\pi f_0\tau) + \alpha\right] \quad \text{(D.6)}$$

where

$$_{f_0}\mathcal{R}_1(\tau) = P_1(f)\cos(2\pi f_0\tau) \quad ; \quad _{f_0}\mathcal{R}_2(\tau) = P_2(f)\cos(2\pi f_0\tau) \quad \text{(D.7)}$$

$$\mathcal{R}_1(\tau) = \int_0^\infty P_1(f)\cos(2\pi f\tau)\,d\tau \quad , \quad \mathcal{R}_2(\tau) = \int_0^\infty P_2(f)\cos(2\pi f\tau)\,d\tau \quad \text{(D.8)}$$

$\mathcal{R}$ and P being the auto-covariance and the power spectral density functions respectively (Ref. 20).

Table of Modal Frequencies for a Square Simply-Supported Panel and a Square Clamped Plate (Theory, Ref. 11)

m^2+n^2	m, n & n, m	cps f_{ss}	cps f_{cL}	m^2+n^2	m, n & n, m	cps f_{ss}	cps f_{cL}
2	1, 1	12.6	23.0	80	4, 8; 8, 4	504	553.9
5	1, 2; 2, 1	31.5	47.4	82	1, 9; 9, 1	516.6	570.8
8	2, 2	50.4	69.7	85	2, 9; 9, 2; 6, 7; 7, 6	535.5	589.8
10	1, 3; 3, 1	63.0	85.1	89	5, 8; 8, 5	560.7	617.5
13	2, 3; 3, 2	81.9	106.0	90	3, 9; 9, 3	567.0	623.1
17	1, 4; 4, 1	107.1	135.6	97	4, 9; 9, 4	611.1	670.1
18	3, 3	113.4	141.8	98	7, 7	617.8	676.7
20	2, 4; 4, 2	126.0	155.8	100	6, 8; 8, 6	630	689.3
25	3, 4; 4, 3	157.5	190.2	101	1, 10; 10, 1	636.3	696.2
26	1.5; 5, 1	163.8	197.3	104	2, 10; 10, 2	655.2	716.1
29	2, 5; 5, 2	182.7	217.5	106	5, 9; 9, 5	667.8	729.8
32	4, 4	201.6	237 2	109	3, 10; 10, 3	686.7	748.0
34	3, 5; 5, 3	214.6	251.0	113	7, 8; 8, 7	711.9	773.8
37	1.6; 6, 1	233.1	271.1	116	4, 10; 10, 4	730.8	794.3
40	2, 6; 6, 2	252.0	290.7	117	6, 9; 9, 6	737.1	801.2
41	4, 5; 5, 4	258.3	297.6	122	1, 11; 11. 1	768.6	835.4
45	3, 6; 6, 3	283.5	324.7	125	2, 11; 11, 2; 5, 10; 10, 5	787.5	856.0
50	1, 7; 7, 1; 5, 5	315.0	357.6	128	8, 8	806.4	874.6
52	4, 6; 6, 4	327.6	371.4	130	3, 11; 11, 3 7, 9; 9, 7	819.0	888.3
53	2, 7; 7, 2	333.9	378.0	136	6, 10; 10, 6	856.8	926.3
58	3, 7; 7, 3	365.4	410.1	137	4, 11, 11, 4	863.1	933.1
61	5, 6; 6, 5	384.3	430.8	145	1, 12; 12, 1 8, 9,; 9, 8	913.5	985.4
65	1, 8; 8, 1 4, 7,; 7, 4	409.5	457.5	146	5, 11; 11. 5	919.8	994.4
68	2, 8; 8, 2	428.4	477.1	148	2, 12; 12, 2	932.4	1004.7
72	6, 6	453.6	504	149	7, 10; 10, 7	938.7	1015.5
73	3, 8; 8, 3	459.9	505.4	153	3, 12; 12, 3	963.9	1037.6
74	5, 7; 7, 5	466.2	512.3	157	6, 11; 11, 6	989.1	1063.5

Steel plate, .008 inch thickness, 11 inches length.
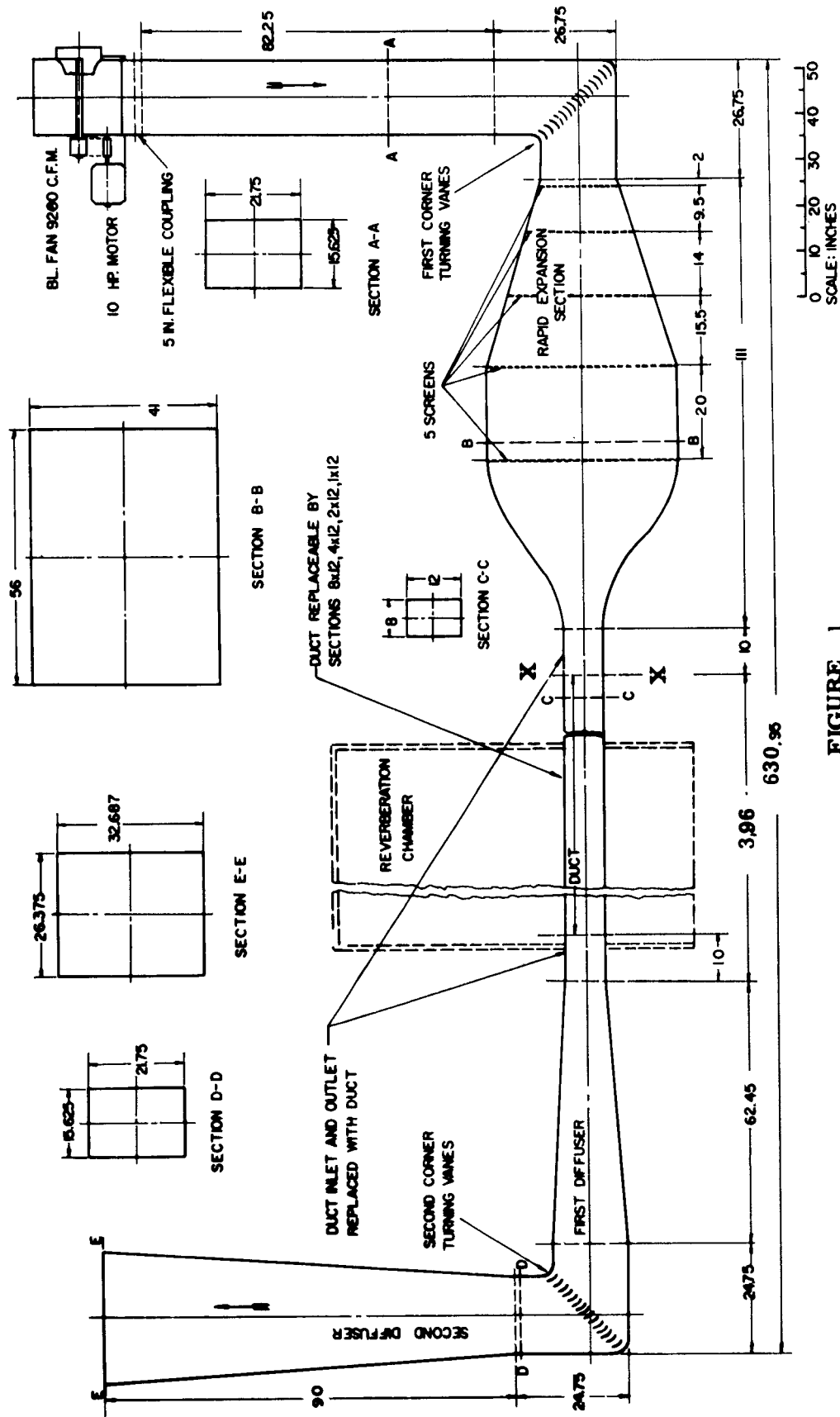
FIGURE 1

GENERAL ARRANGEMENT OF THE U. T. I. A. S. LOW-NOISE AIR DUCT

FLOW DIRECTION

PANEL EXPOSED SURFACE

PANEL CLAMPING SURFACES

x'

y'

PANEL FRAME
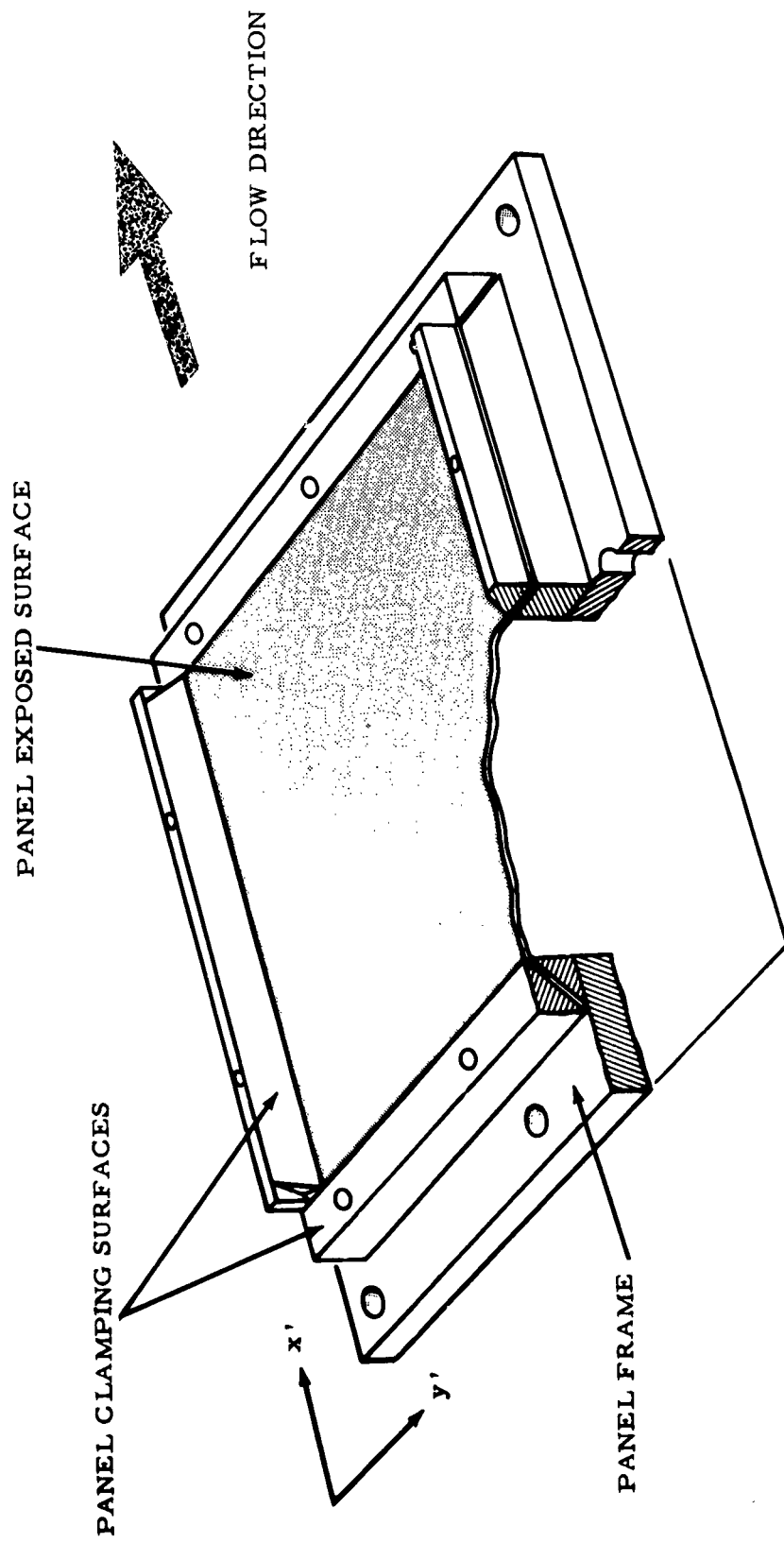
FIGURE 2   SKETCH OF A TEST PANEL MOUNTED IN ITS FRAME SHOWING THE
SURFACE TO BE EXPOSED TO THE TURBULENCE IN VIEW
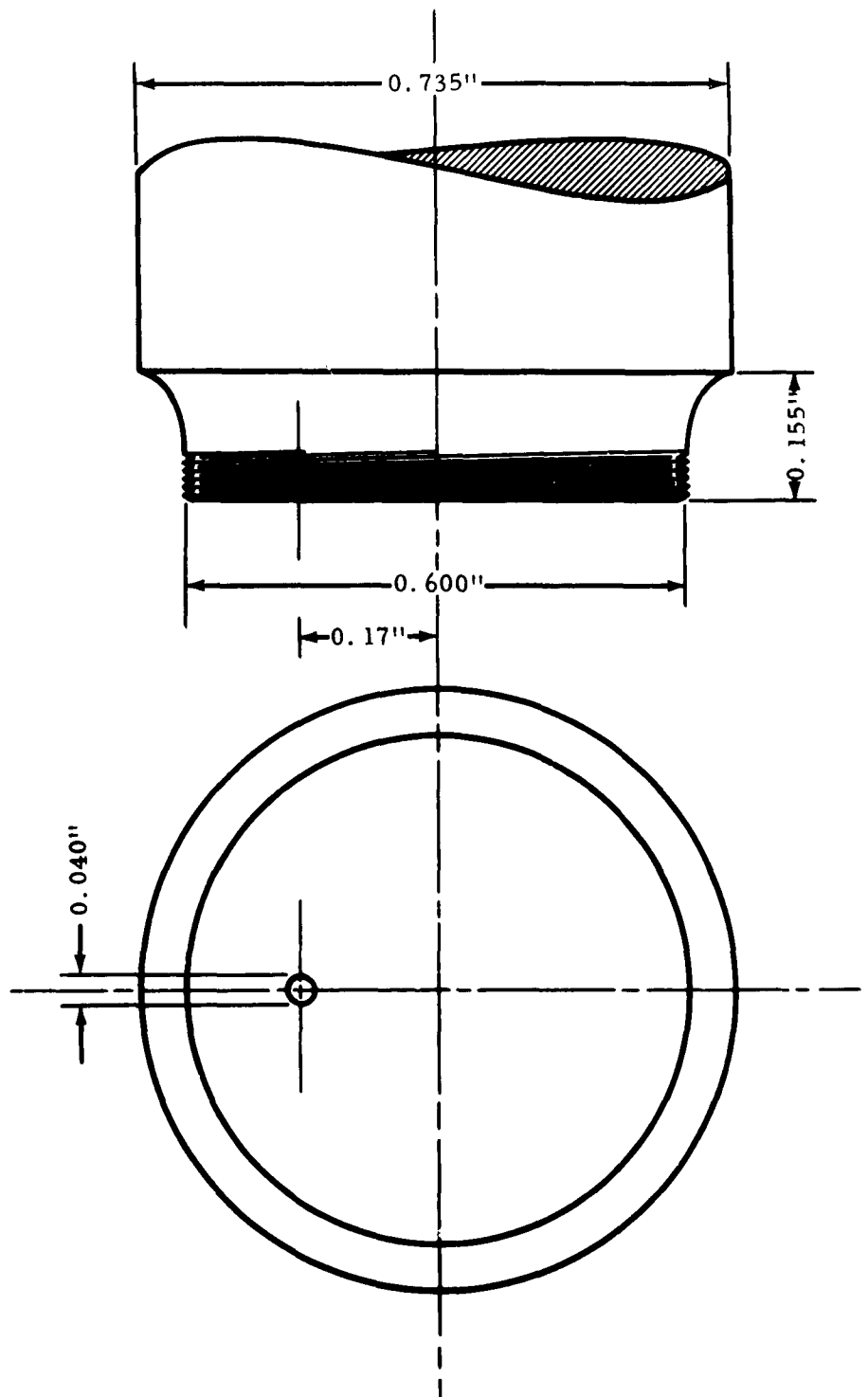
FIGURE 3   A SKETCH OF AN ALTEC LANSING PIN HOLE
MICROPHONE

CROSS SECTION THRU A-A.

STAINLESS
STEEL

TEFLON

0.500"

0.300"

0.125"

0.570"

0.735"

SENSING
ELEMENT

A

A
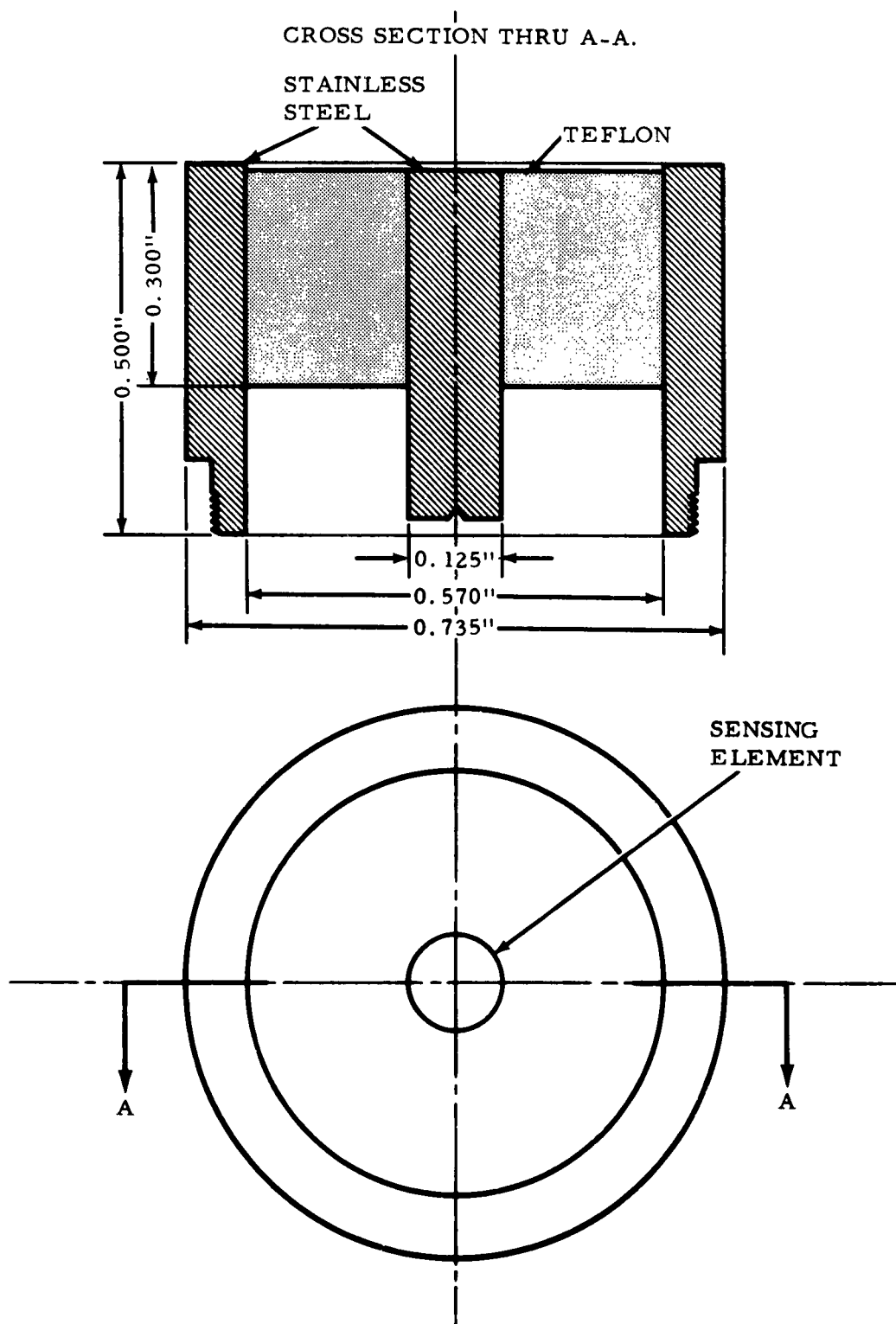
FIGURE 4 A SKETCH OF THE SHATTUCK CAPACITANCE - TYPE
DISPLACEMENT PROBE
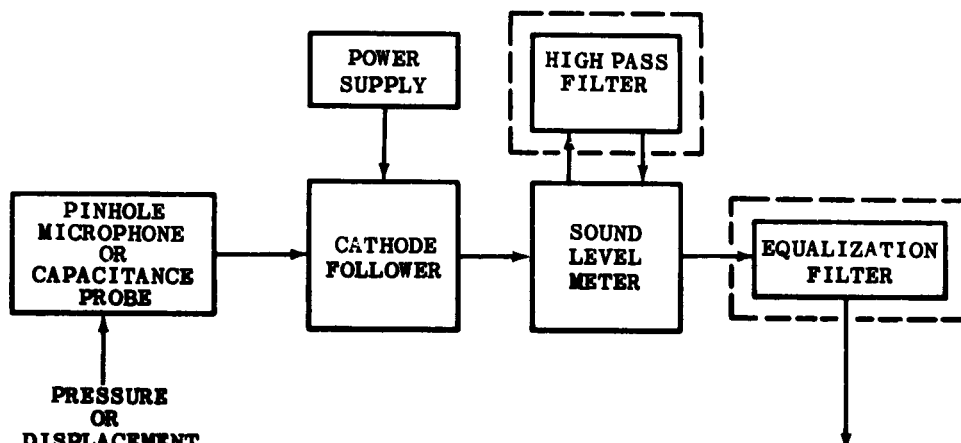
FIGURE 5A. FUNCTIONAL DIAGRAM OF THE PRESSURE AND
DISPLACEMENT MEASUREMENT SYSTEM
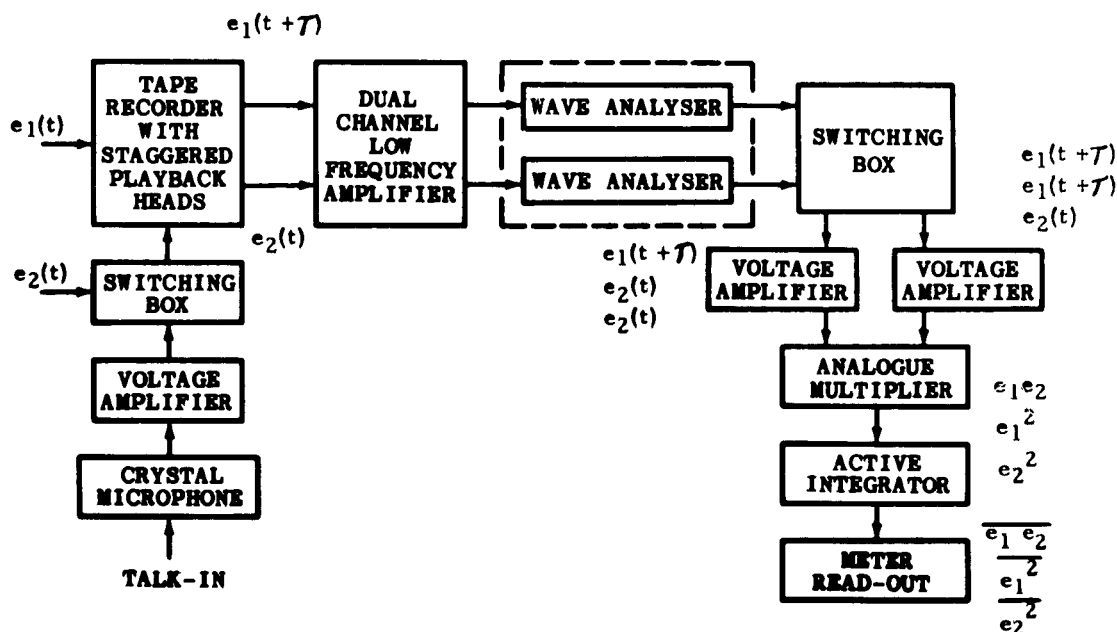
FIGURE 5B. FUNCTIONAL DIAGRAM OF THE ELECTRONIC CORRELATOR
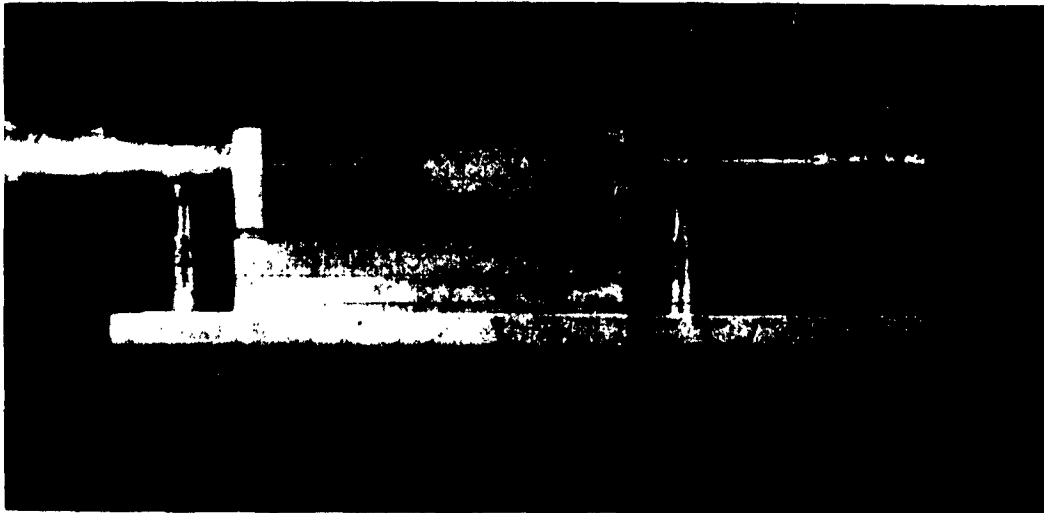
FIG. 6   STAGGERED-HEAD TAPE RECORDER PLAYBACK
          ASSEMBLY FOR INTRODUCING TIME DELAY
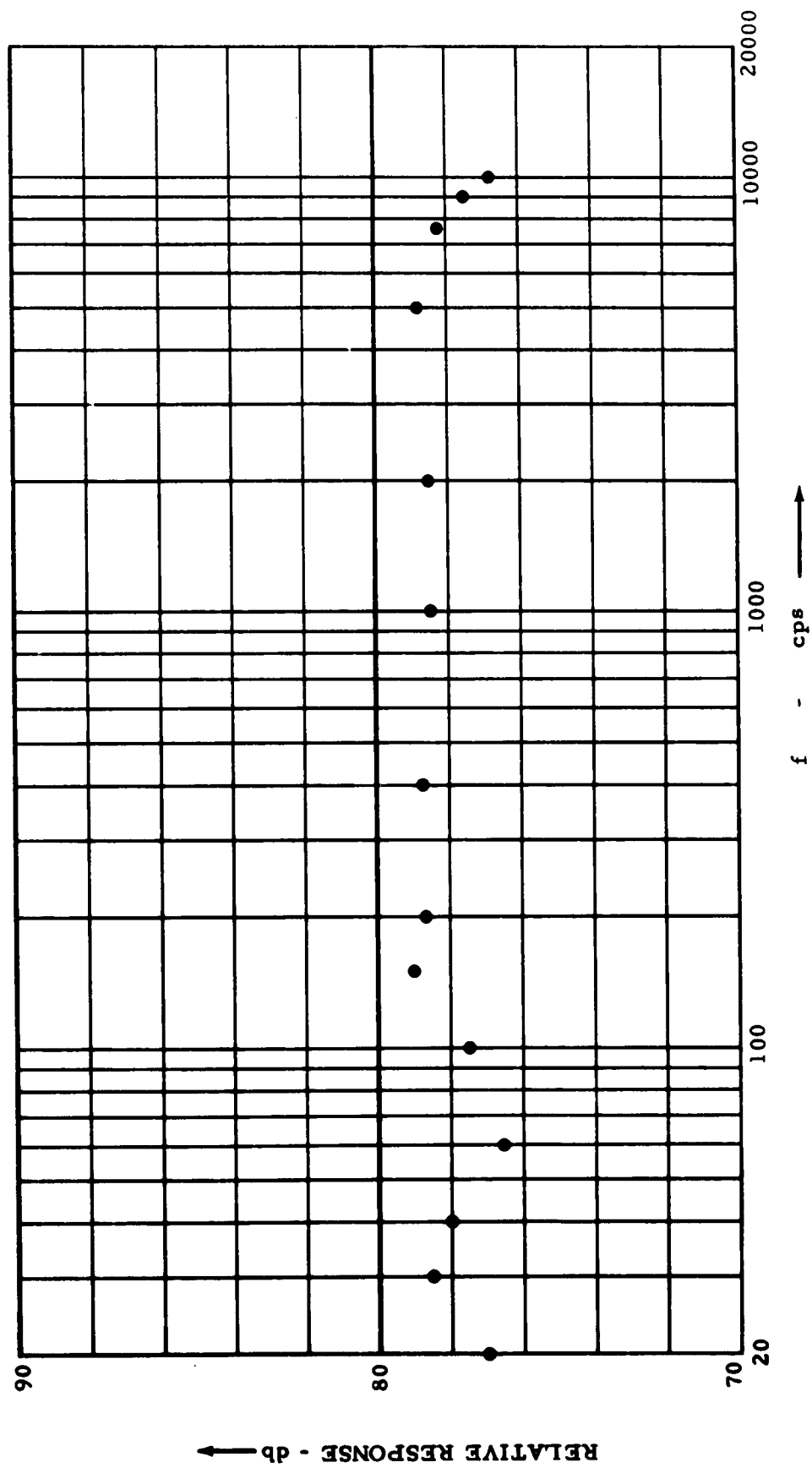
FIGURE 7 FREQUENCY RESPONSE OF ELECTRONIC CORRELATOR
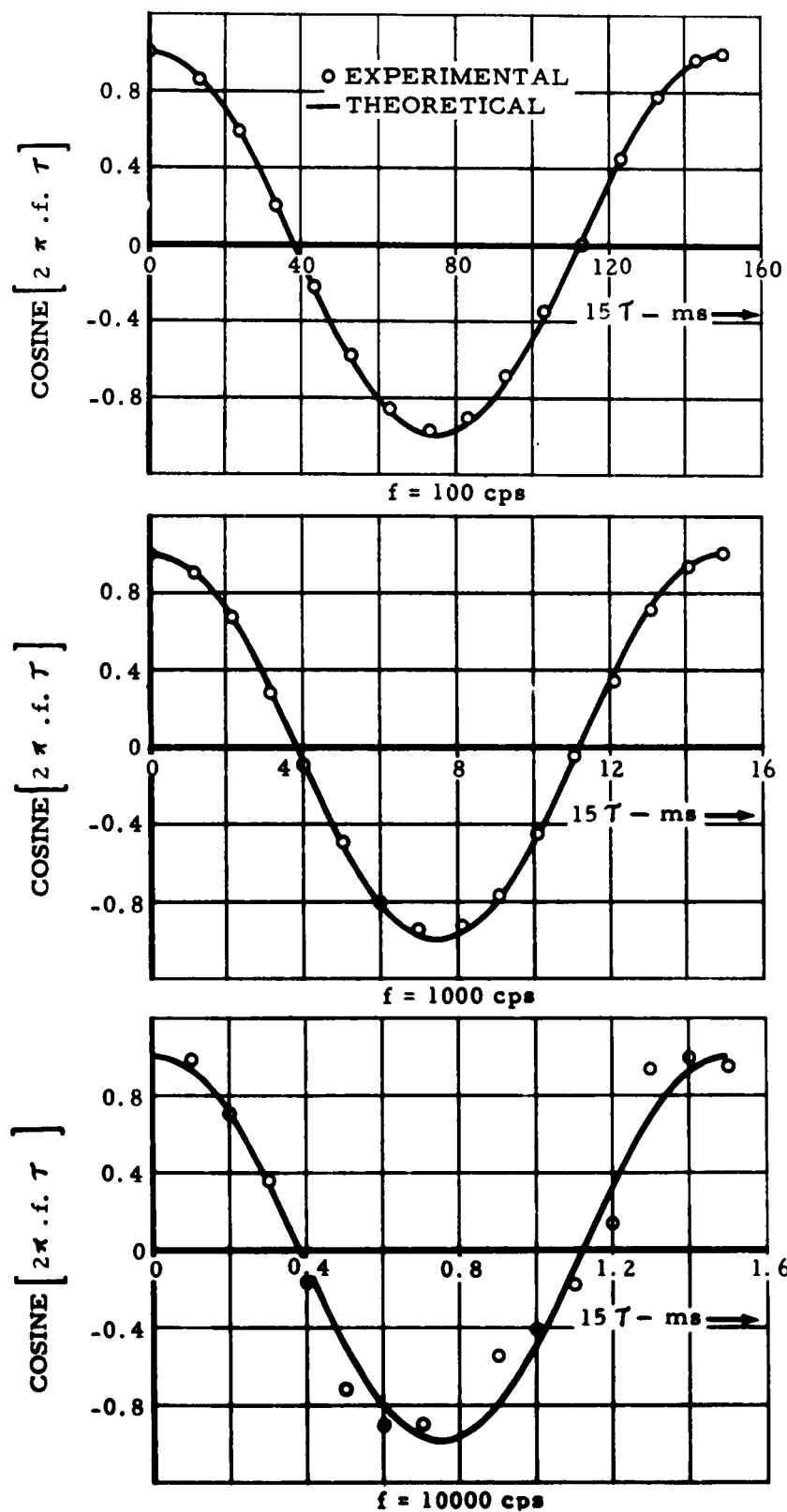
FIGURE 8   THE AUTO-CORRELATION OF SINE WAVES (CARRIED OUT ON THE ELECTRONIC CORRELATOR)

FLOW DIRECTION

EXPOSED SURFACE

MICROPHONE LOCATING HOLES

FRAME

x'

y'

SECTION VIEW SHOWING
MICROPHONE IN POSITION

SECTION VIEW SHOWING
LOCATING HOLES BLANKED
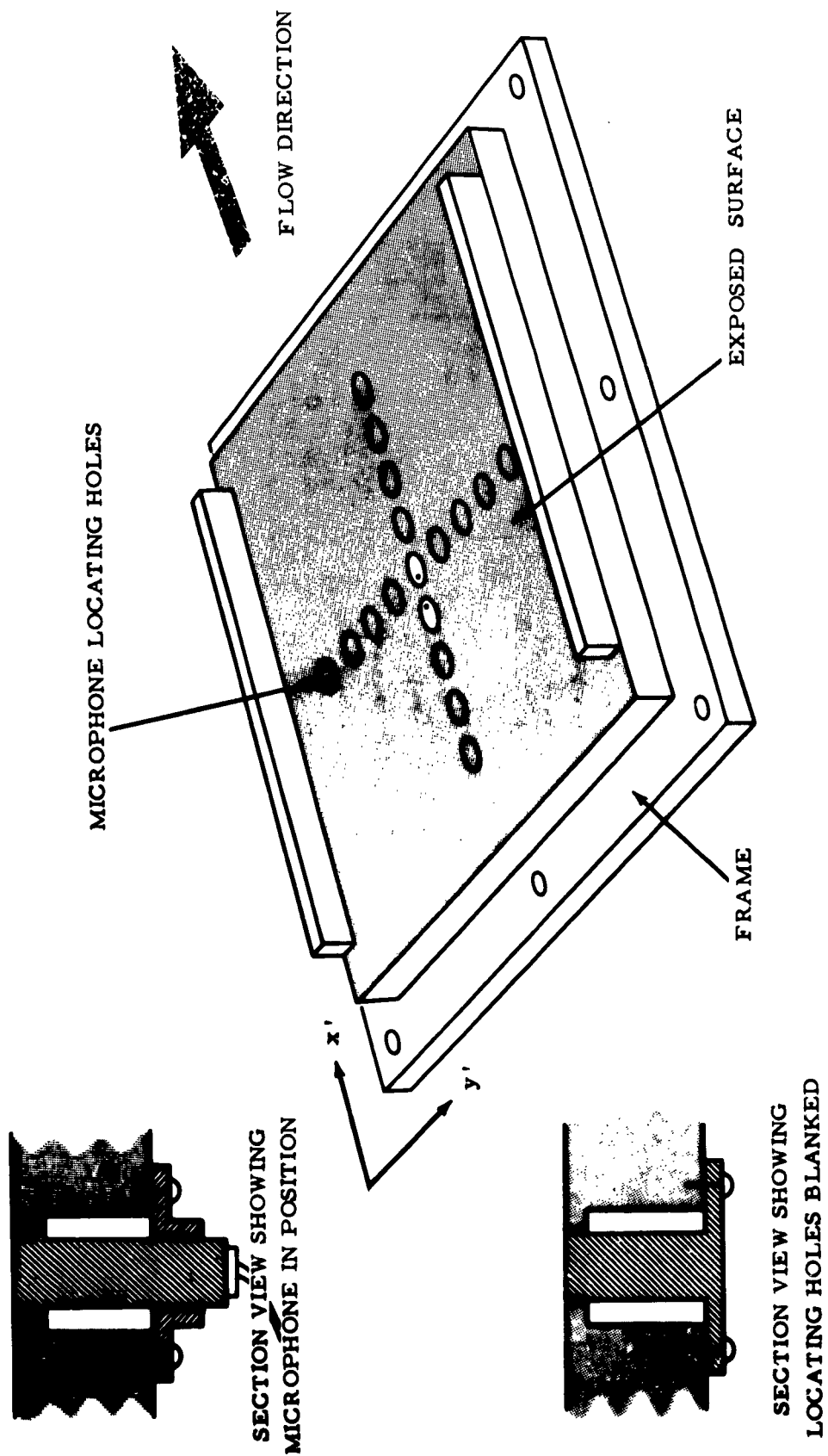
FIGURE 9   SKETCH OF THE MICROPHONE FRAME SHOWING THE SURFACE
TO BE EXPOSED TO THE TURBULENCE IN VIEW

8 in. DUCT

▲ 170 fps, 0.008 in. PANEL IN POSITION,
  4.5 ft DOWNSTREAM OF PANEL STATION
○ 172 fps, MICROPHONE FRAME IN POSITION,
  4.5 ft DOWNSTREAM OF PANEL STATION (REF. 4)
◇ 172 fps, MICROPHONE FRAME IN POSITION,
  3.5 ft UPSTREAM OF PANEL STATION (REF. 4)

1 in. DUCT

△○ 185.5 fps, MICROPHONE FRAME IN POSITION,
   AT PANEL STATION
◇ 189 fps, MICROPHONE FRAME IN POSITION,
  5.5 in DOWNSTREAM OF PANEL STATION (REF. 4)
△ 191 fps, MICROPHONE FRAME IN POSITION,
  7.5 in. UPSTREAM OF PANEL STATION (REF. 4)
▲ 202.7 fps, 0.002 in. PANEL IN POSITION,
  AT PANEL STATION

FIGURE 10   DUCT VELOCITY PROFILES
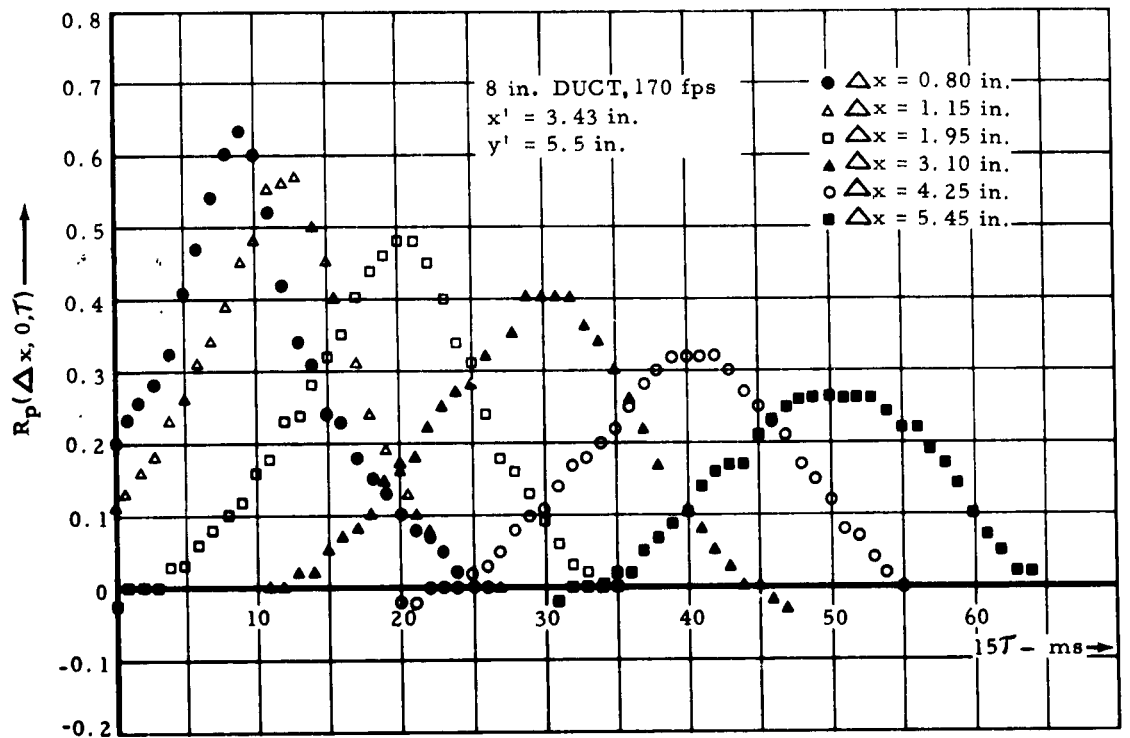
FIGURE 11A
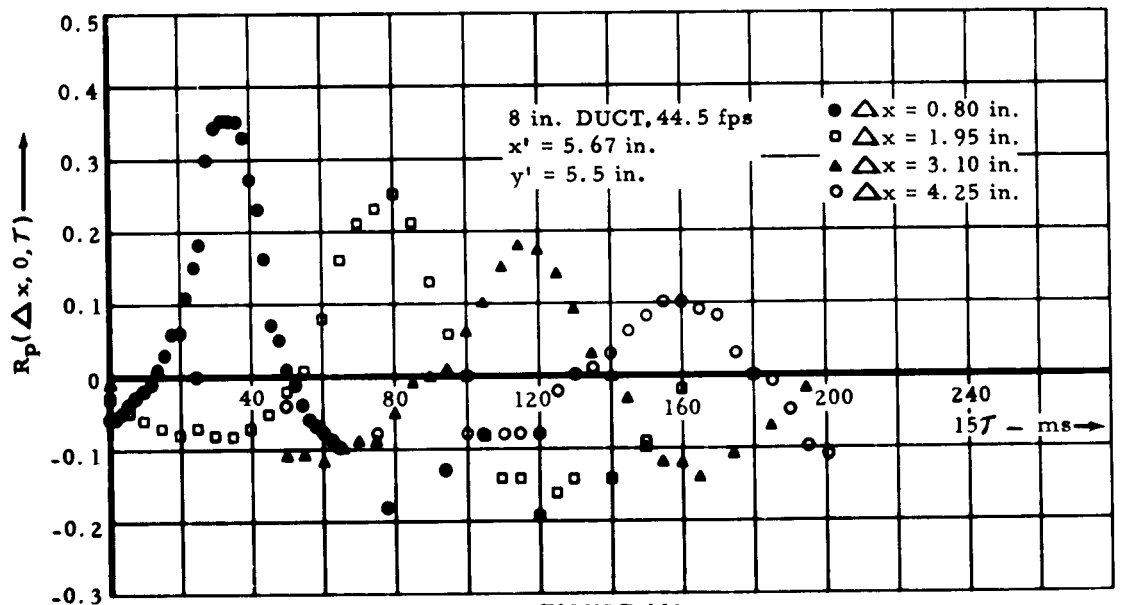
FIGURE 11B

FIGURE 11A, B LONGITUDINAL TWO-POINT SPACE-TIME CORRELATION
OF THE WALL PRESSURE FLUCTUATIONS
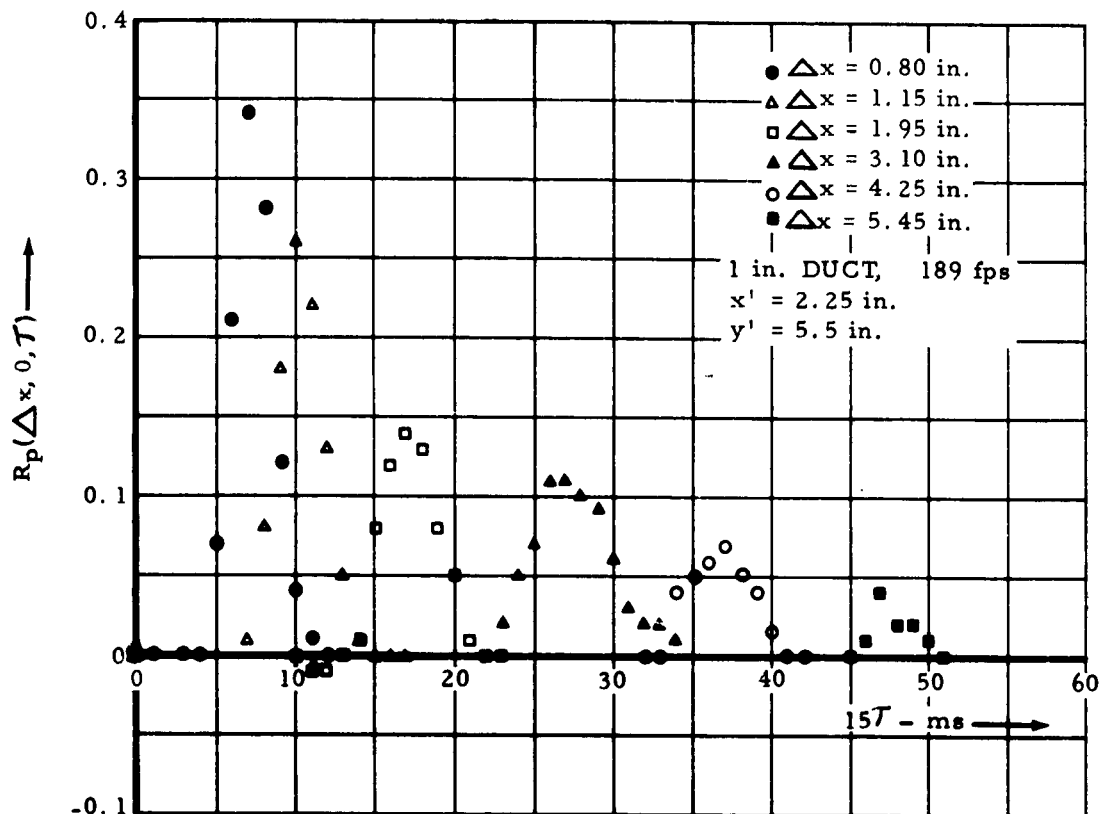
FIGURE 11C
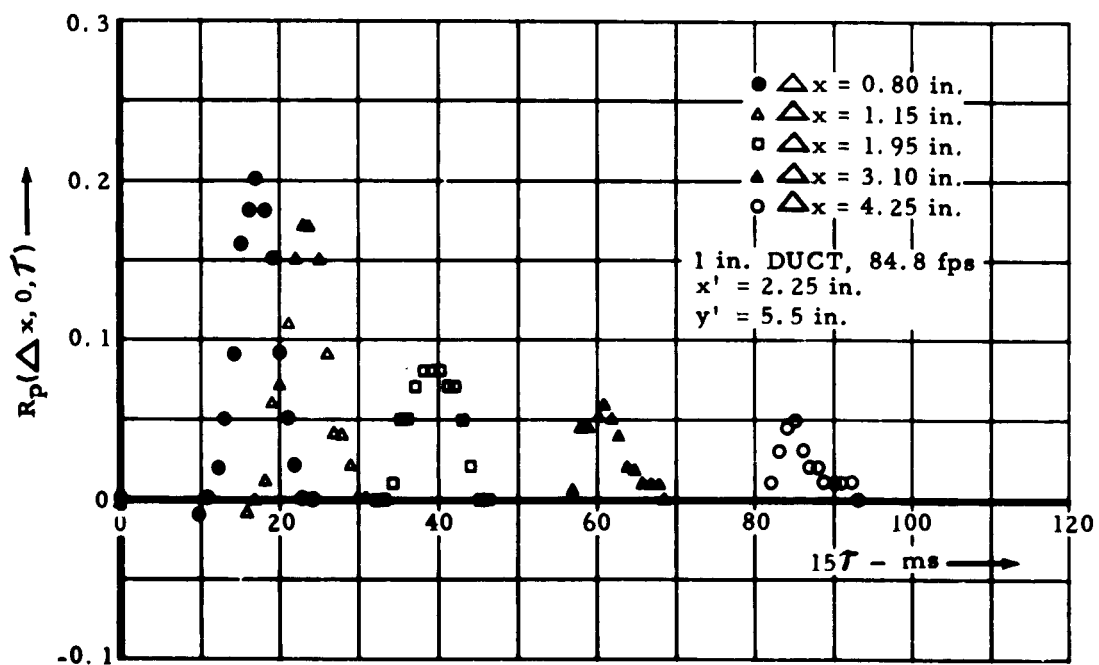
FIGURE 11D

FIGURE 11C, D   LONGITUDINAL TWO-POINT SPACE-TIME CORRELATION
OF THE WALL PRESSURE FLUCTUATIONS
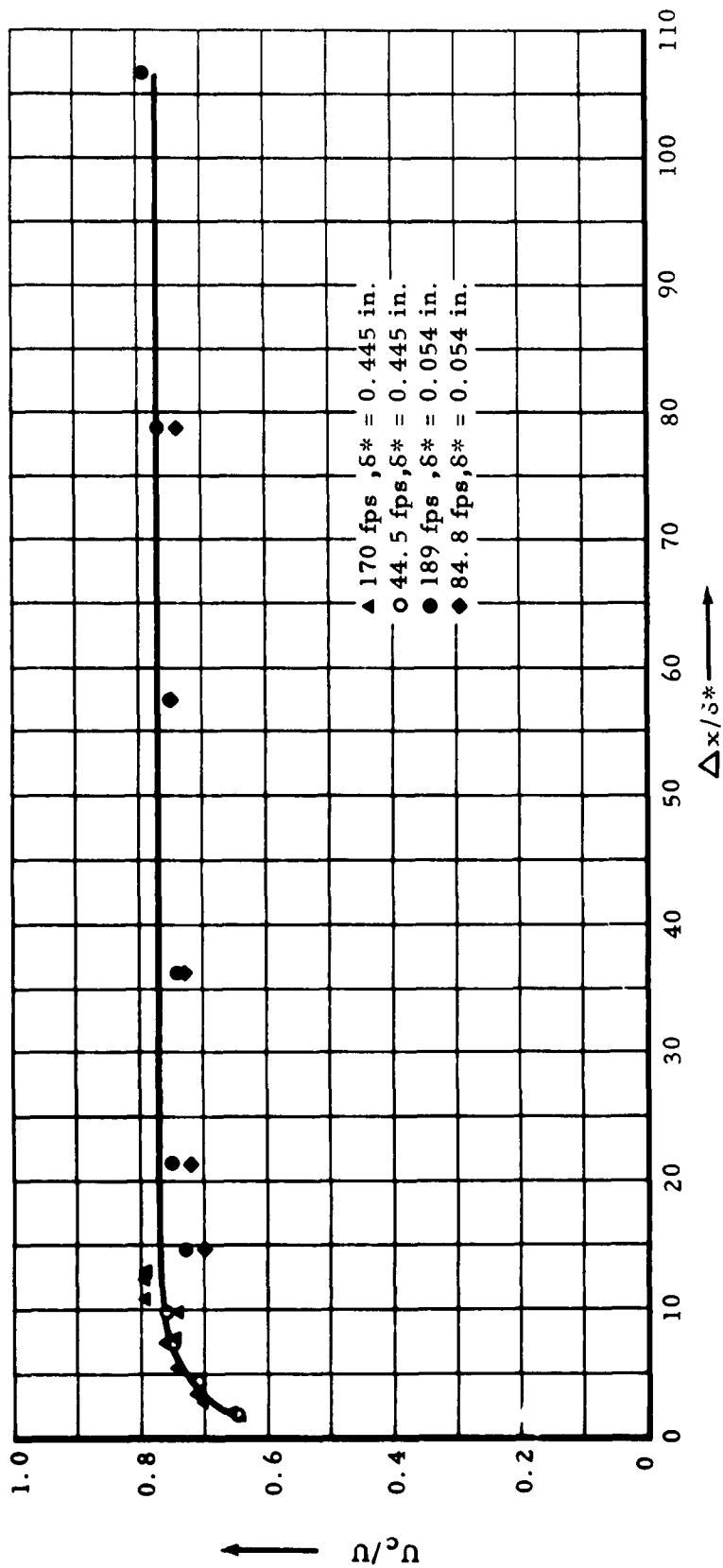
FIGURE 12A   MEAN CONVECTION SPEED OF PRESSURE - PRODUCING EDDIES
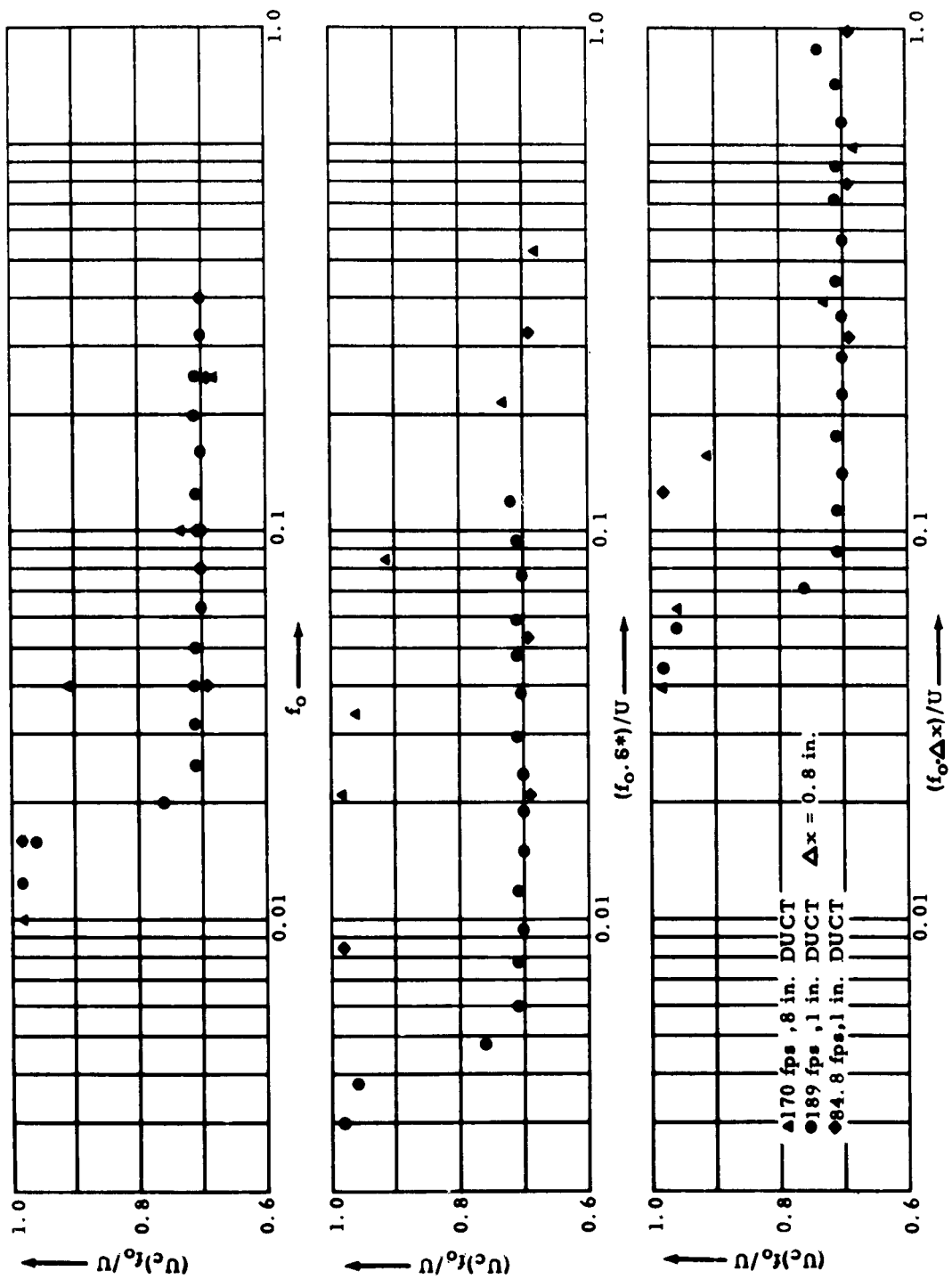
FIGURE 12B   MEAN CONVECTION SPEED OF PRESSURE - PRODUCING
EDDIES FOR 1/3 OCTAVE BANDS
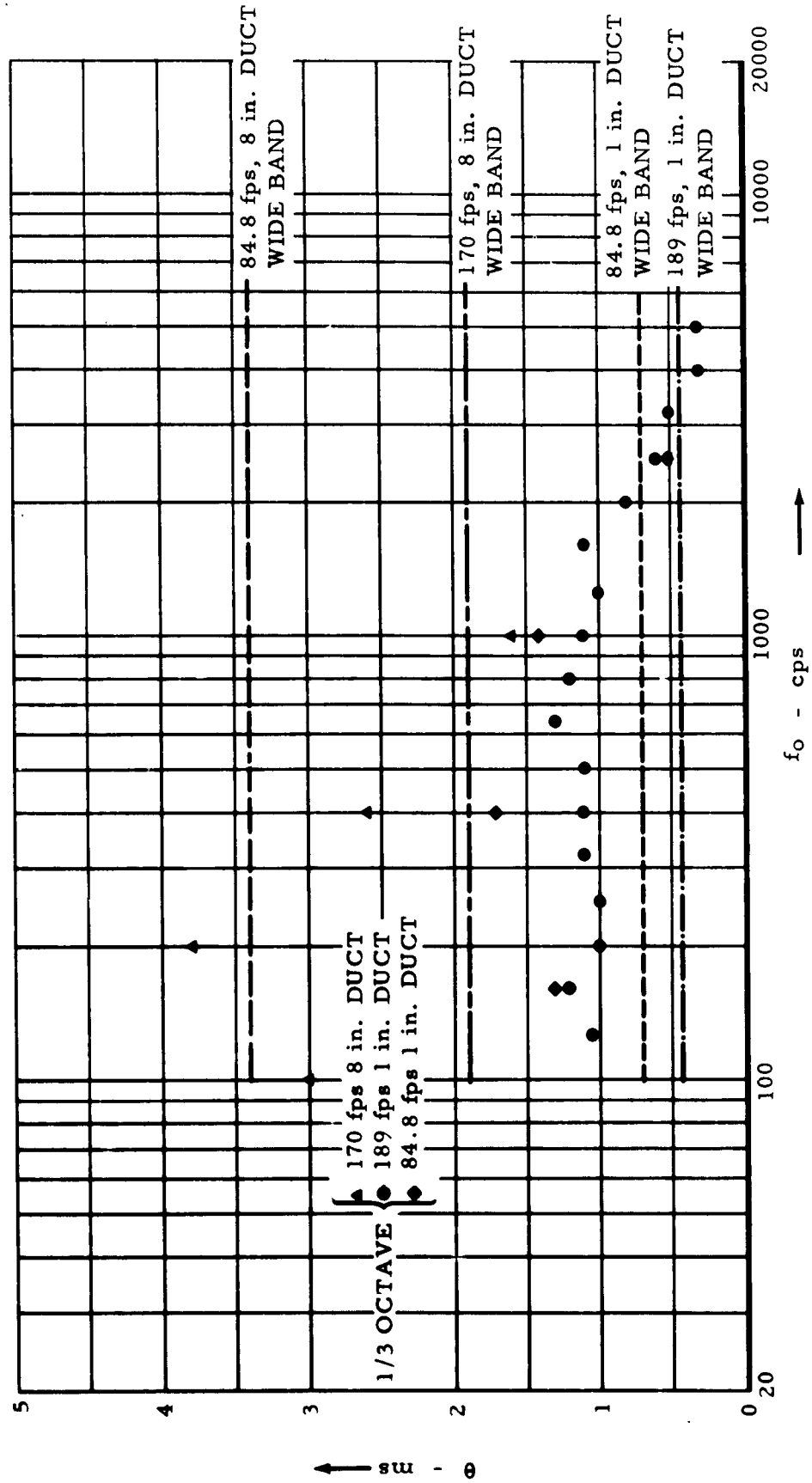
FIGURE 13   MEAN LIFETIME OF PRESSURE PRODUCING EDDIES
FOR VARIOUS FREQUENCY BANDS
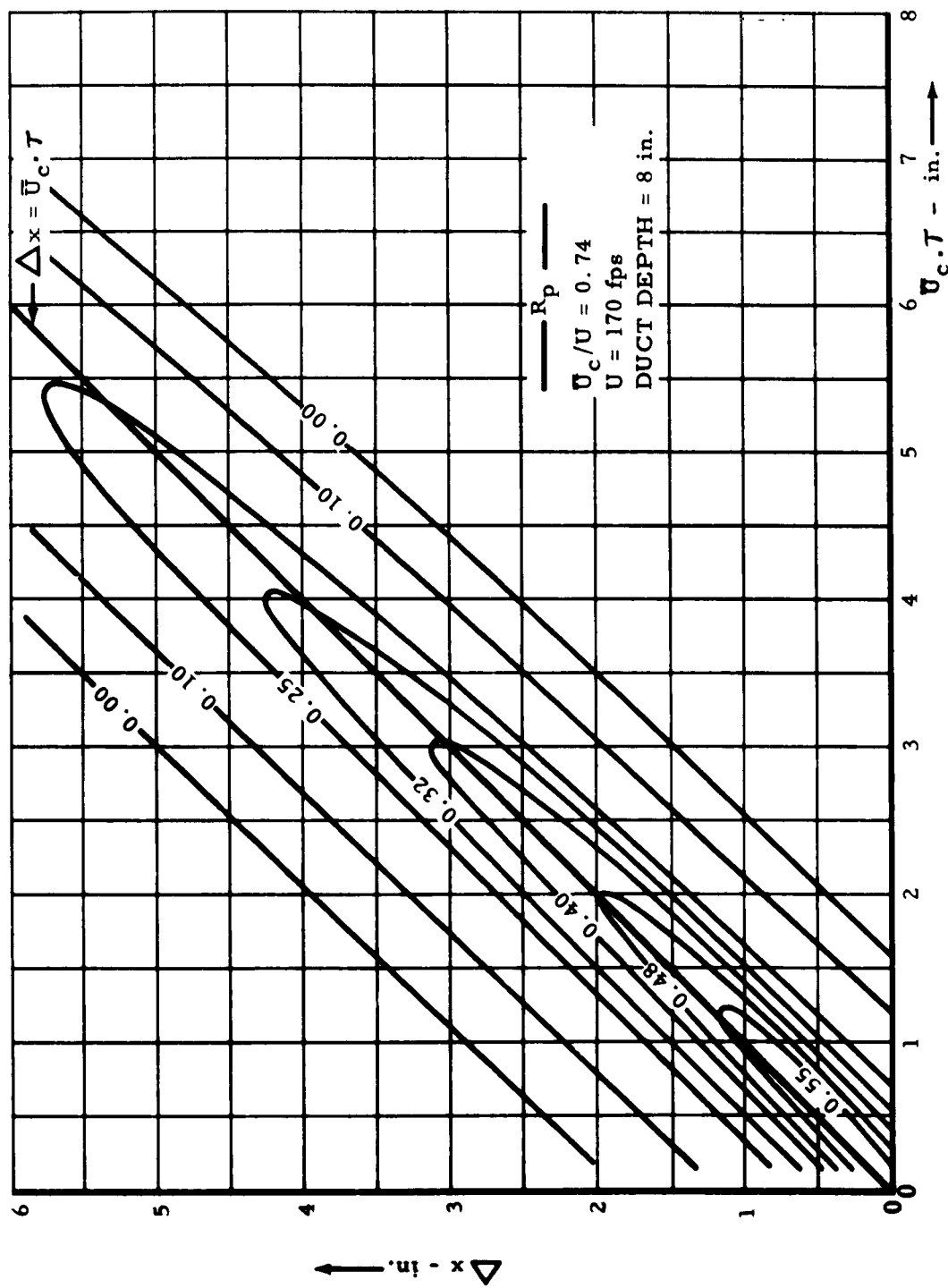
FIGURE 14 LINES OF CONSTANT LONGITUDINAL CORRELATION:
WALL PRESSURE FLUCTUATIONS.
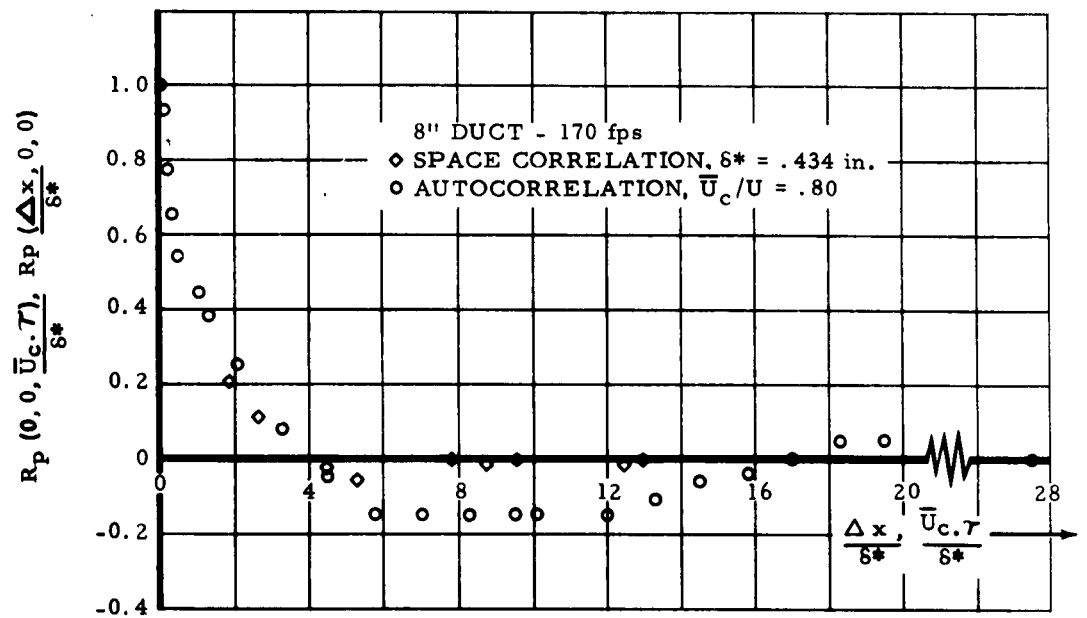
FIGURE 15A
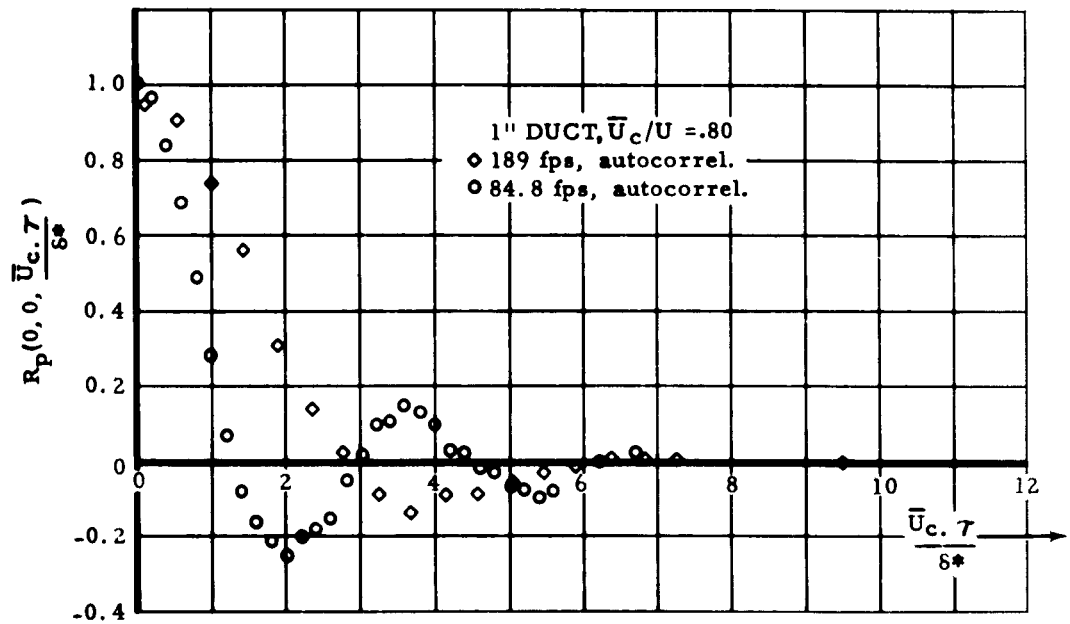
FIGURE 15B

FIGURE 15A, B   LONGITUDINAL AUTOCORRELATION AND SPACE
CORRELATION OF THE WALL PRESSURE FLUCTUATIONS
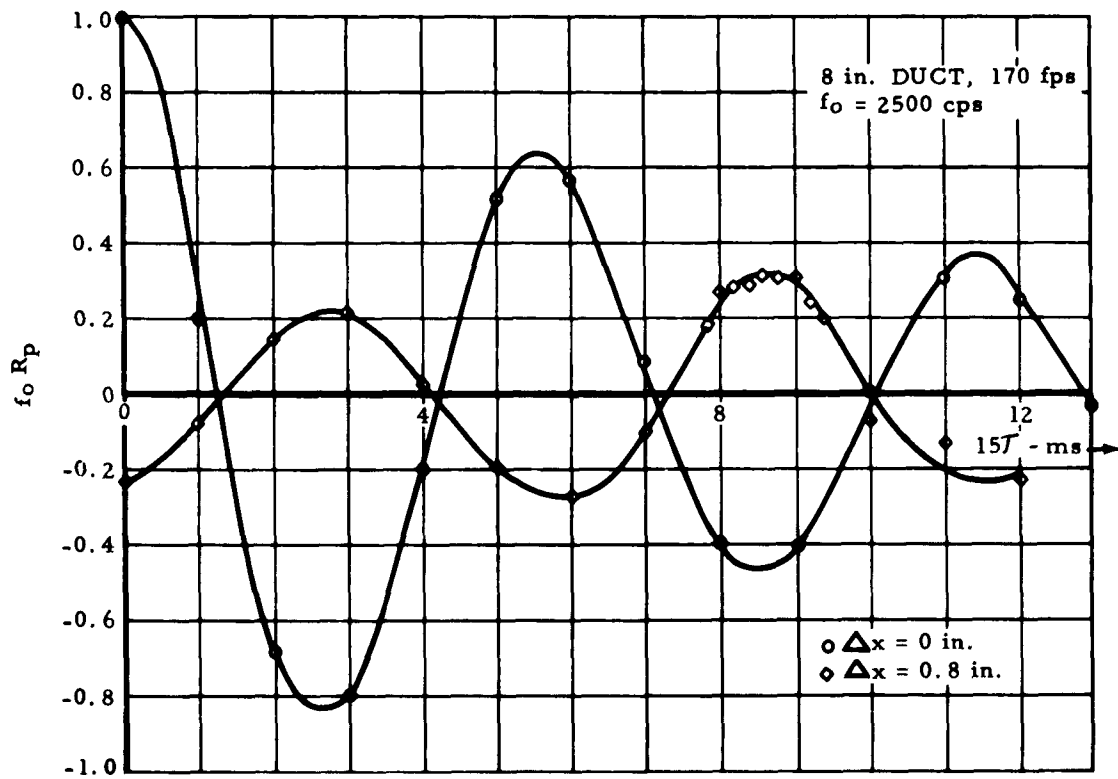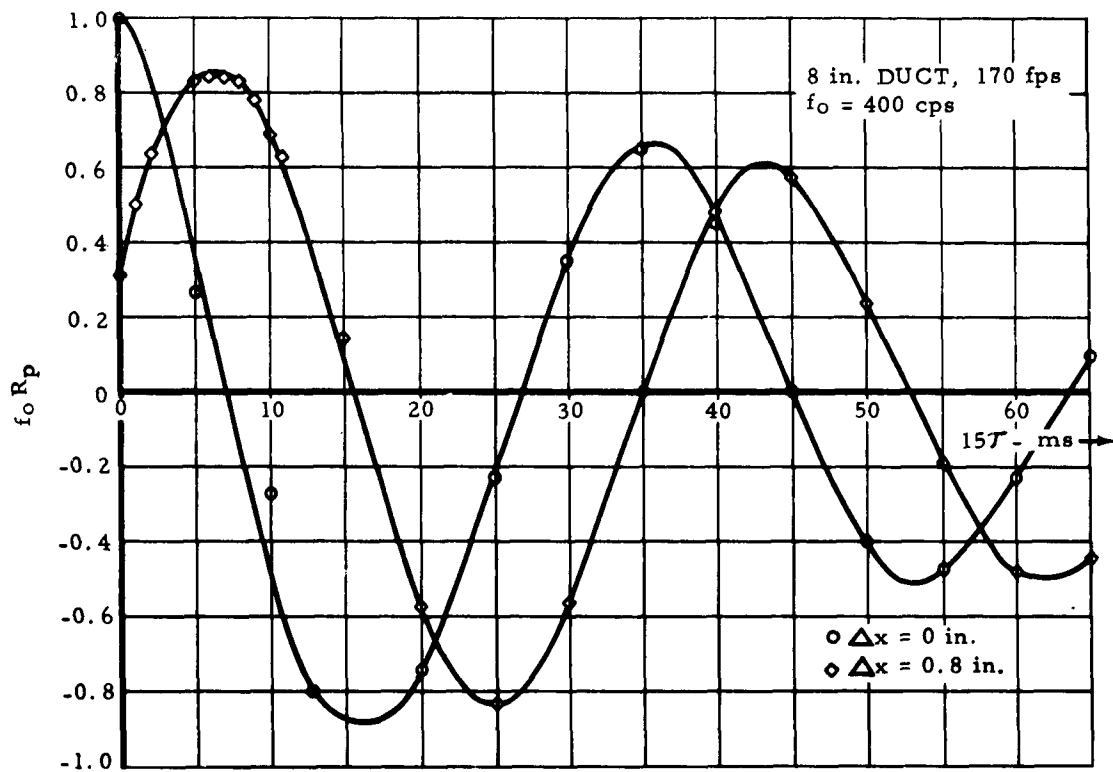
FIGURE 16A   LONGITUDINAL TWO-POINT SPACE-TIME CORRELATION OF THE WALL PRESSURE FLUCTUATIONS IN 1/3 OCTAVE BANDS
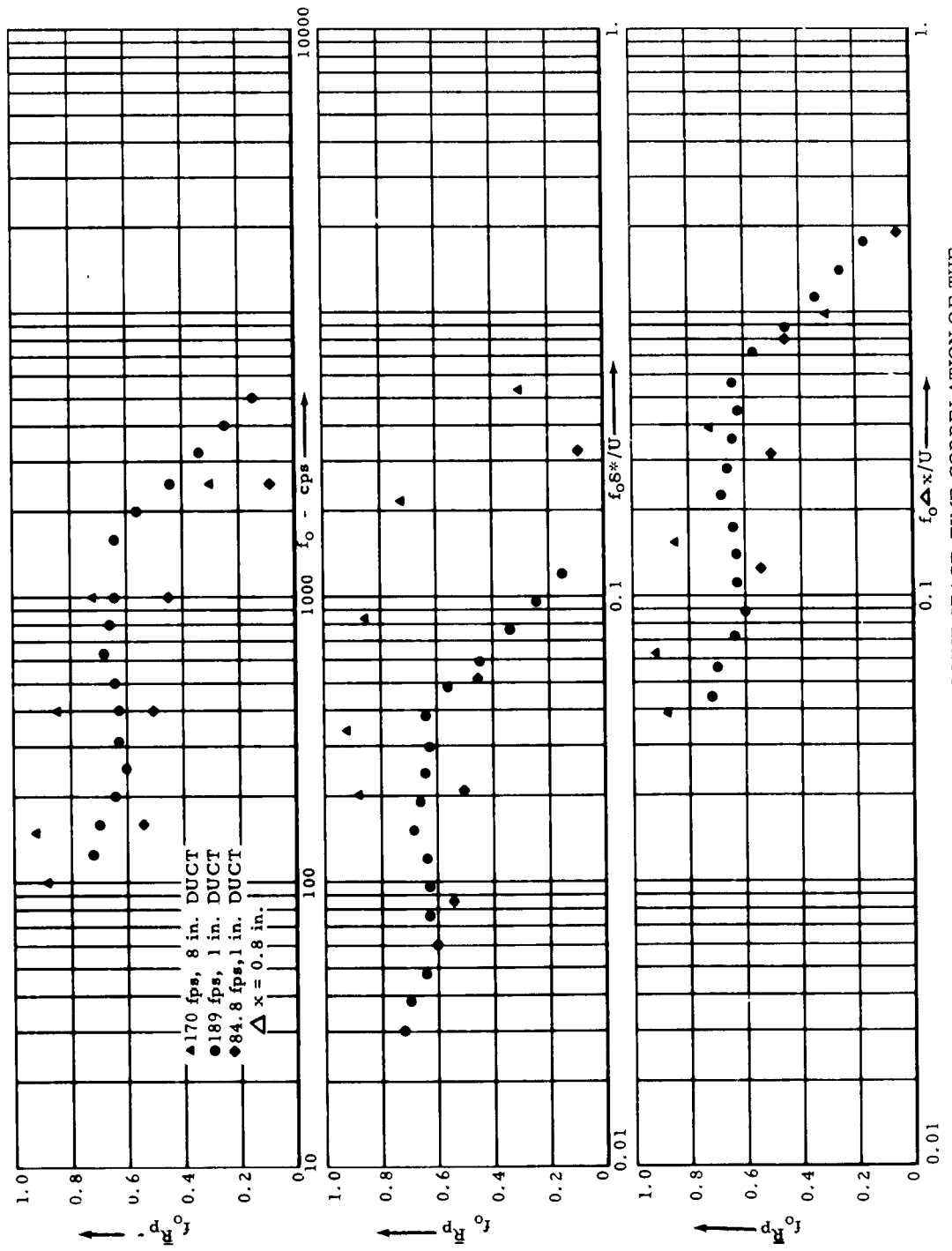
FIGURE 16B LONGITUDINAL TWO-POINT SPACE-TIME CORRELATION OF THE
WALL PRESSURE FLUCTUATIONS IN 1/3 OCTAVE BANDS
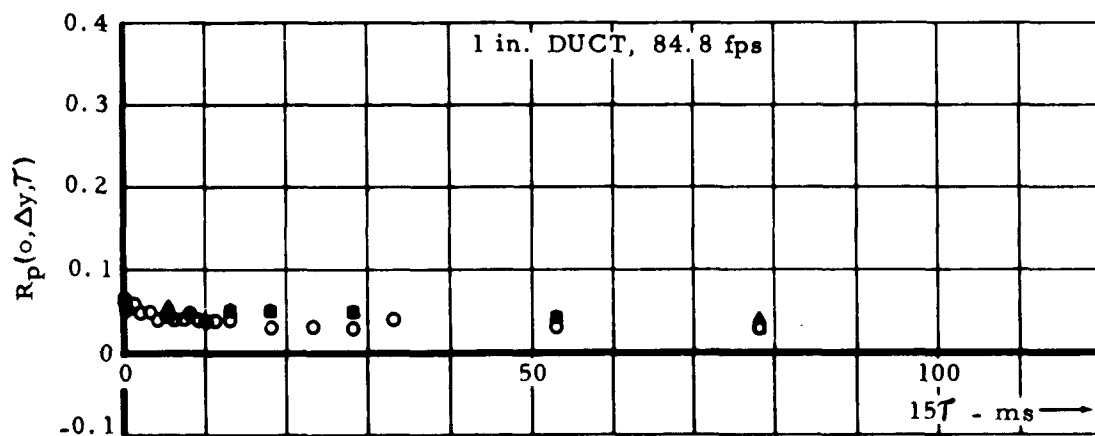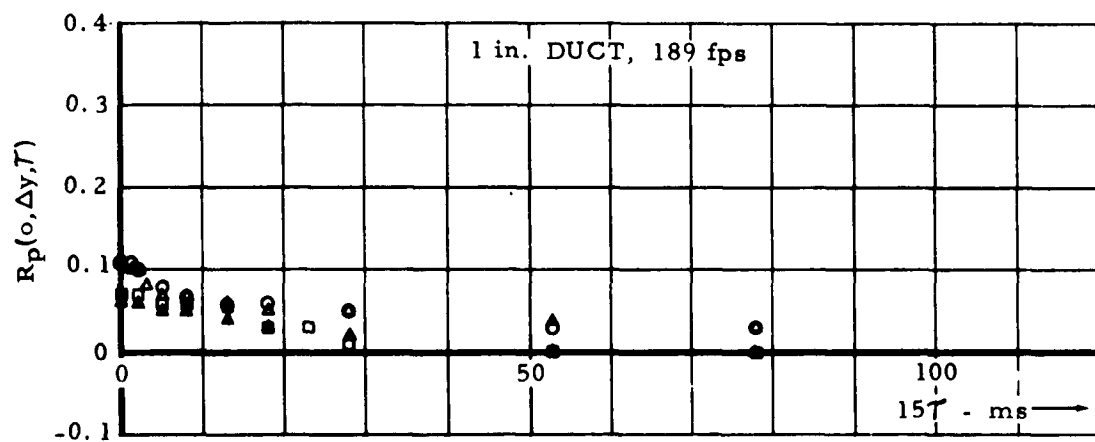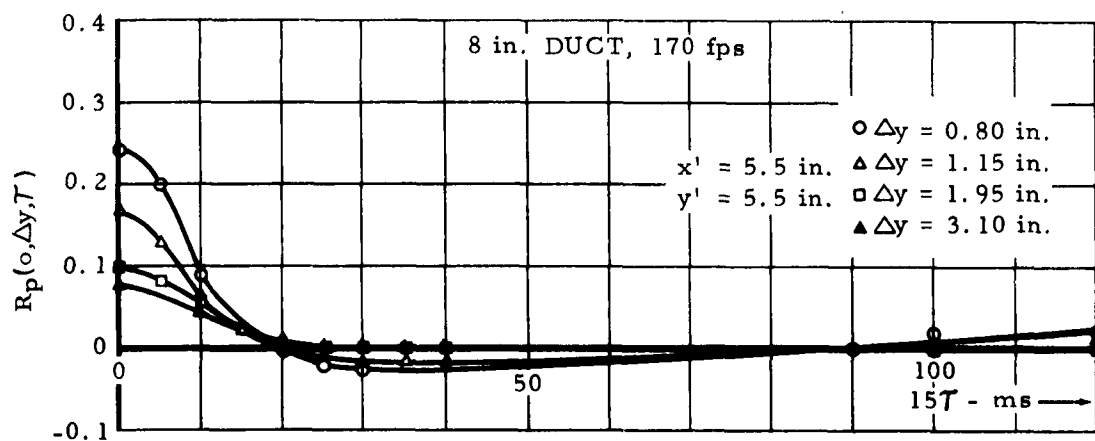
FIGURE 17   LATERAL TWO-POINT SPACE-TIME CORRELATION
OF THE WALL-PRESSURE FLUCTUATIONS
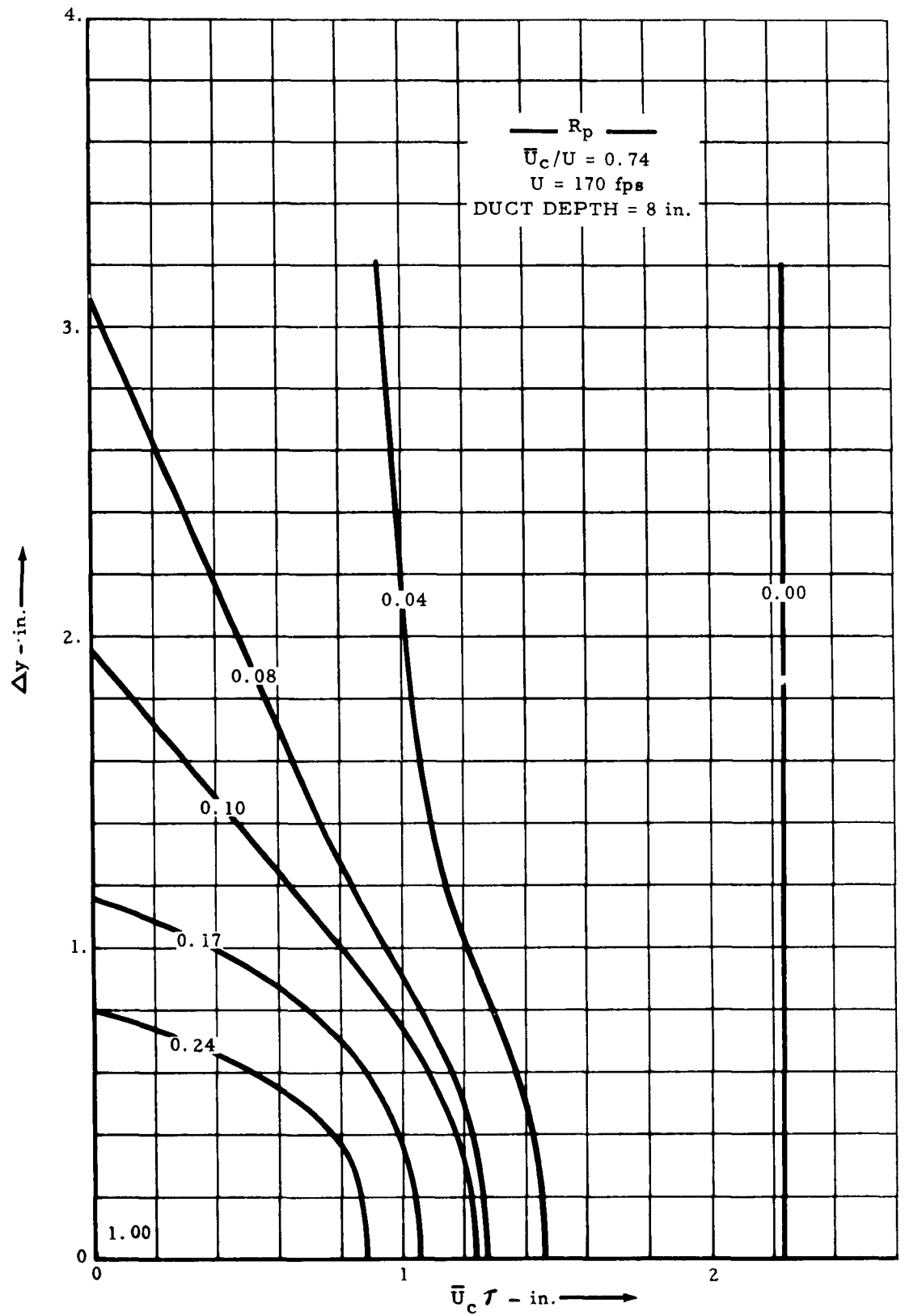
FIGURE 18   LINES OF CONSTANT LATERAL CORRELATION:
WALL PRESSURE FLUCTUATIONS
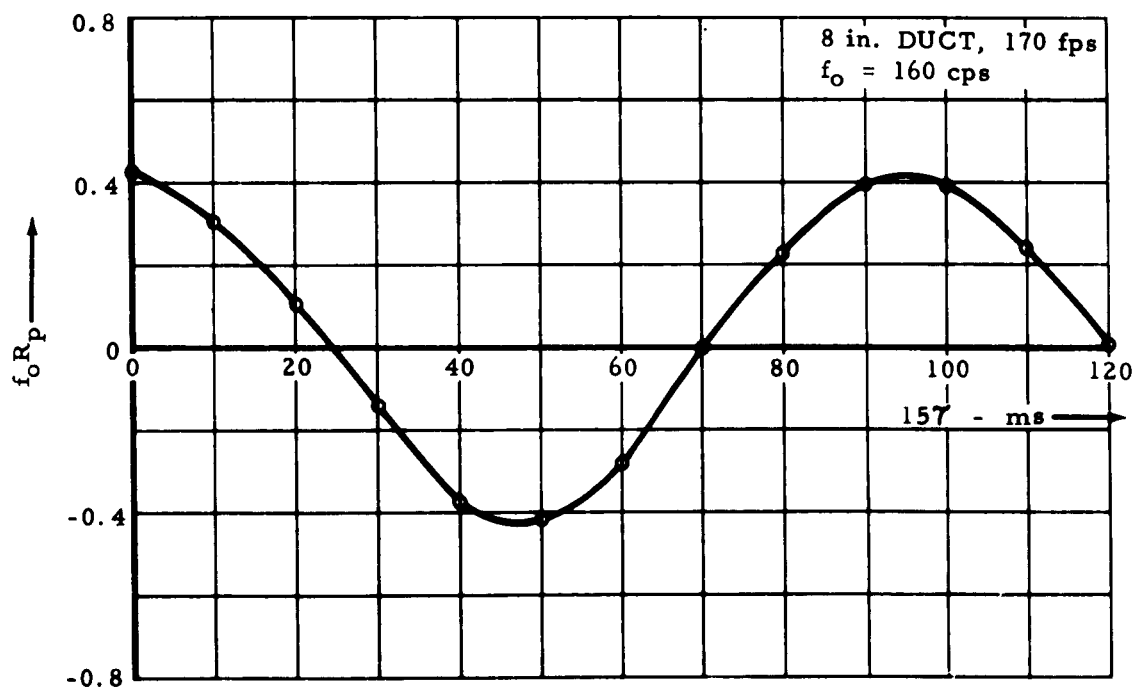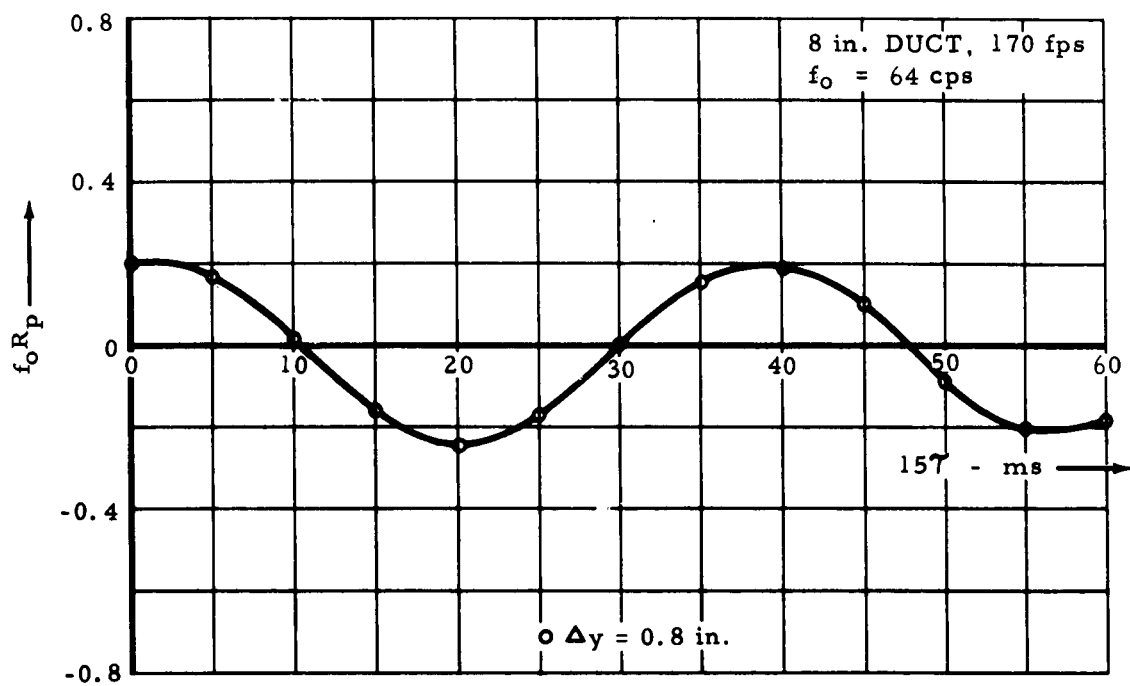
FIGURE 19   LATERAL TWO-POINT SPACE-TIME
CORRELATION OF WALL PRESSURE
FLUCTUATIONS IN 1/3 OCTAVE BANDS.
PANEL CENTRE
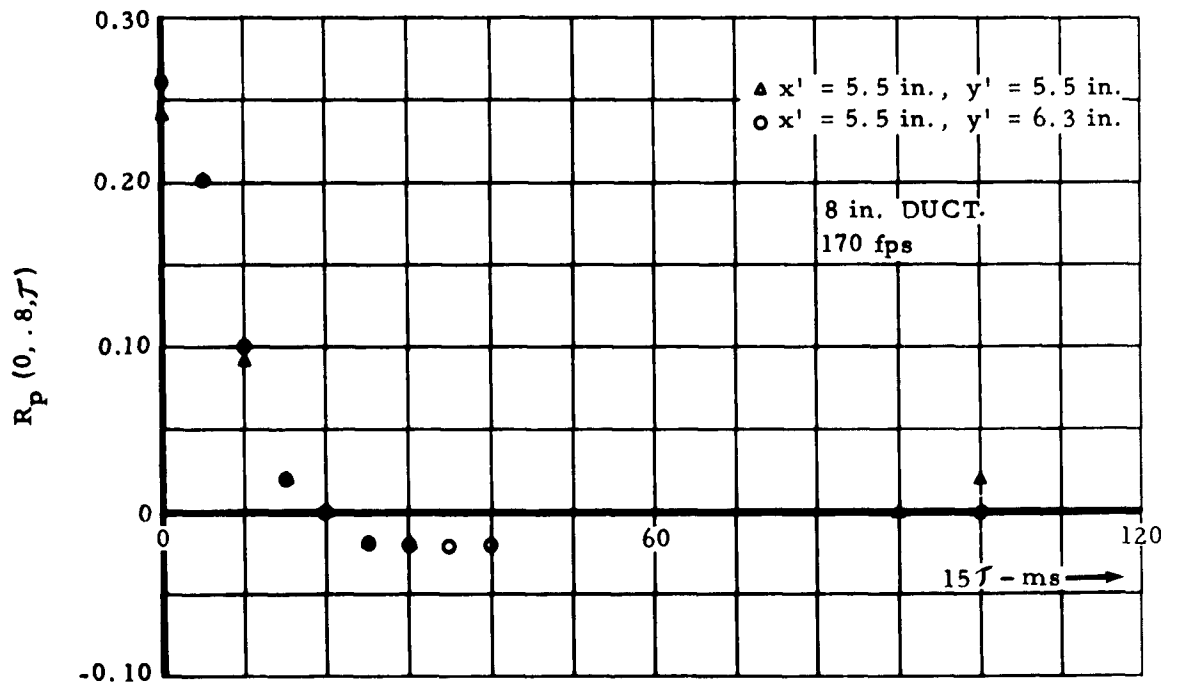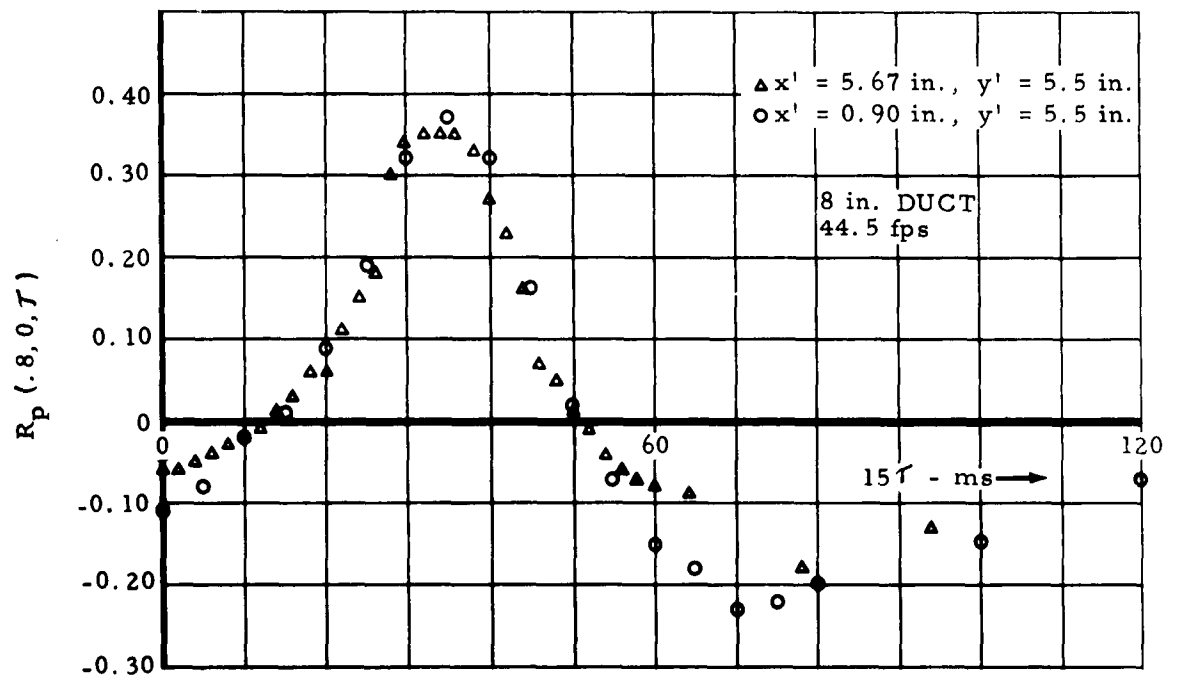
FIGURE 20   HOMOGENEITY CHARACTERISTICS OF THE DUCT
WALL PRESSURE FIELD
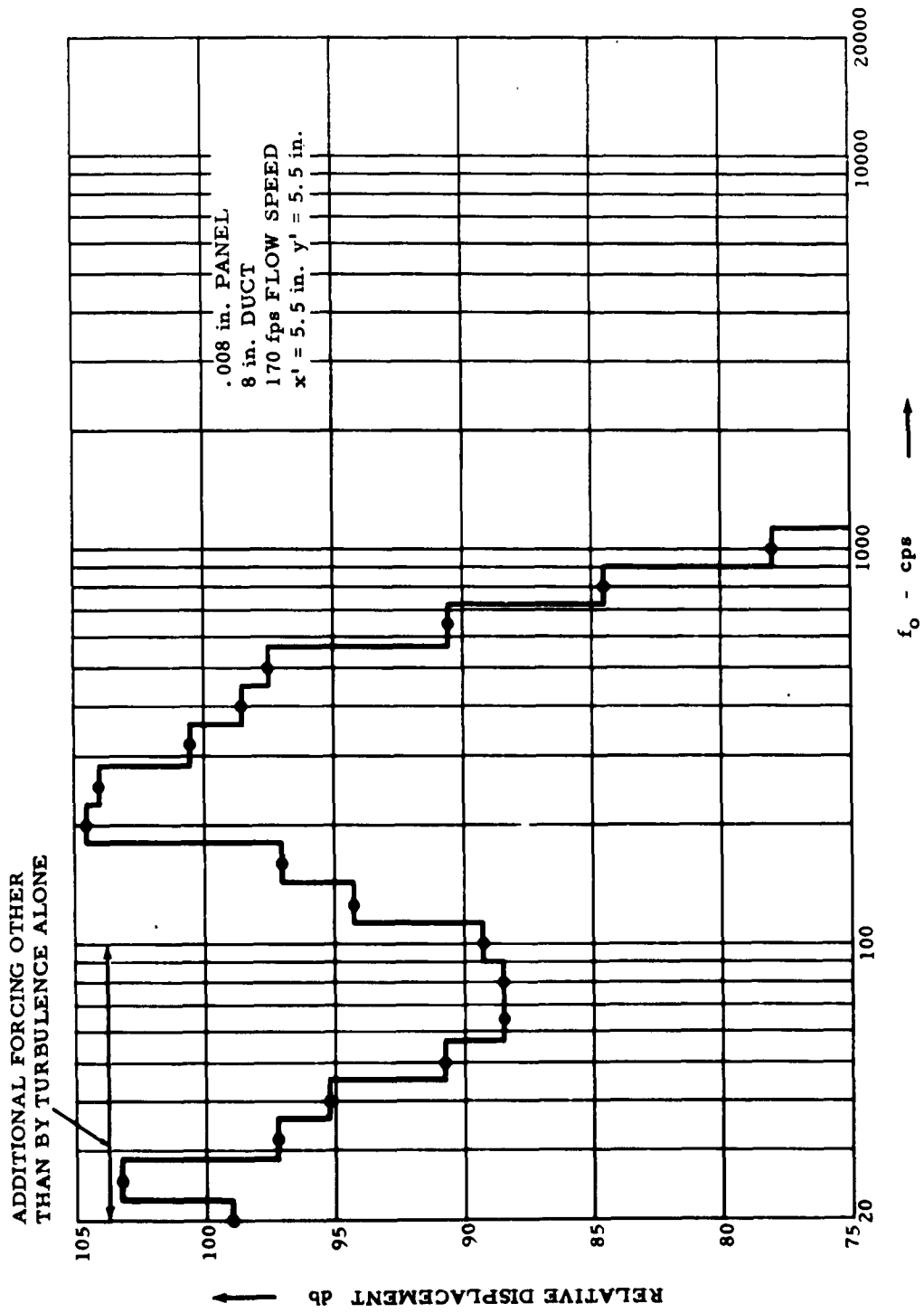
FIGURE 21A   PANEL VIBRATION FREQUENCY RESPONSE   1/3 OCTAVE

ADDITIONAL FORCING OTHER
THAN BY TURBULENCE ALONE

.002 in. PANEL
8 in. DUCT
189 fps FLOW SPEED
x' = 5.5 in., y' = 5.5 in.

f_o - cps

RELATIVE DISPLACEMENT - db

FIGURE 21B   PANEL VIBRATION FREQUENCY RESPONSE, 1/3 OCTAVE

.002 in. PANEL
8 in. DUCT
170 fps FLOW SPEED
x' = 5.5 in., y' = 5.5 in.

RELATIVE DISPLACEMENT - db

f_o - cps
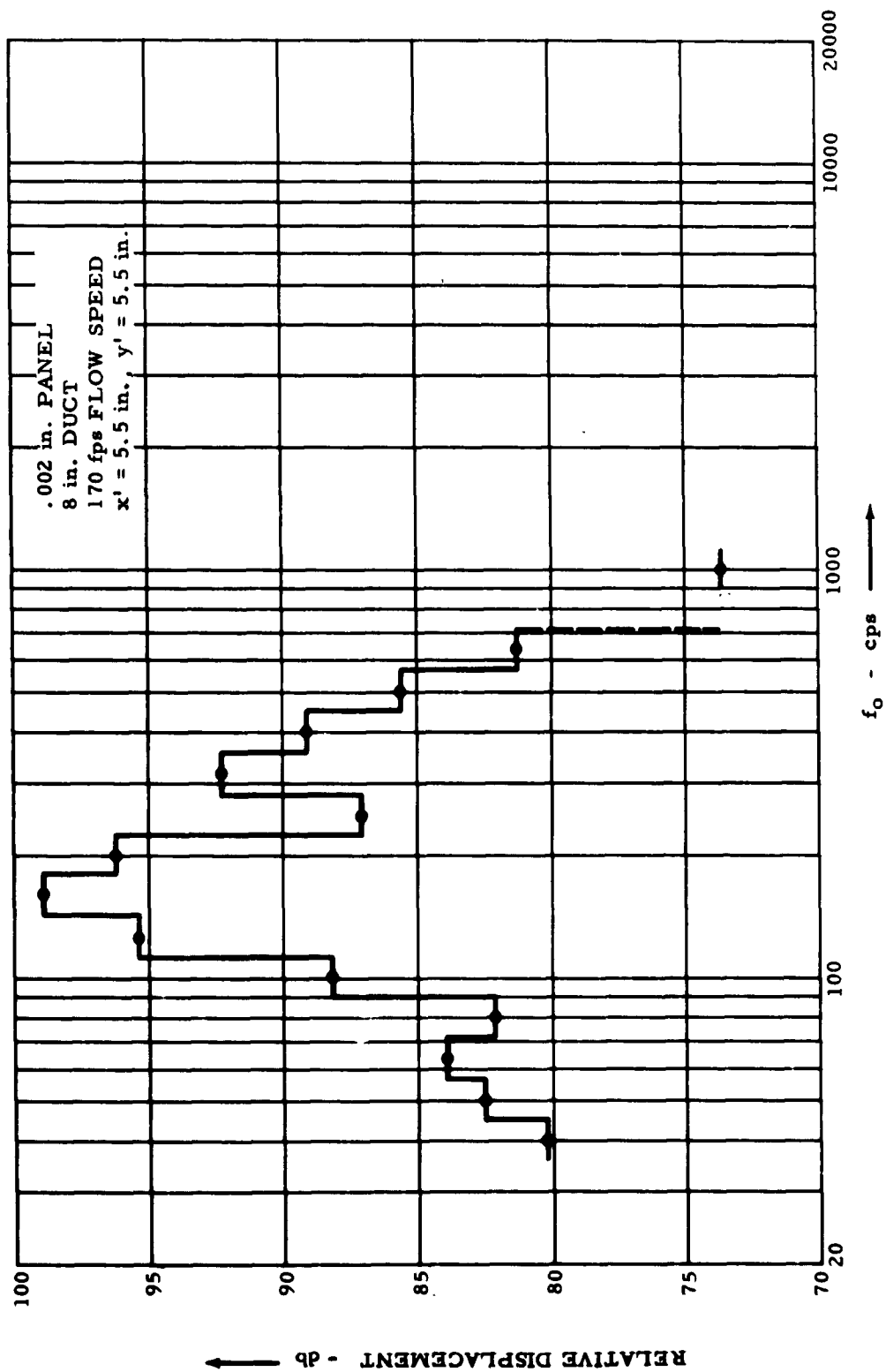
FIGURE 21C   PANEL VIBRATION FREQUENCY RESPONSE, 1/3 OCTAVE
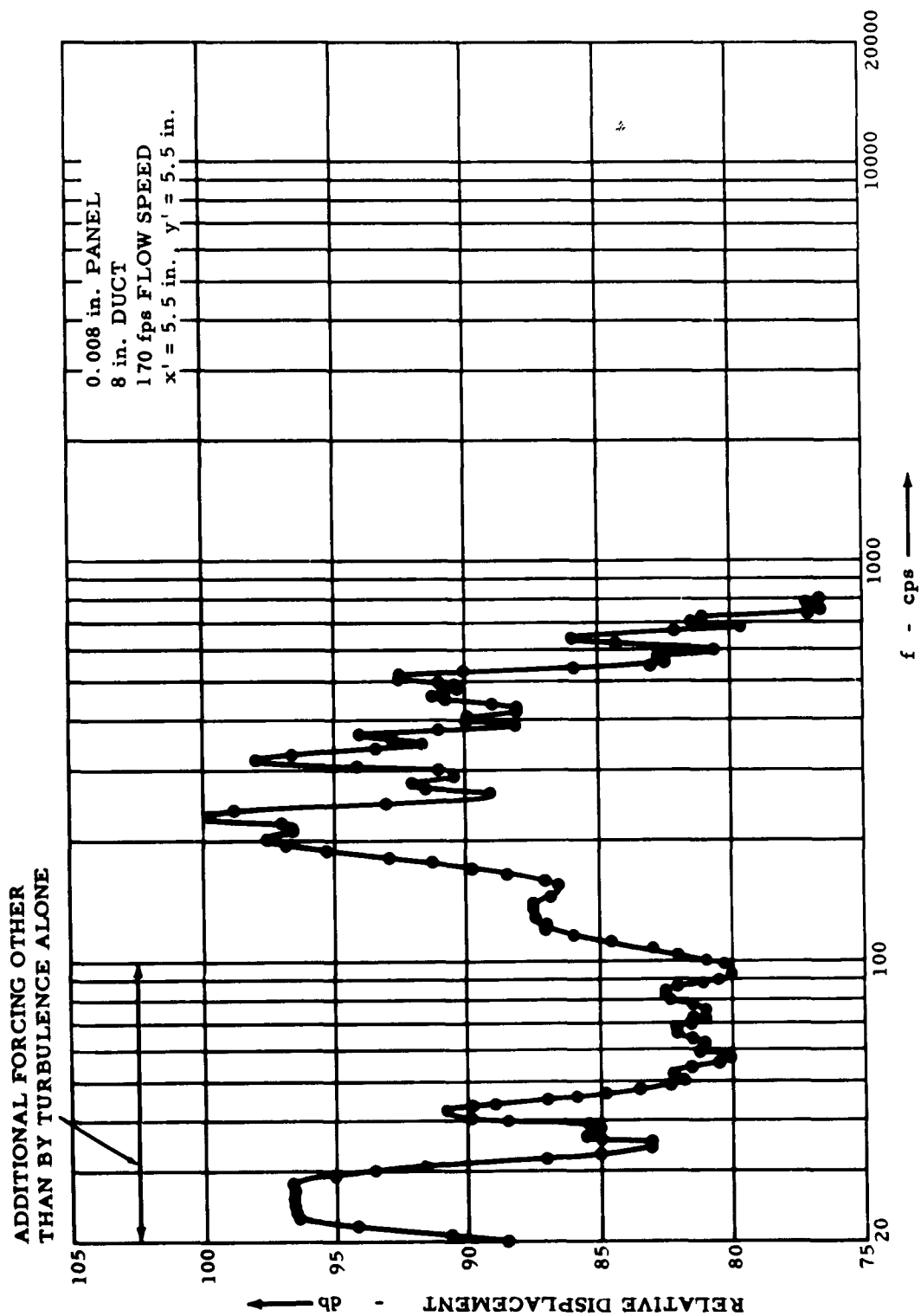
FIGURE 22A   PANEL VIBRATION FREQUENCY RESPONSE, NARROW BAND
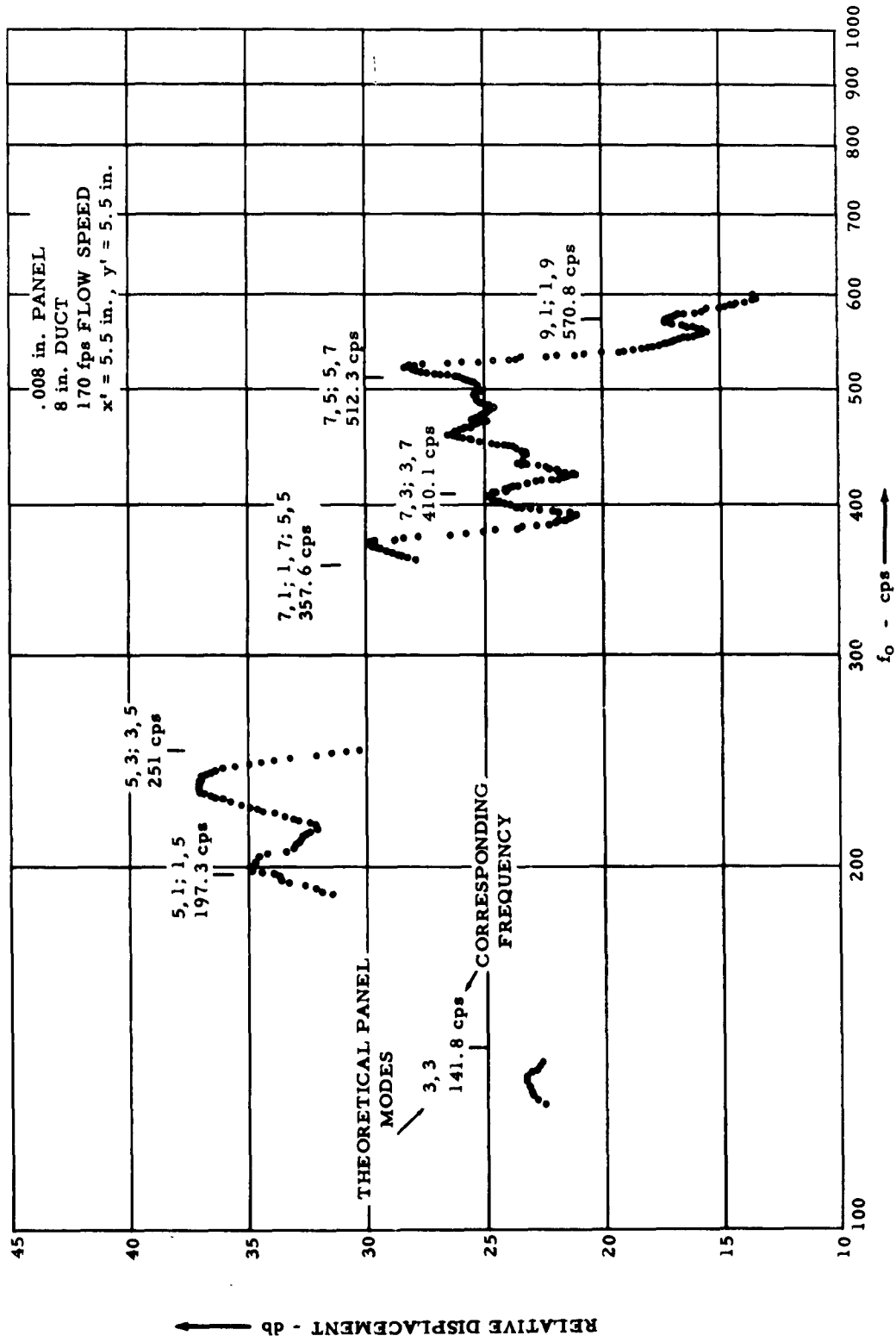
FIGURE 22B   PANEL VIBRATION FREQUENCY RESPONSE,
IN-TUNE HIGH SELECTIVITY
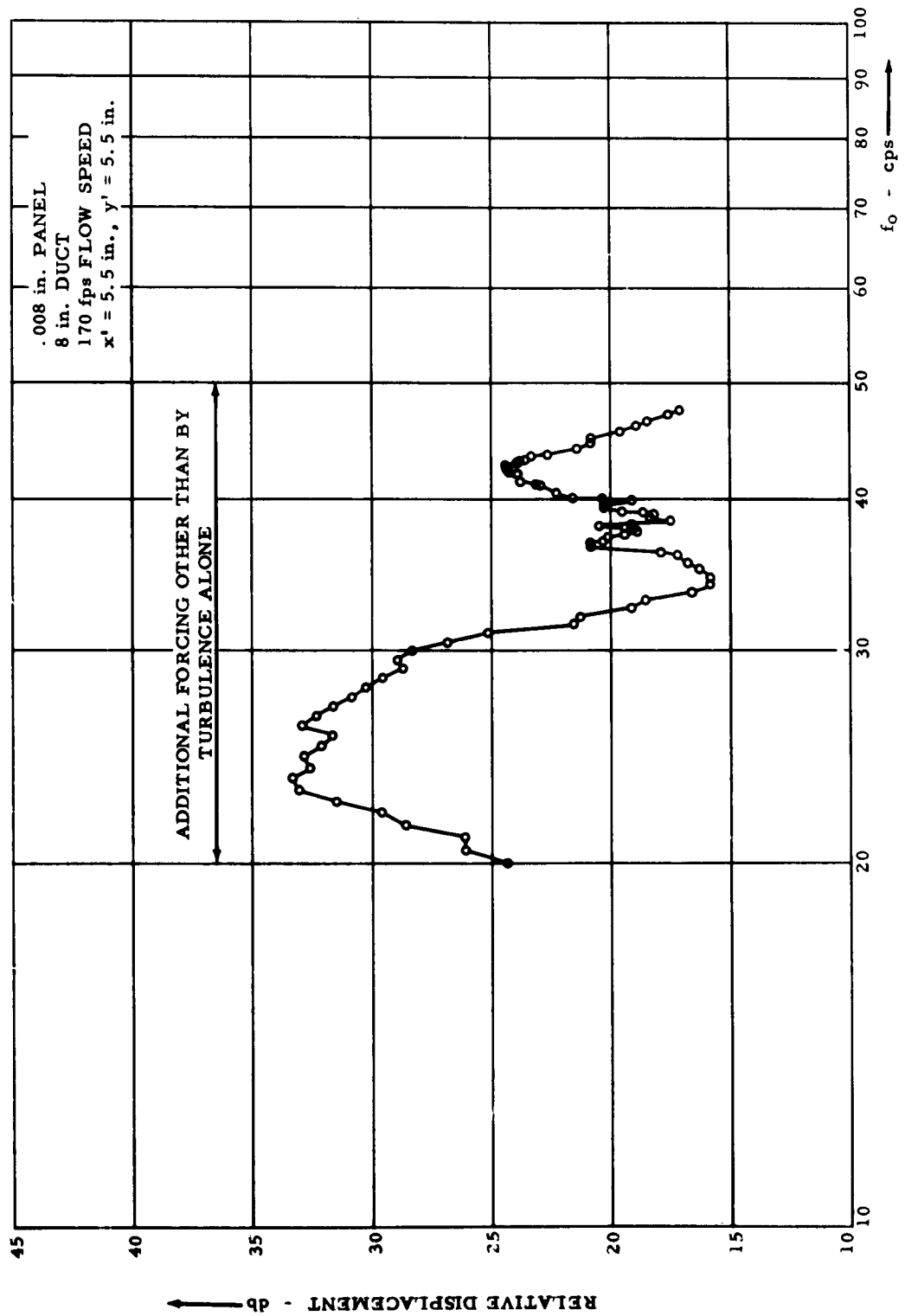
FIGURE 22C   PANEL VIBRATION FREQUENCY RESPONSE,
IN-TUNE HIGH SELECTIVITY
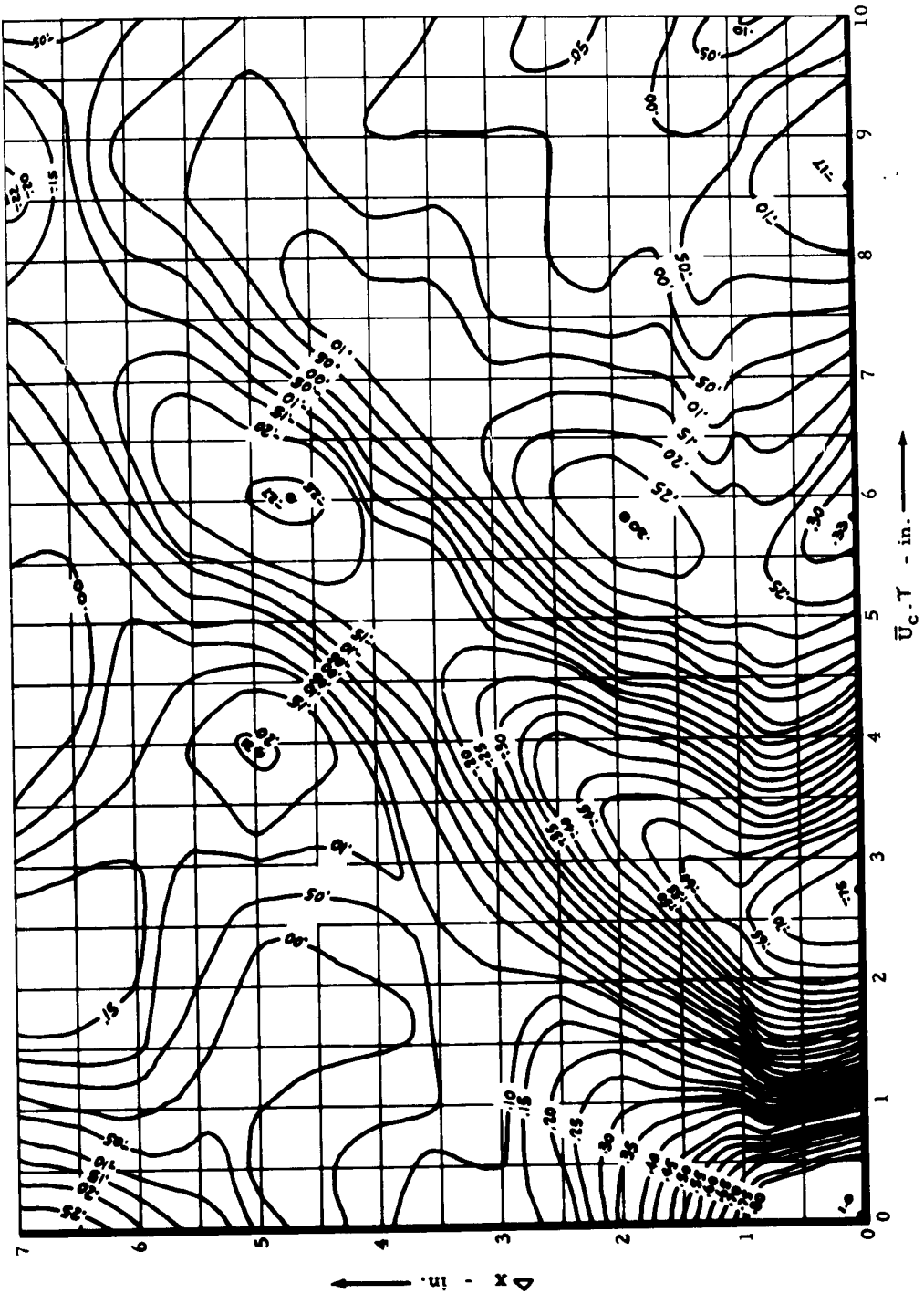
.008 in. PANEL, 170 fps FLOW SPEED, 8 in. DUCT, $\bar{U}_c/U = 0.74$

FIGURE 23   LINES OF CONSTANT LONGITUDINAL CORRELATION
PANEL VIBRATION
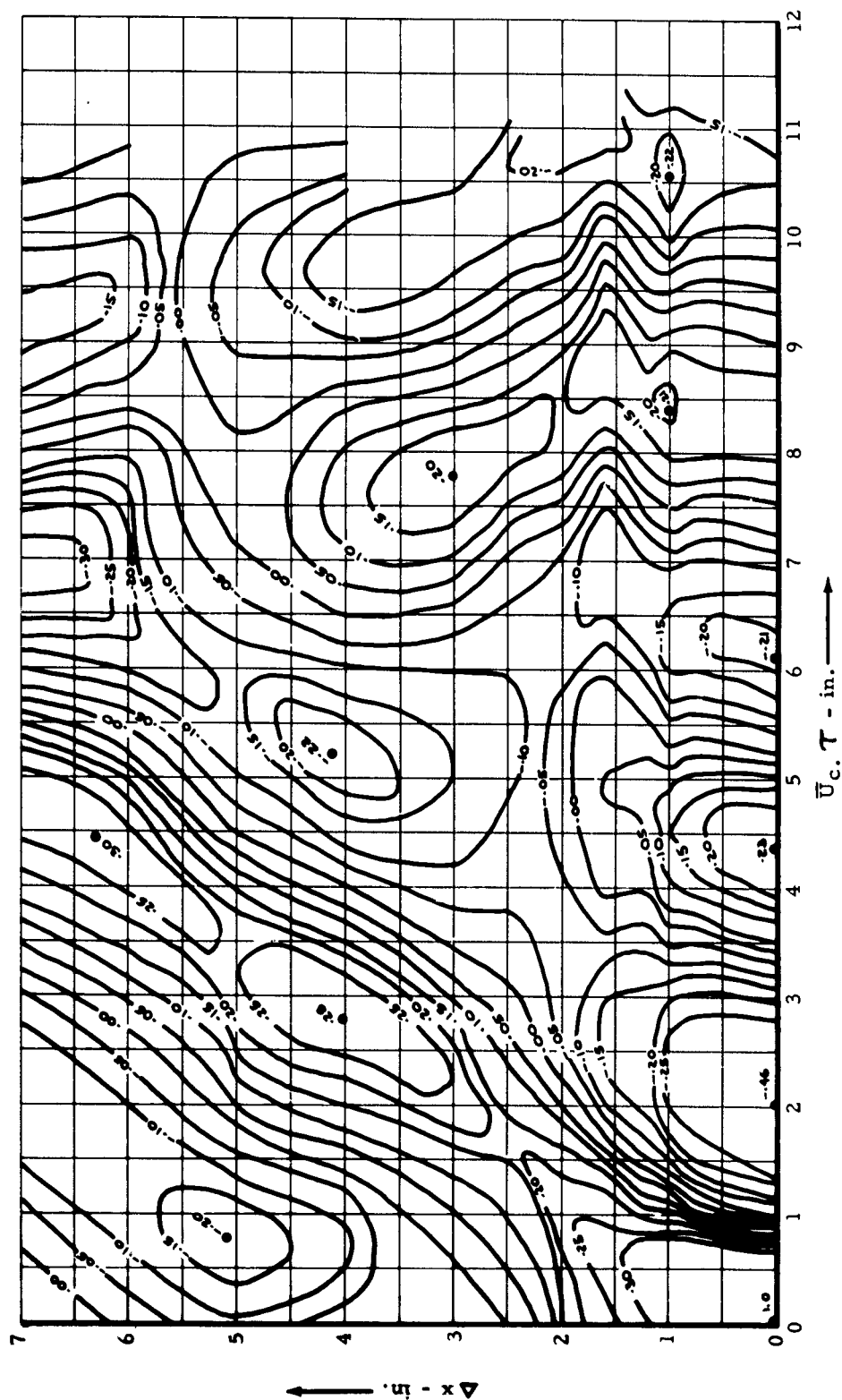
.002 in. PANEL, 189 fps. FLOW SPEED, 1 in. DUCT, $\bar{U}_c/U = 0.74$

FIGURE 24   LINES OF CONSTANT LONGITUDINAL CORRELATION,
PANEL VIBRATION
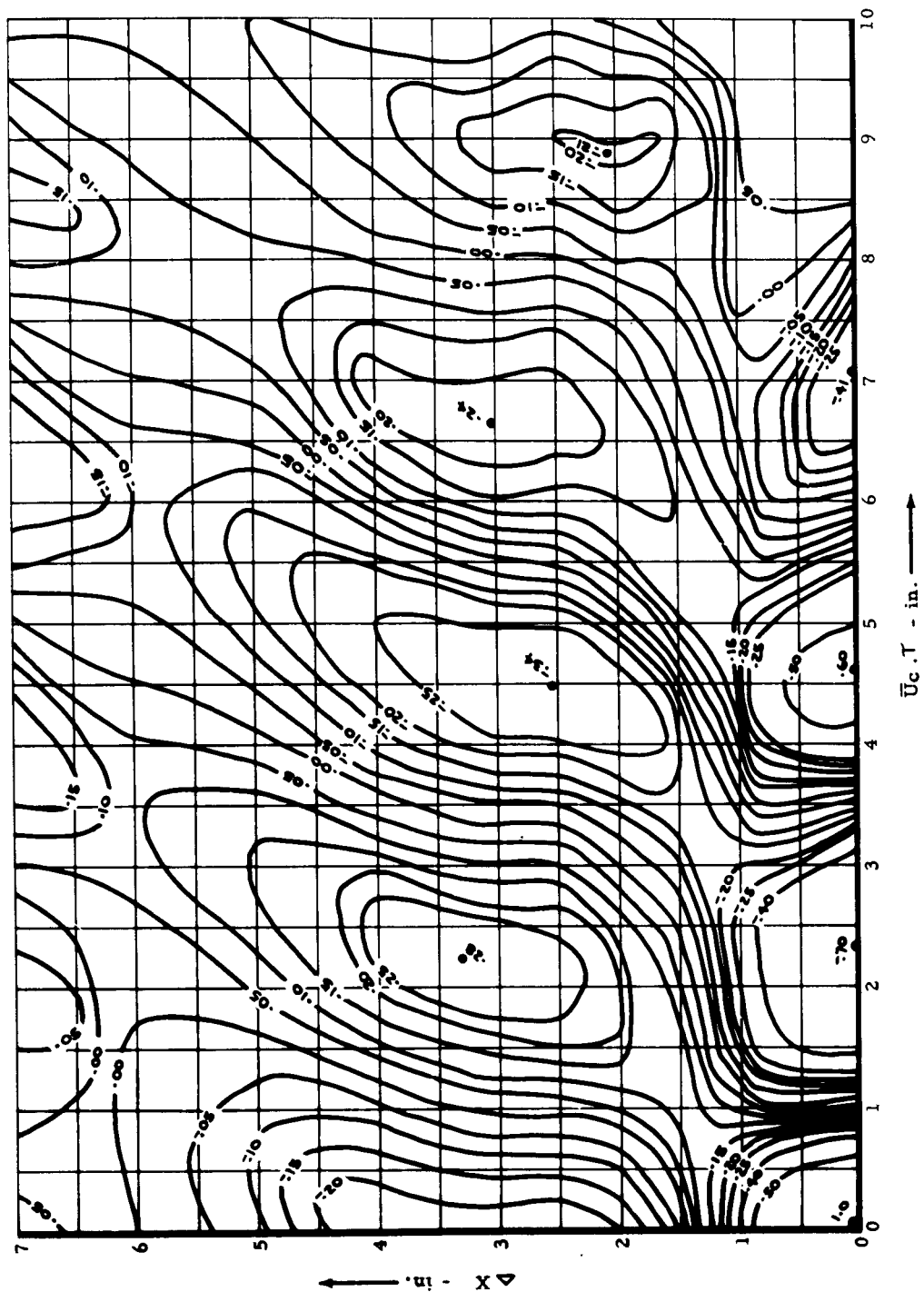
.002 in. PANEL, 84.8 fps FLOWSPEED, 1 in. DUCT, $\bar{U}_c/U = 0.74$

FIGURE 25   LINES OF CONSTANT LONGITUDINAL CORRELATION
PANEL VIBRATION
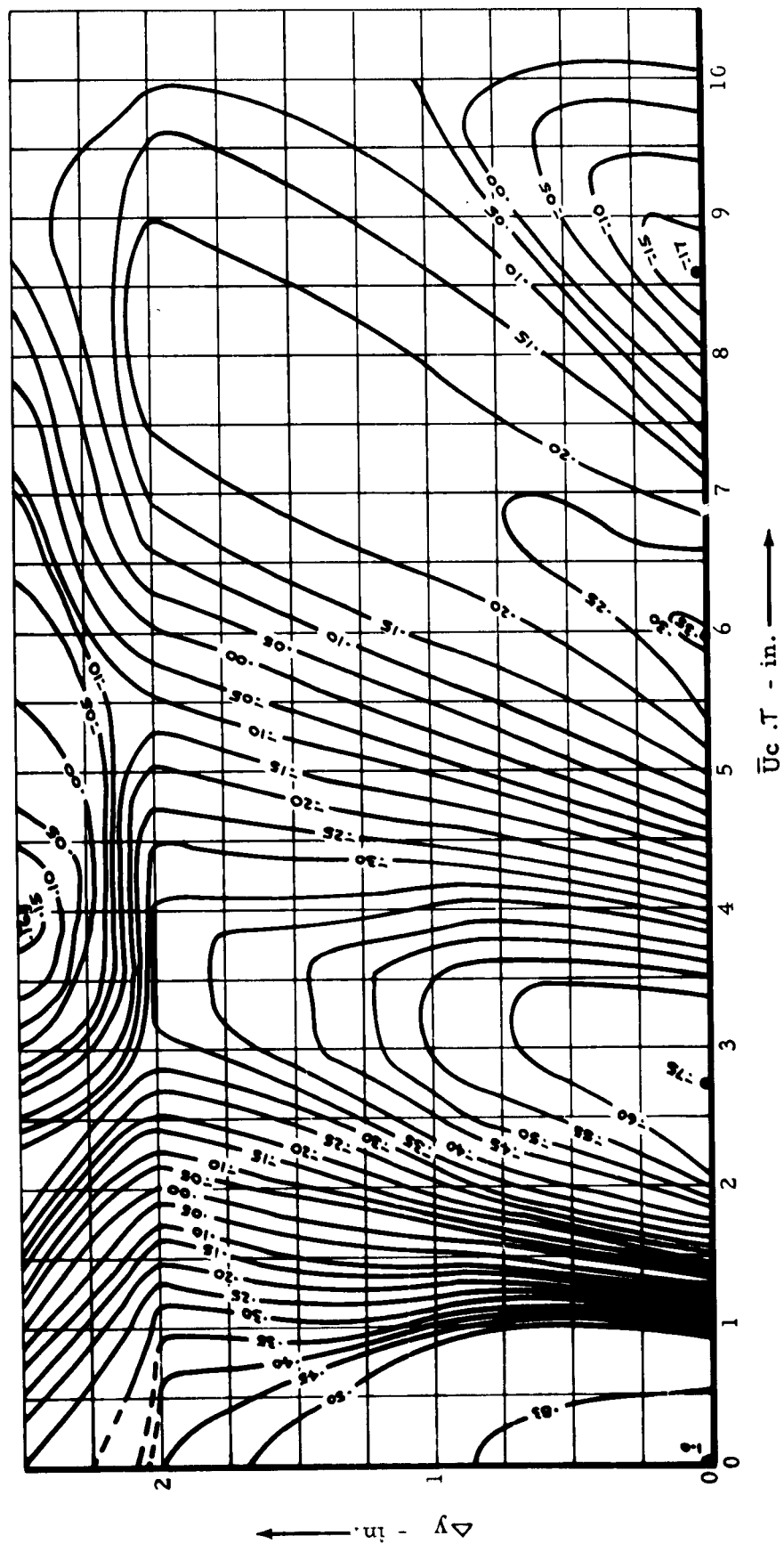
.008 in. PANEL, 170 fps FLOWSPEED, 8 in. DUCT, $\bar{U}_c/U = 0.74$

FIGURE 26   LINES OF CONSTANT LATERAL CORRELATION
PANEL VIBRATION
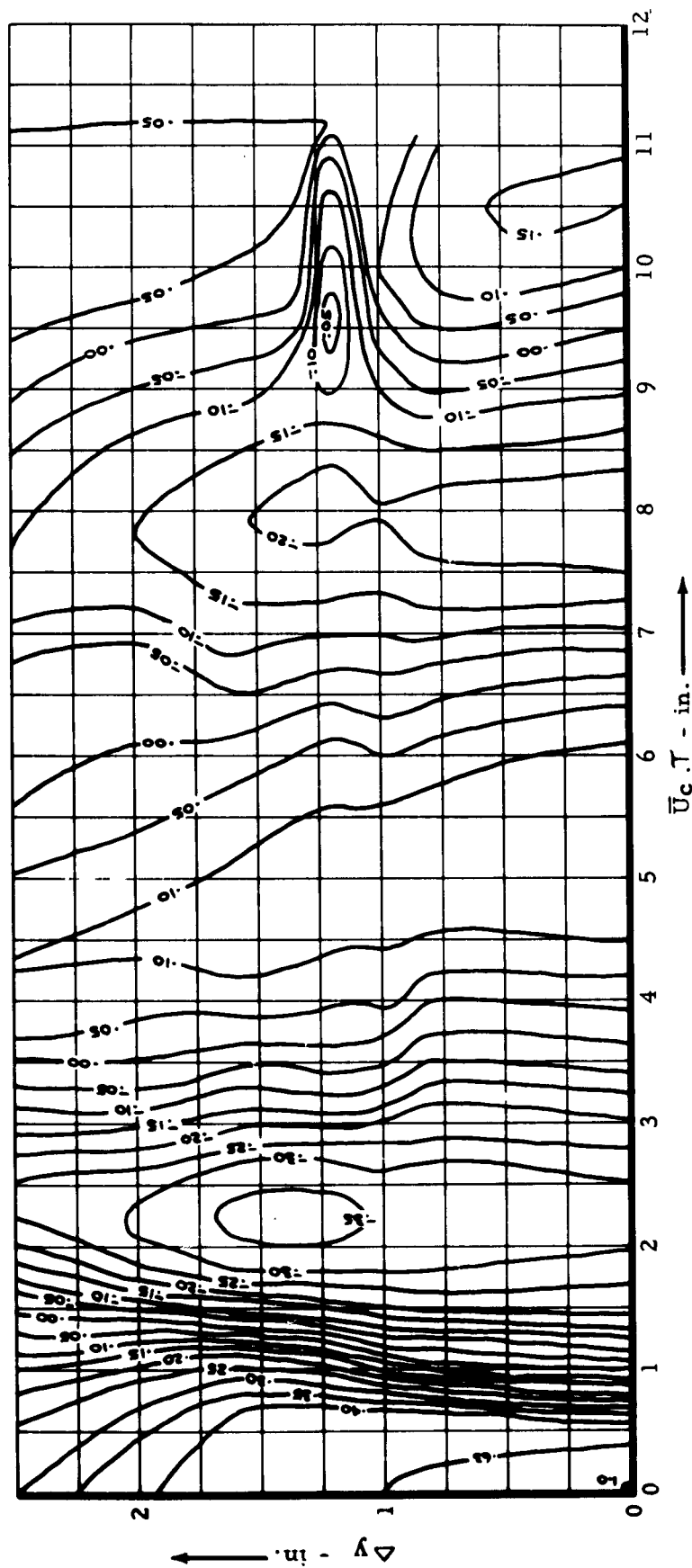
.002 in. PANEL, 189 fps FLOWSPEED, 1 in. DUCT, $\bar{U}_c/U = 0.74$

FIGURE 27   LINES OF CONSTANT TRANSVERSE CORRELATION
PANEL VIBRATION
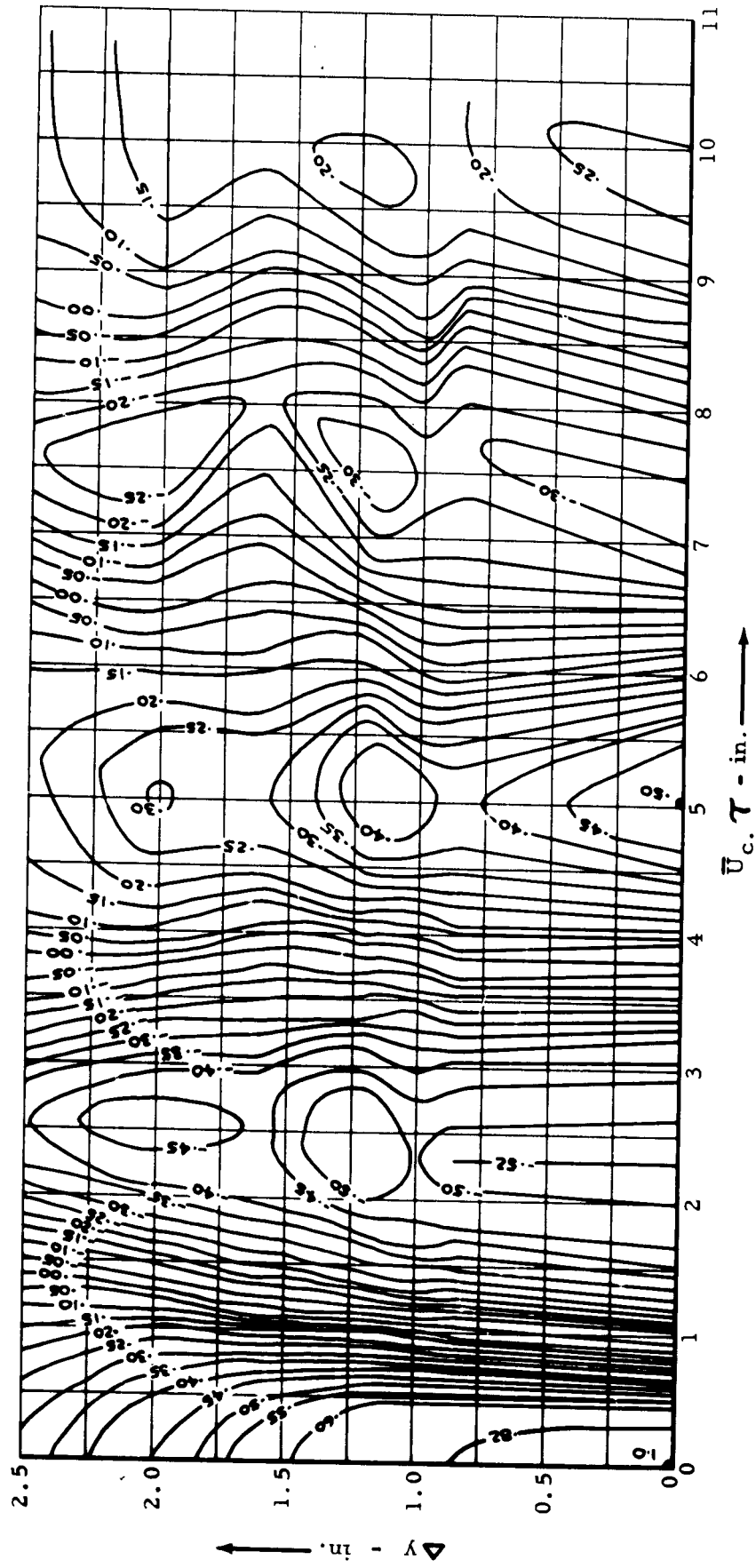
.002 in. PANEL, 84.8 fps. FLOW SPEED, 1 in. DUCT, $\overline{U}_c/U = 0.74$

FIGURE 28   LINES OF CONSTANT TRANSVERSE CORRELATION,
PANEL VIBRATION
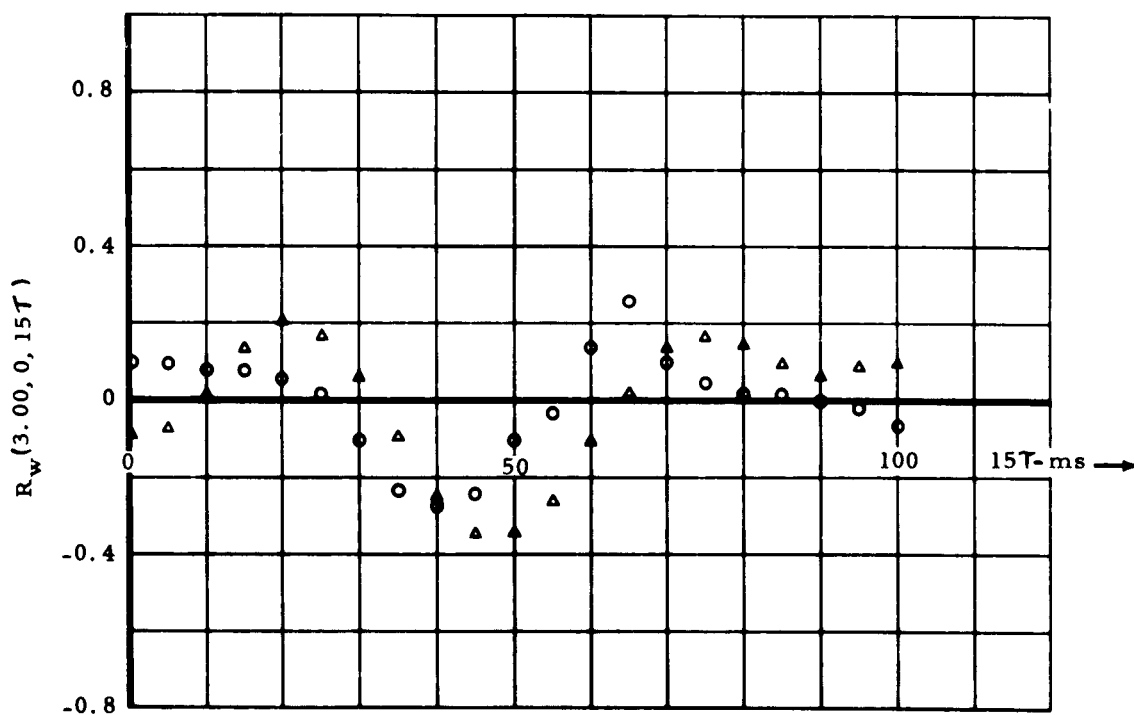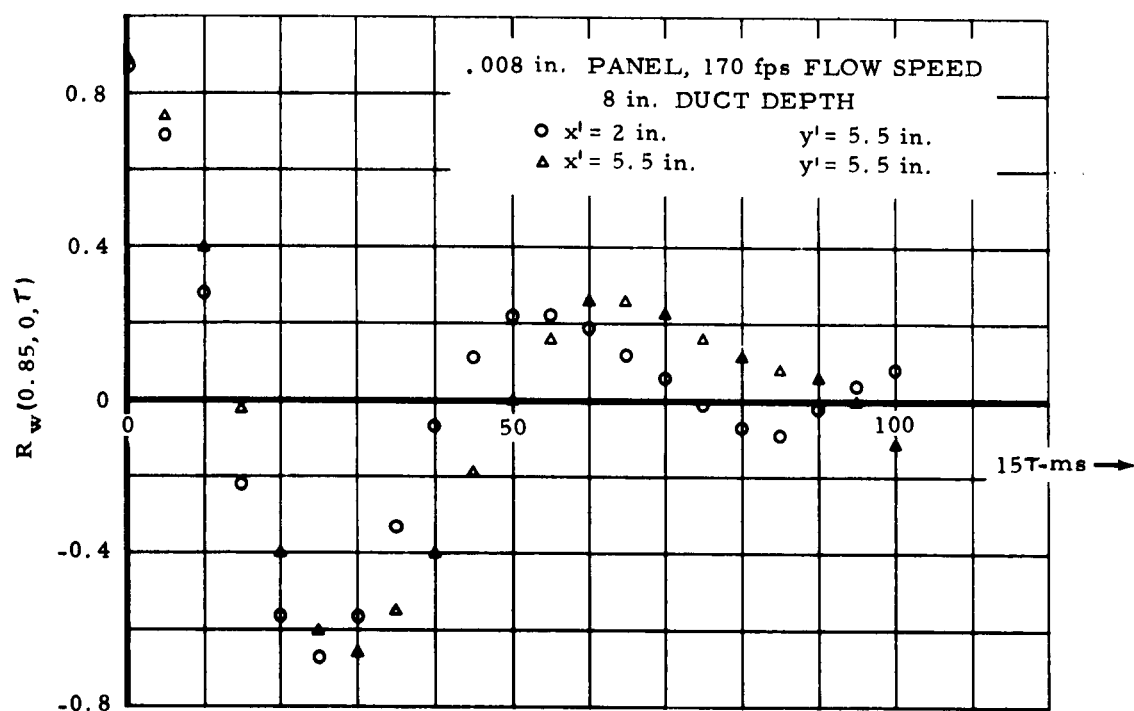
FIGURE 29   LONGITUDINAL TWO-POINT SPACE-TIME CORRELATION
OF THE PANEL VIBRATION
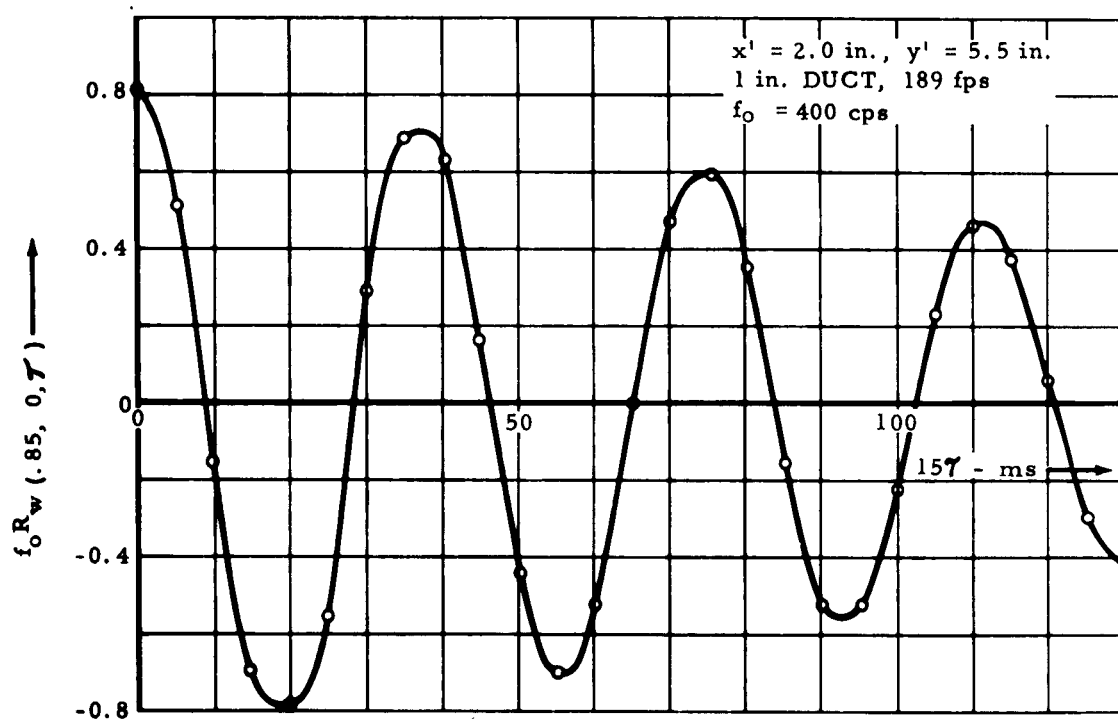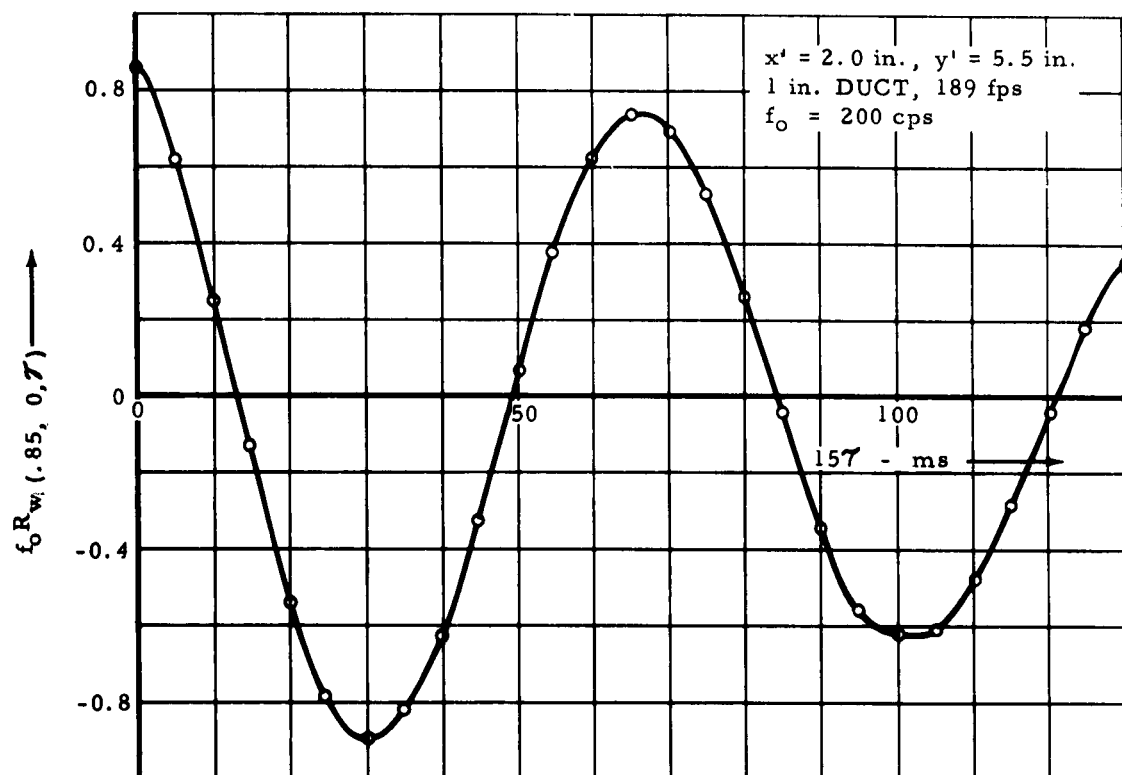
FIGURE 30   LONGITUDINAL TWO-POINT SPACE-TIME
CORRELATION OF THE PANEL VIBRATION
IN 1/3 OCTAVE BANDS
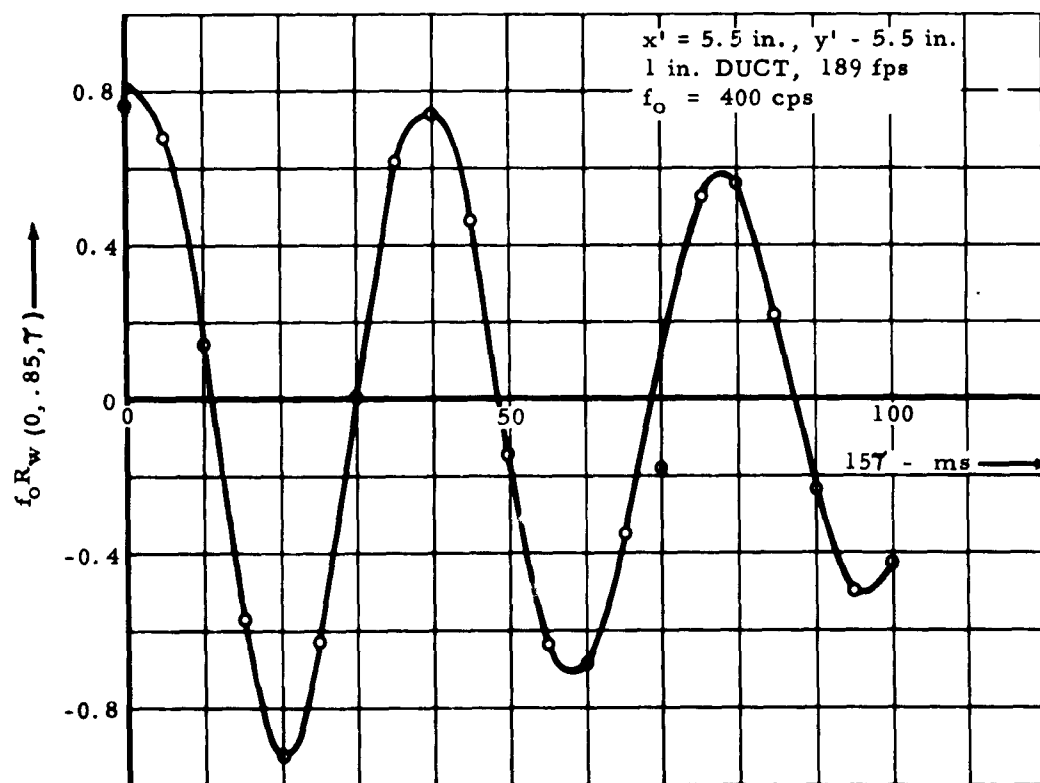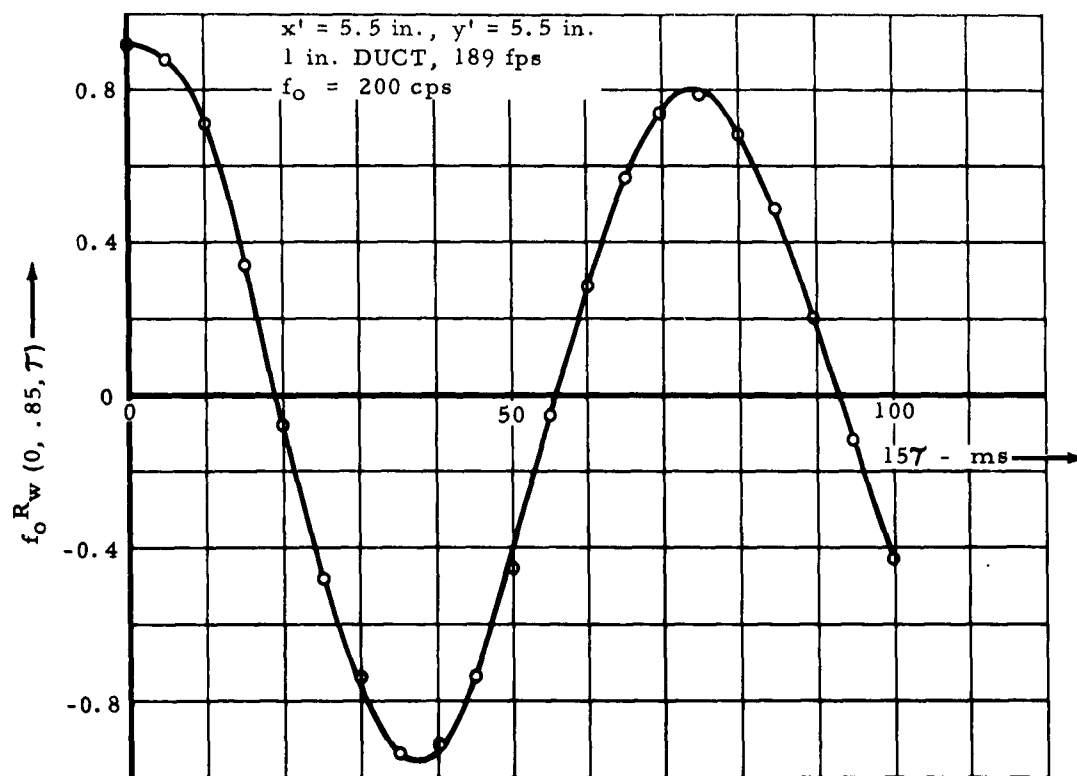
FIGURE 3) LATERAL TWO-POINT SPACE-TIME CORRELATION
OF THE PANEL VIBRATION IN 1/3 OCTAVE BANDS
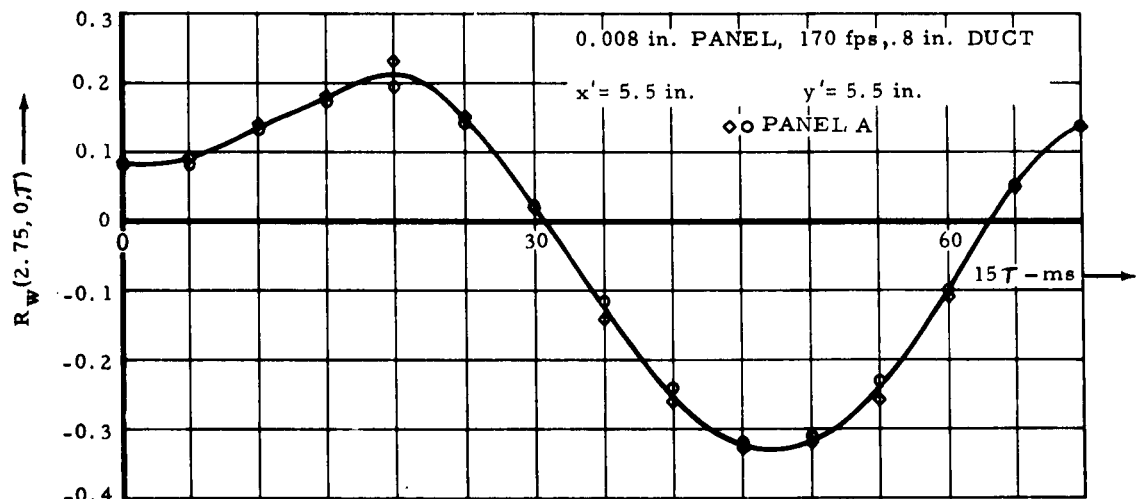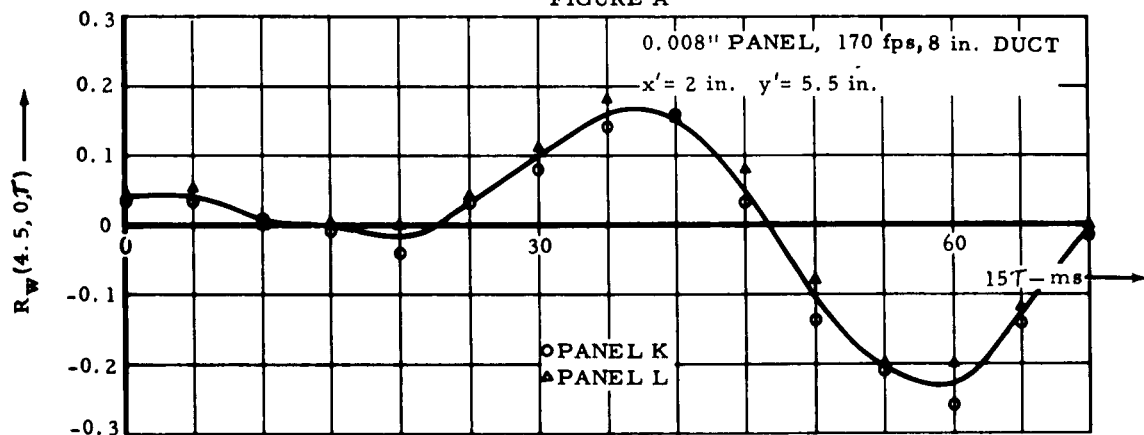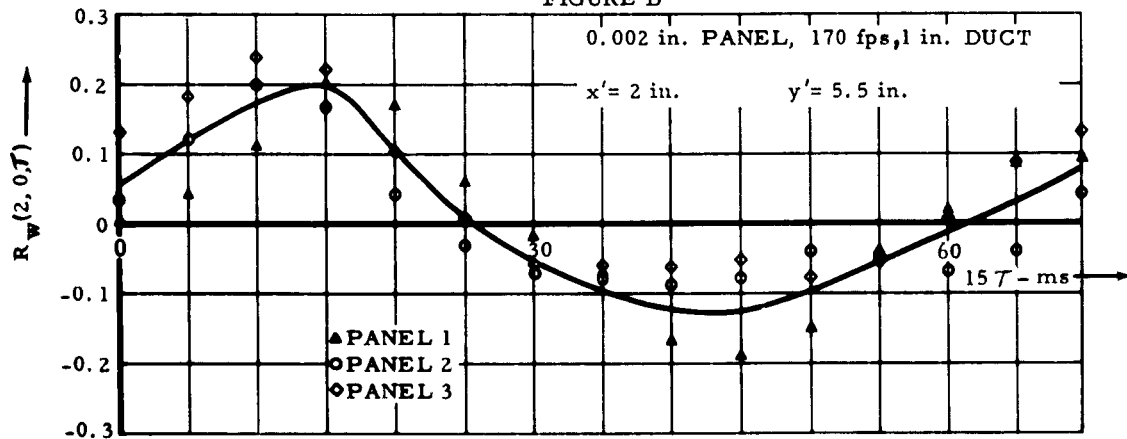
FIGURE 32A   PANEL VIBRATION REPEATABILITY TESTS:
1 PANEL, 2 SIGNAL SAMPLES
FIGURE 32B, C   PANEL VIBRATION REPEATABILITY TESTS:
3 DIFFERENT PANELS
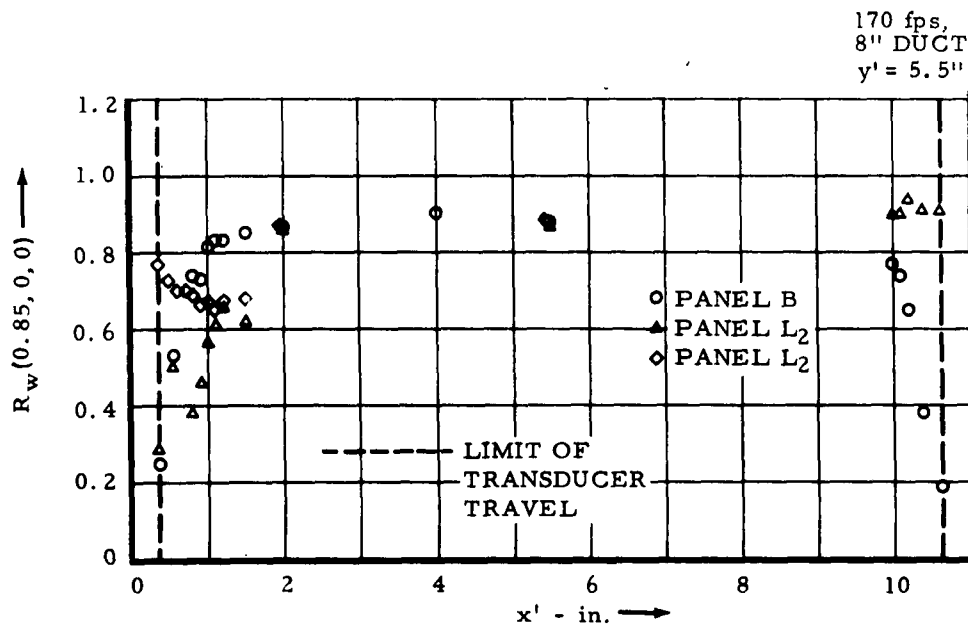
FIGURE 33 A
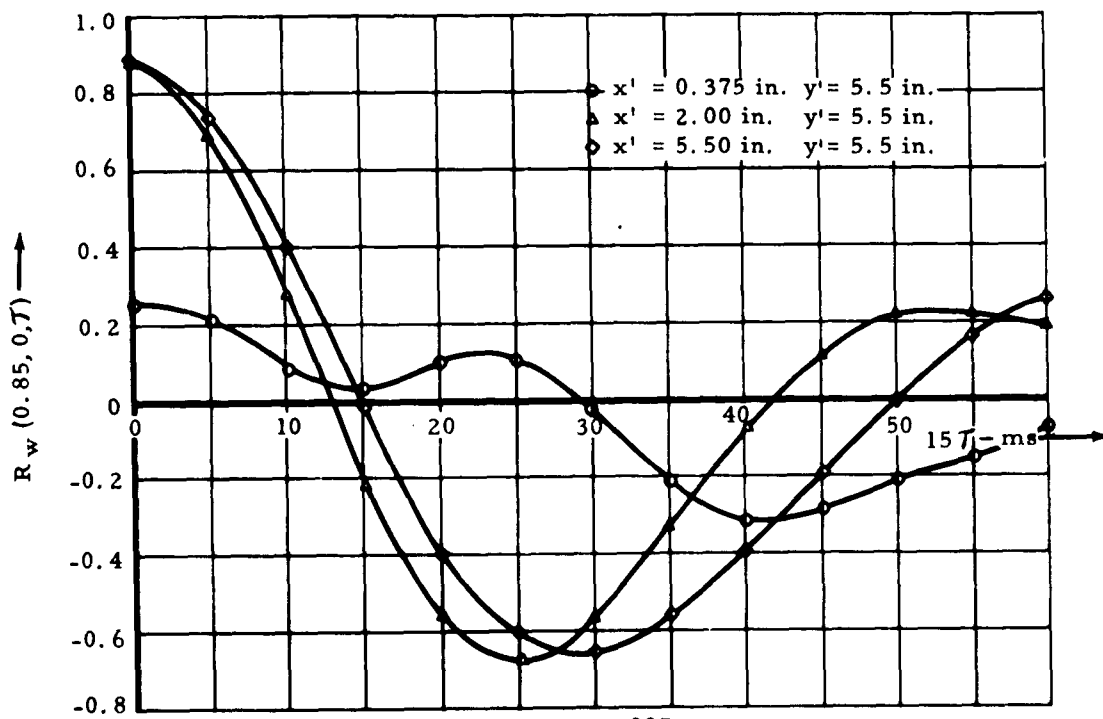
FIGURE 33B

8" DUCT, 170 fps,

FIGURE 33A, B   THE EFFECT OF EDGE CLAMPING AND BENDING ON
THE PANEL DISPLACEMENT CORRELATION, 0.008 in.
PANEL
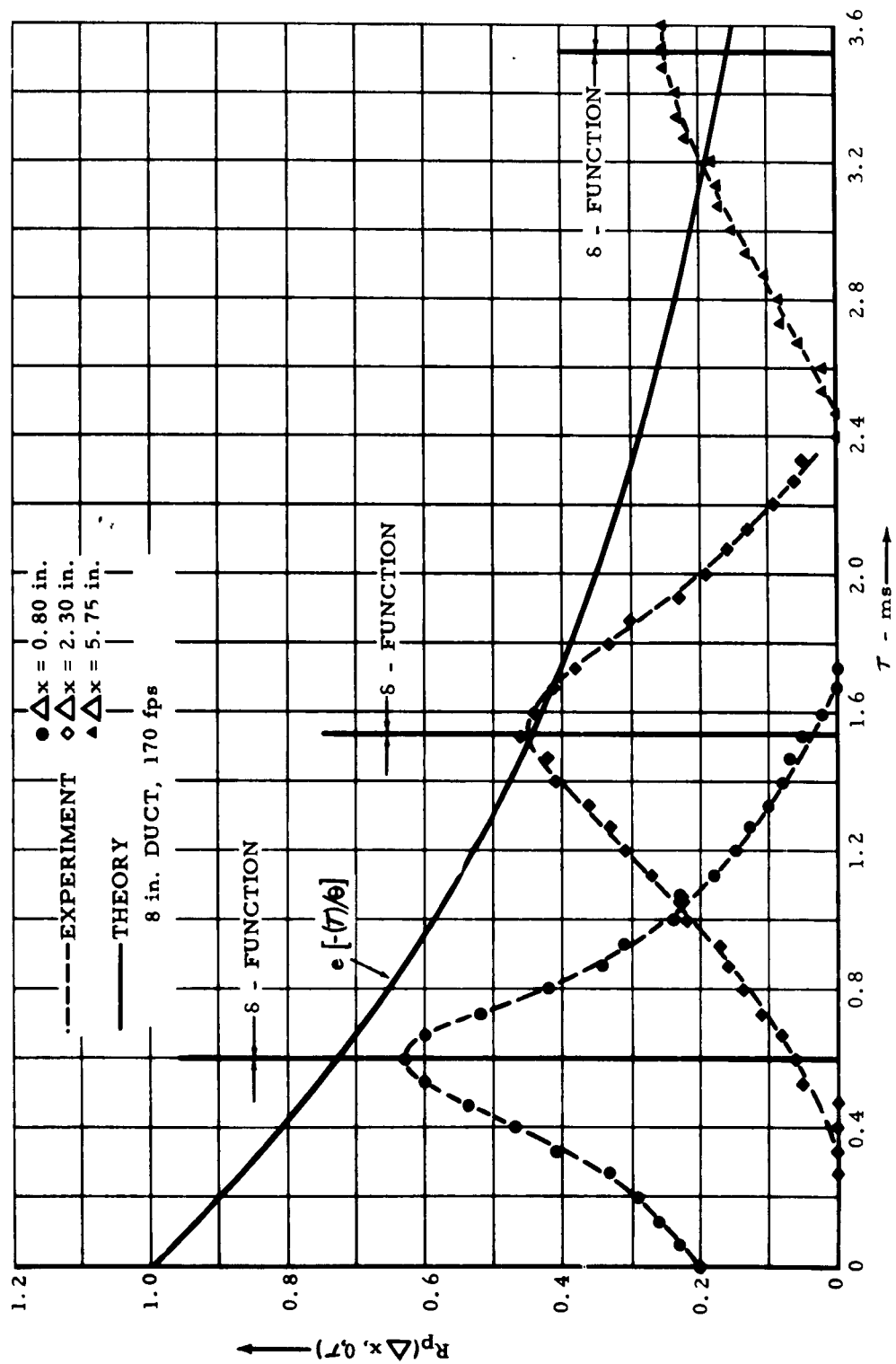
FIGURE 34   COMPARISON OF THE δ-FUNCTION PRESSURE
CORRELATION WITH ITS EXPERIMENTAL
COUNTERPART

$\sim a_{mn} = 0.478 \ \omega_{mn}^{1/3}$

$\sim a_{mn} = \dfrac{3100}{\omega_{mn}}$

f - cps

a_{mn}
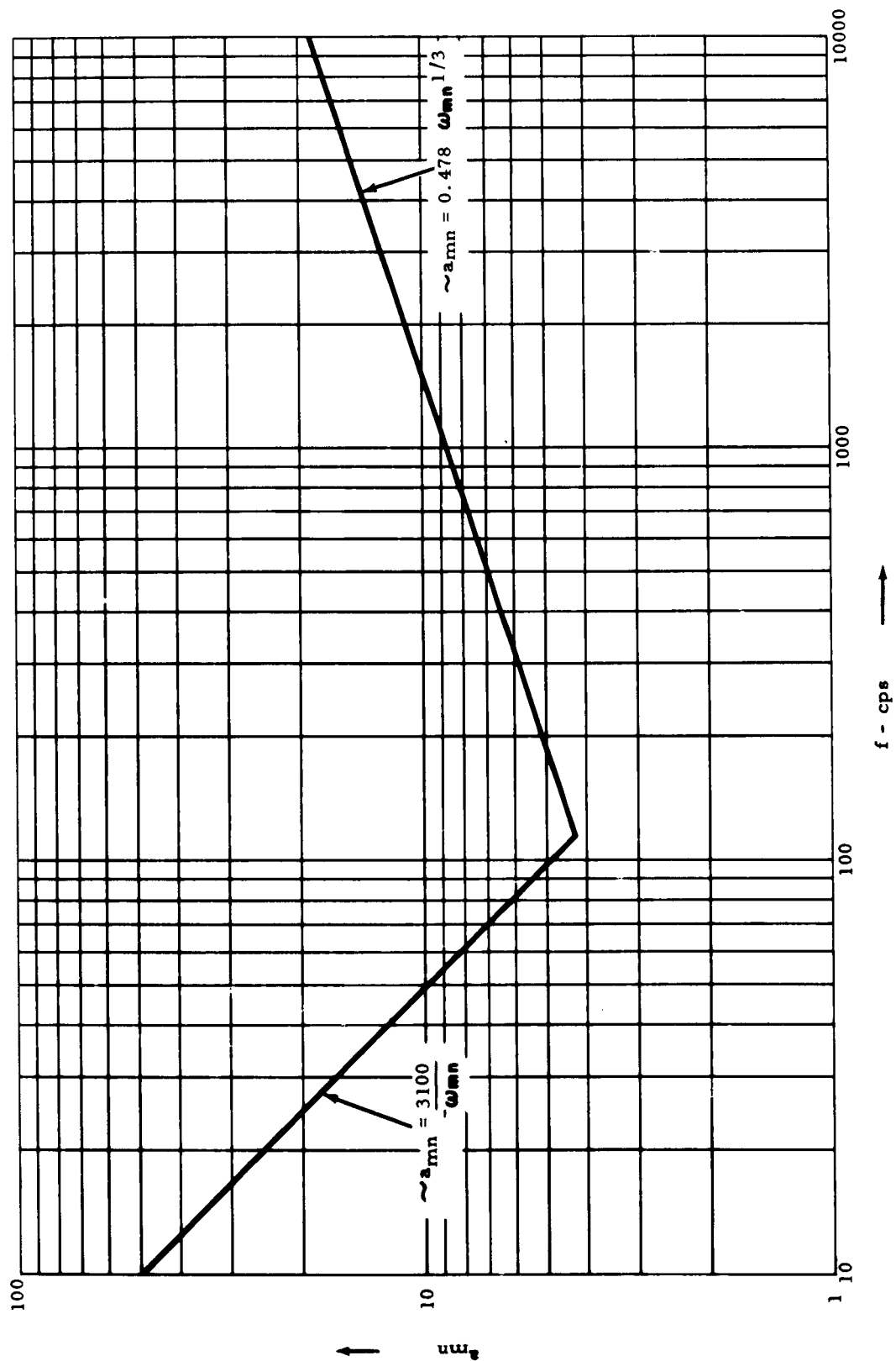
FIGURE 35   THE MODAL DAMPING FOR AN 0.008 INCH STEEL PANEL
(BASED ON EXPERIMENTAL DATA FROM UTIA REPT. NO. 87)

$$\frac{U_p}{U_c} = \cos \gamma = \frac{\lambda}{\lambda_x}$$

$$\therefore \quad U_p^2 = \sqrt{\frac{B}{M}} \, \omega_{mn}$$

$$\therefore \quad \omega_{mn} = \sqrt{\frac{M}{B}} \, U_c^2 \cos^2 \gamma$$
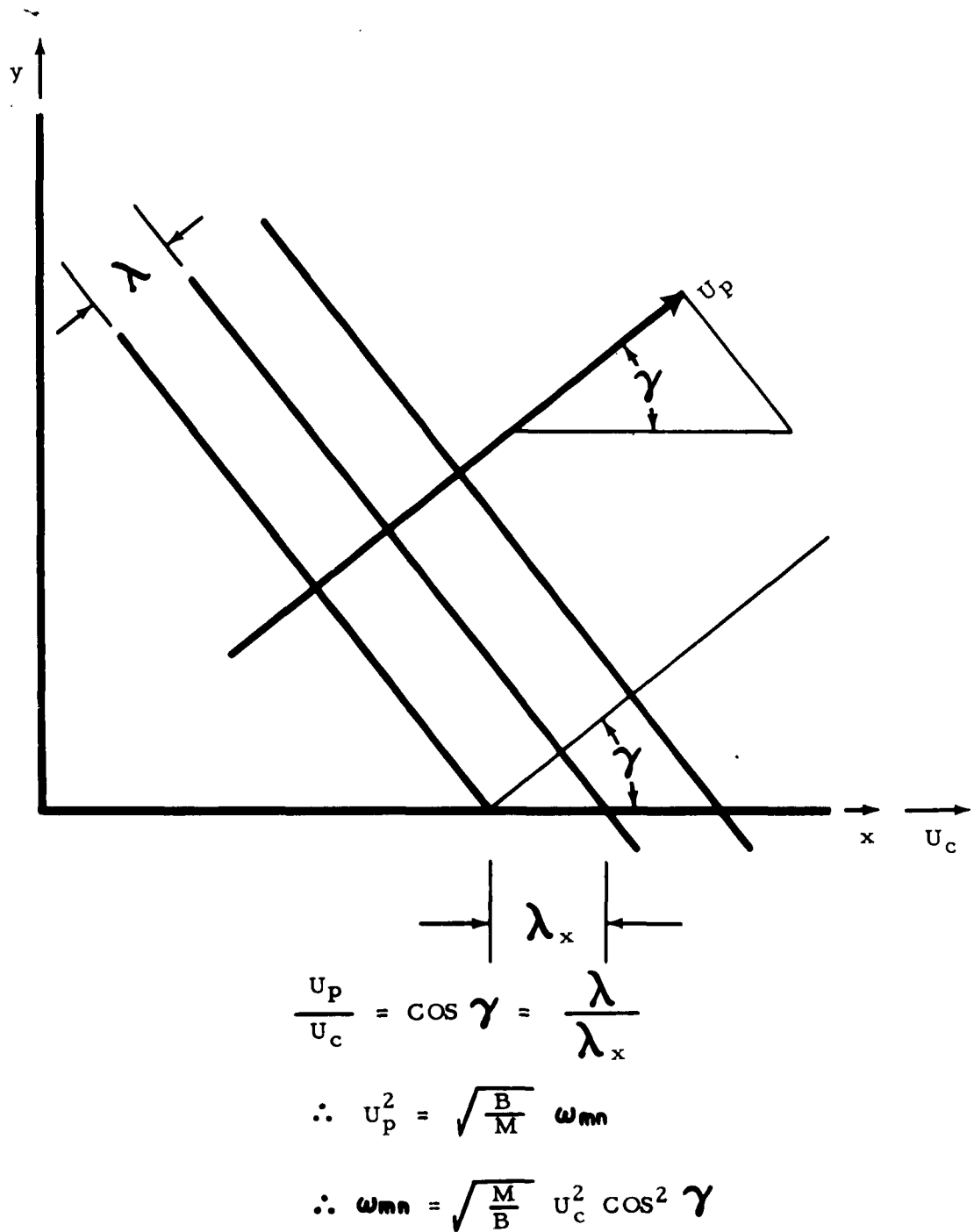
FIGURE 36   PRESSURE AND FLEXURAL WAVE MATCHING
PROCESS AT COINCIDENCE
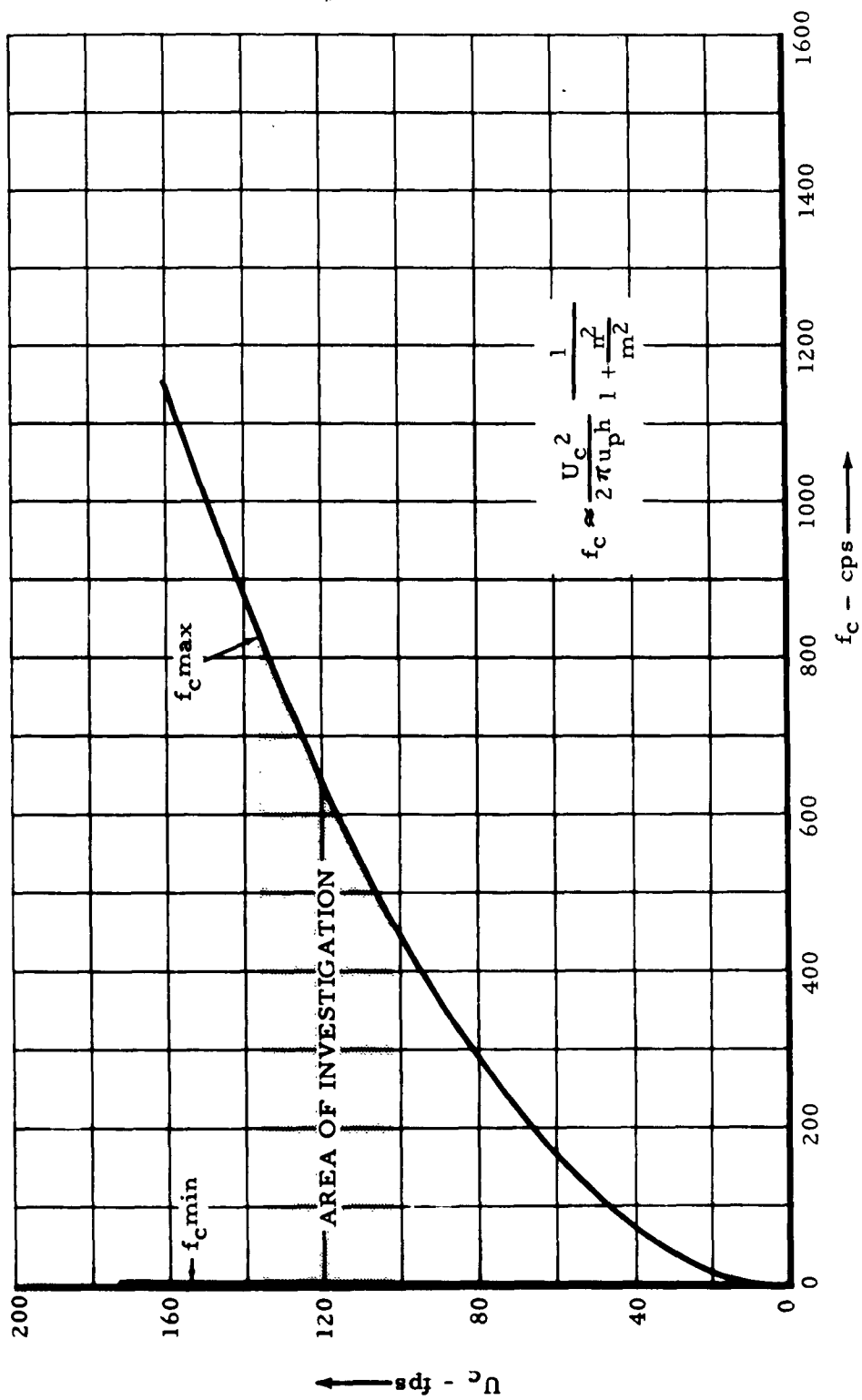
FIGURE 37 COINCIDENCE FREQUENCY RANGE FOR AN 0.008 in.
STEEL PANEL (SQUARE)

$$f_c \approx \frac{U_c^2}{2\tau u_p h} \; \frac{1}{1 + \frac{n^2}{m^2}}$$

f_c — cps

U_c — fps

.008 in. PANEL
8 in. DUCT
170 fps FLOW SPEED
$x' = 5.5$ in., $y' = 5.5$ in.
$M, N, P = 11, 11, 11$
$\sqrt{\overline{w^2}} = .001832$ in.

f - cps

RELATIVE DISPLACEMENT - db
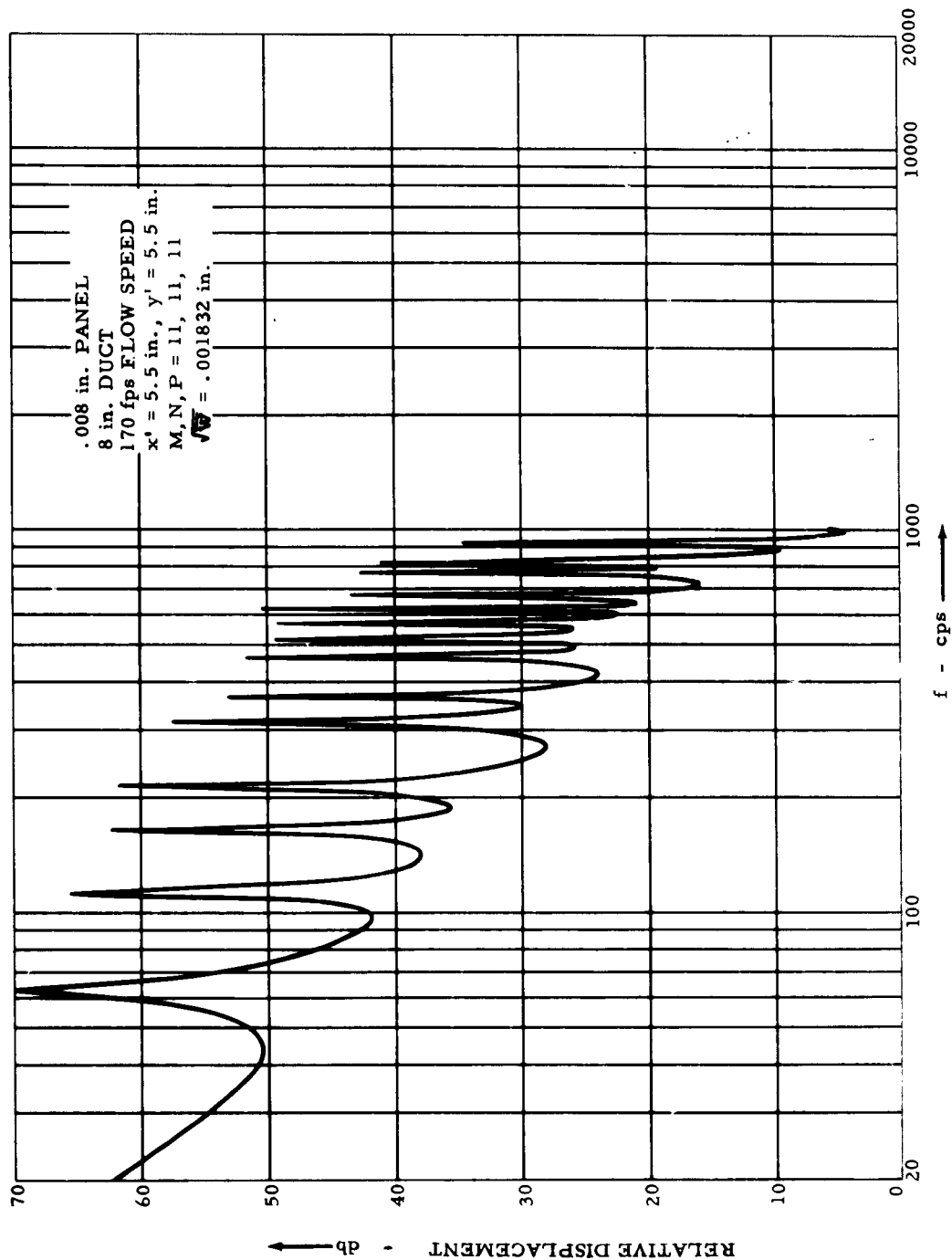
FIGURE 38   THEORETICAL PANEL VIBRATION FREQUENCY RESPONSE
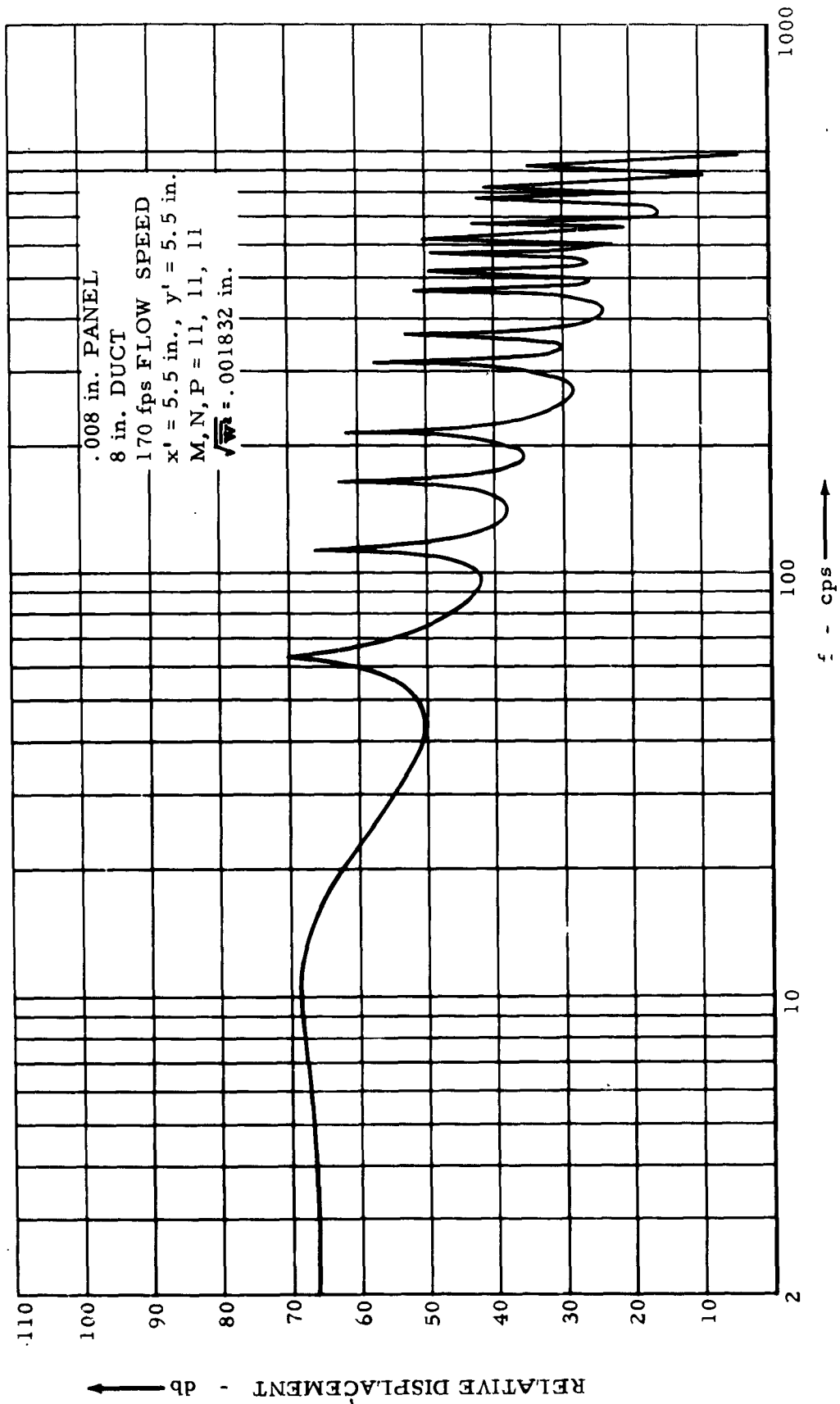
FIGURE 38 Continued. THEORETICAL PANEL VIBRATION FREQUENCY RESPONSE

.008 in. PANEL
8 in. DUCT
170 fps FLOW SPEED
x' = 5.5 in., y' - 5.5 in.
M, N, P ≡ 11, 11, 11
modes with frequencies
of 100 cps or less
excluded.
$\sqrt{\overline{W^2}}$ = .000620 in.

70
60
50
40
30
20
10

100
1000
10000

f - cps

RELATIVE DISPLACEMENT - db
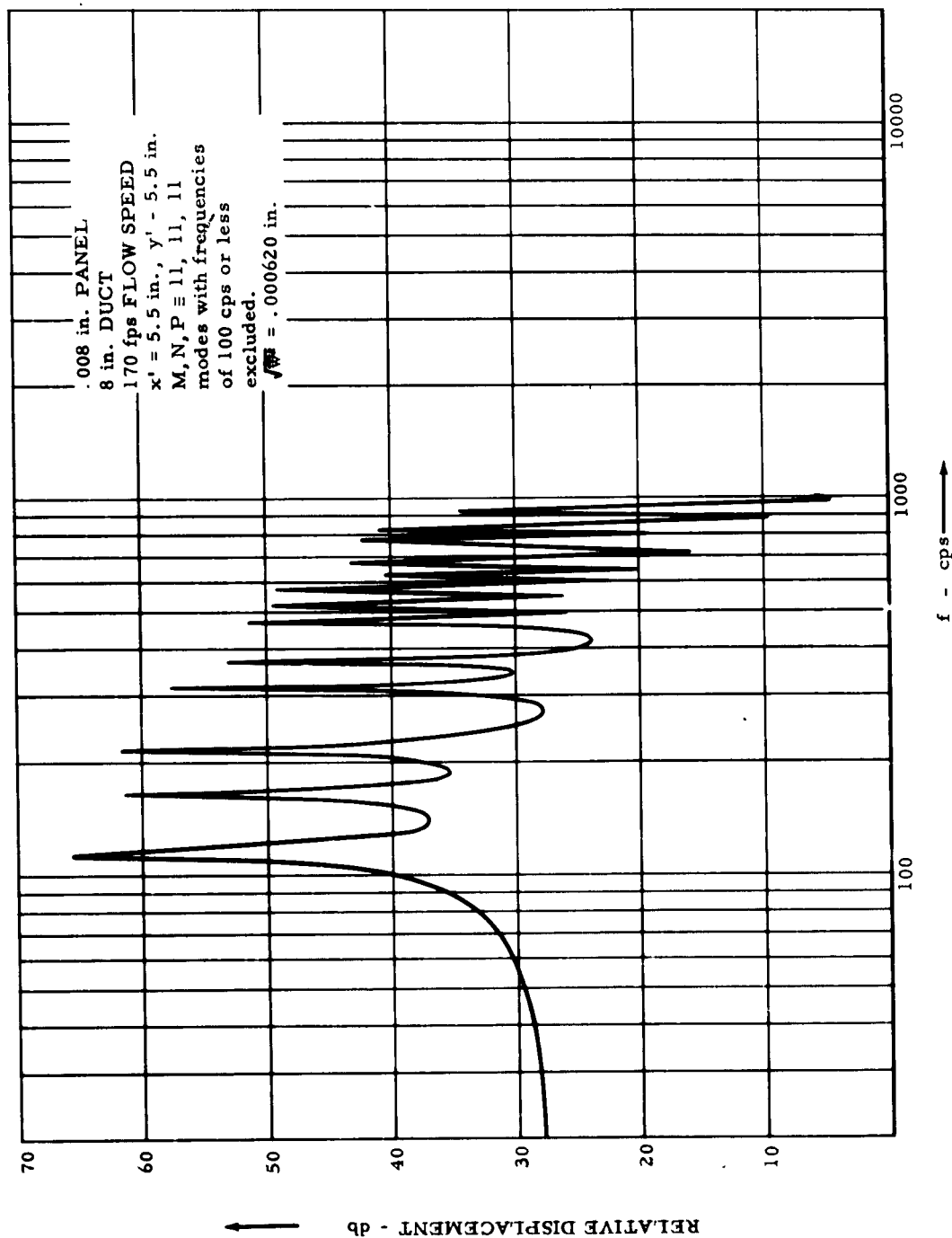
FIGURE 39   THEORETICAL PANEL VIBRATION FREQUENCY RESPONSE
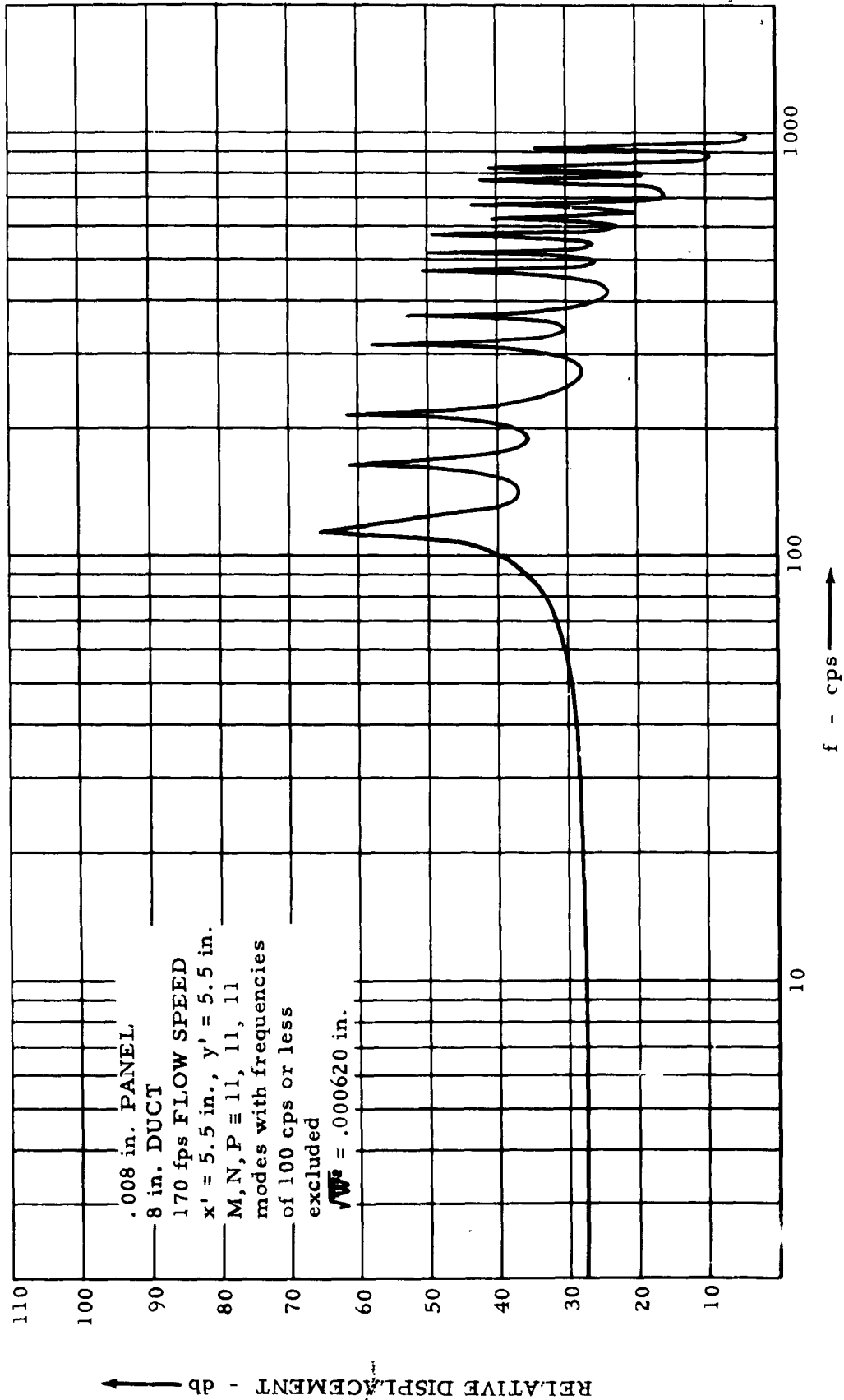
FIGURE 39 Continued. THEORETICAL PANEL VIBRATION FREQUENCY RESPONSE

.008 in. PANEL,
8 in. DUCT
170 fps FLOW SPEED
x' = 5.5 in., y' = 5.5 in.
M, N, P = 11, 11, 11
modes with frequencies
of 100 cps or less
excluded
$\sqrt{W^2}$ = .000620 in.

f - cps

RELATIVE DISPLACEMENT - db

.008 in. PANEL, 170 fps FLOW SPEED, 8 in.DUCT, $\bar{U}_c/U = 0.74$
$f_{co} - 120$ cps, $(M \times N \times P)$ max $= 11 \times 11 \times 11$
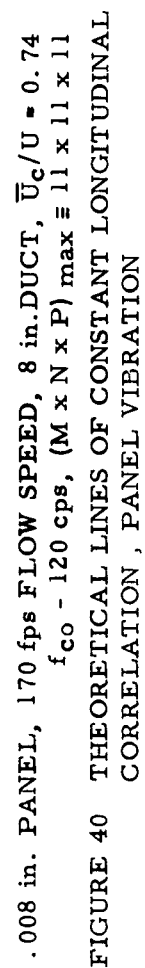
FIGURE 40   THEORETICAL LINES OF CONSTANT LONGITUDINAL
CORRELATION, PANEL VIBRATION
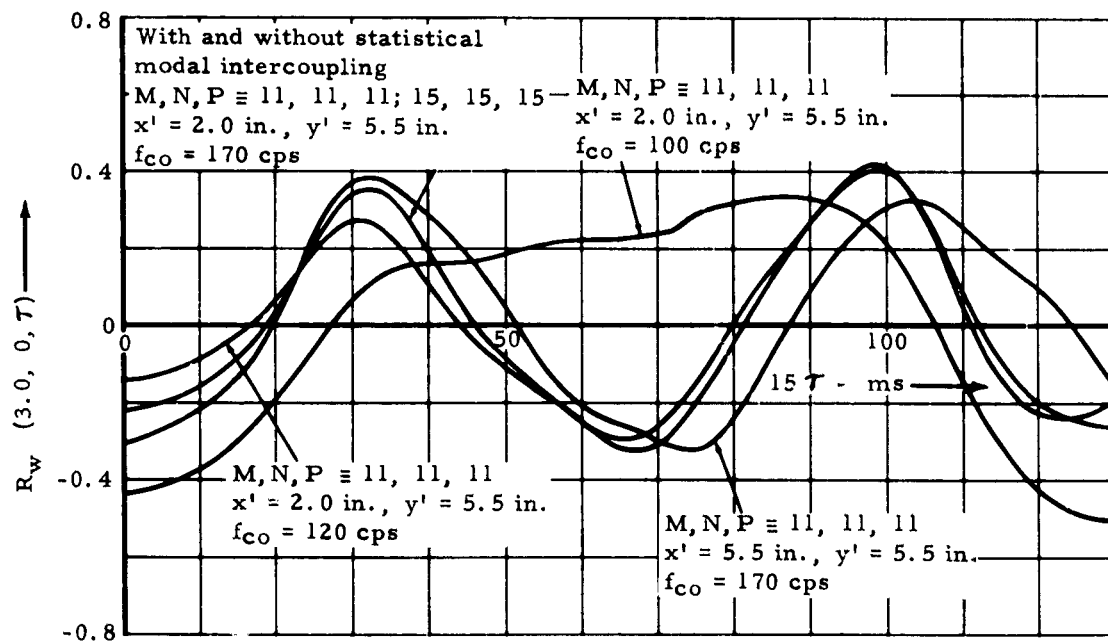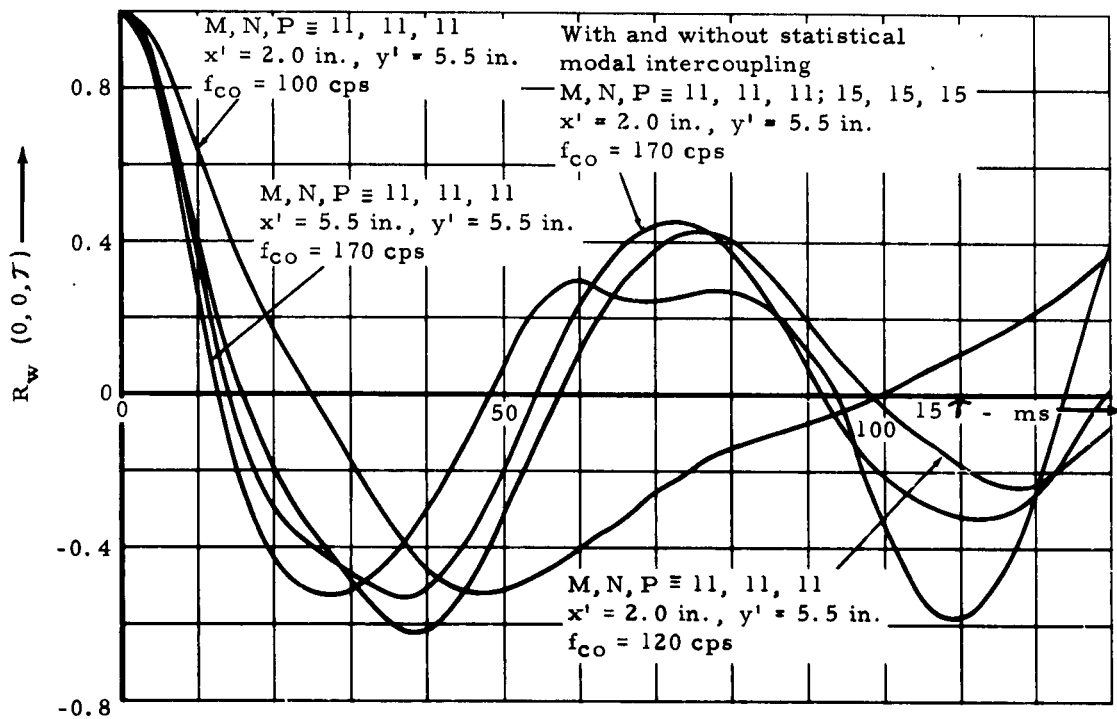
.008 in. PANEL, 170 fps FLOW SPEED, 8 in. DUCT

FIGURE 41   THEORETICAL LONGITUDINAL TWO-POINT
SPACE-TIME CORRELATION OF THE PANEL
DISPLACEMENT
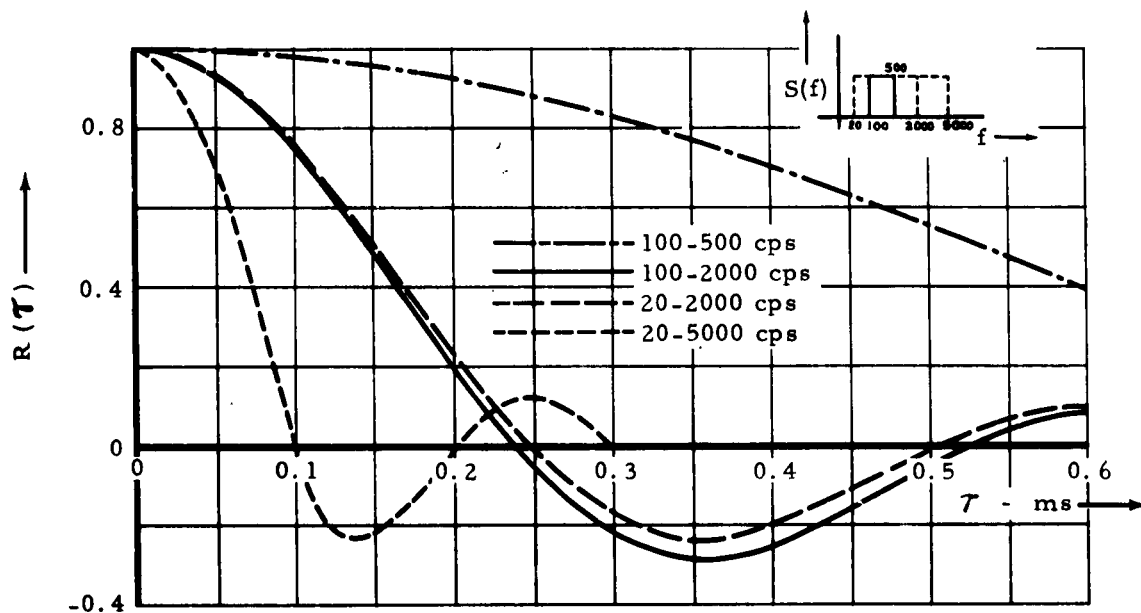
FIGURE C-1
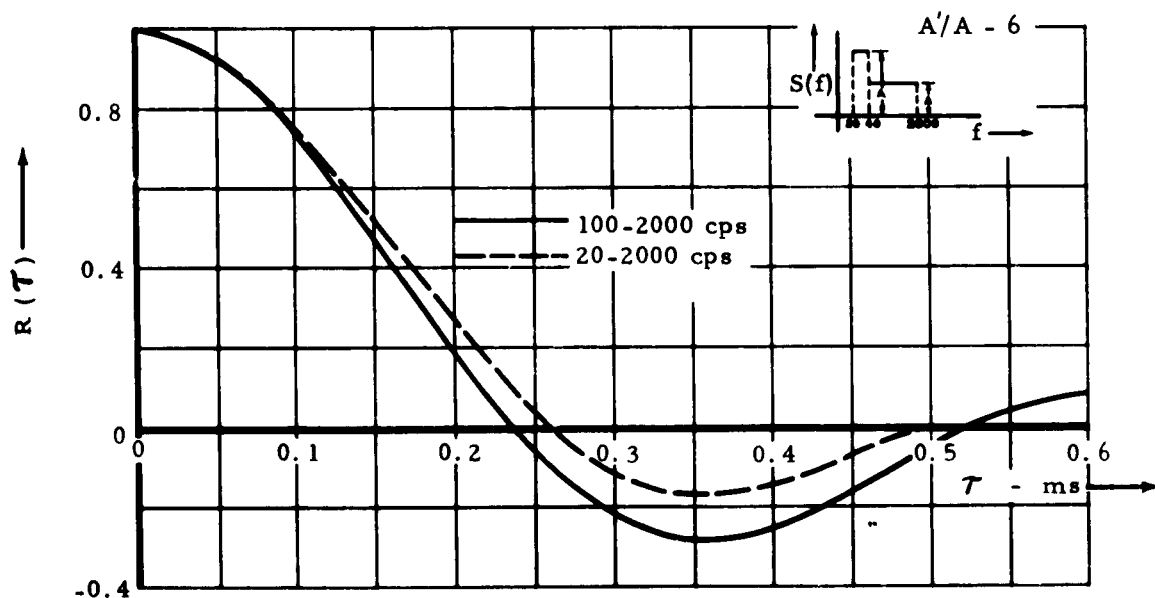
FIGURE C-2

FIGURE C-1, C-2   EFFECTS OF SPECTRAL BAND WIDTH AND RELATIVE
AMPLITUDE ON AUTO-CORRELATION

UTIAS REPORT NO. 98

Institute for Aerospace Studies, University of Toronto

Turbulence-Induced Panel Vibration

M. Y. el Baroudi   February, 1964   29 pages   43 figures

1. Vibration of Plates   2. Turbulence   3. Structural Dynamics
4. Aerodynamic Noise   5. Boundary Layer Noise   6. Acoustics
I. el Baroudi, M. Y.   II. UTIAS Report No. 98

Motivated by the problem of boundary-layer induced panel noise, a detailed study has been made of the transverse vibration of 11 x 11 inch steel panels flush-mounted in the wall of a turbulent flow duct. Panel thicknesses were .002 and .008 inch. Duct cross sections were 1 x 12 and 8 x 12 inches, and flow speeds were about 60 to 200 feet per second. The characteristics of the exciting pressure field at the wall and of the resultant vibration of the sample panels were investigated using statistical techniques. Relief charts of the experimental two-point space-time correlation of panel vibration versus longitudinal separation and time-delay showed pronounced oblique ridges and valleys discernable in a more random pattern. These are interpreted as running waves (with a speed equal to that of the pressure field convection) with an irregular pattern superposed. For comparison, Dyer's idealized theoretical model of the panel response was developed and programmed for a digital computer. The calculated relief plot of correlation showed qualitative agreement with the experimental results.

Available copies of this report are limited. Return this card to UTIAS, if you require a copy.